Titre: Title:	Low-Profile Antennas for Aircraft Communication Systems
Auteur: Author:	Amna Ikram
Date:	2018
Type:	Mémoire ou thèse / Dissertation or Thesis
Référence: Citation:	Ikram, A. (2018). Low-Profile Antennas for Aircraft Communication Systems [Thèse de doctorat, École Polytechnique de Montréal]. PolyPublie. https://publications.polymtl.ca/3763/

URL de PolyPublie: PolyPublie URL:	https://publications.polymtl.ca/3763/
Directeurs de recherche: Advisors:	Jean-Jacques Laurin
Programme: Program:	Génie électrique

UNIVERSITÉ DE MONTRÉAL

LOW-PROFILE ANTENNAS FOR AIRCRAFT COMMUNICATION SYSTEMS

AMNA IKRAM

DÉPARTEMENT DE GÉNIE ÉLECTRIQUE

ÉCOLE POLYTECHNIQUE DE MONTRÉAL

THÈSE PRÉSENTÉE EN VUE DE L'OBTENTION

DU DIPLÔME DE PHILOSOPIAE DOCTOR

(GÉNIE ÉLECTRIQUE)

DÉCEMBRE 2018

Cette thèse intitulée :

LOW-PROFILE ANTENNAS FOR AIRCRAFT COMMUNICATION SYSTEMS

présentée par: IKRAM Amna

en vue de l'obtention du diplôme de : Philosophiae Doctor

a été dûment acceptée par le jury d'examen constitué de :

M. Wu Ke, Ph. D., président

M. LAURIN Jean-Jacques, Ph. D., membre et directeur de recherche

M. AKYEL Cevdet, D. Sc., membre

M. DESLANDES Dominic, Ph. D., membre externe

DEDICATION

To my parents!

May they rest in peace in heaven!

ACKNOWLEDGEMENTS

RÉSUMÉ

Dans les aéronefs, les antennes sont utilisées pour les communications ainsi que pour différents systèmes de navigation allant de 30 MHz à 4 GHz et plus. Le positionnement des antennes sur l'aéronef est crucial pour les systèmes avioniques. Les antennes de type « lame » (*blade antennas*) sont généralement utilisées dans l'aéronef pour divers systèmes de communication. L'antenne lame est essentiellement un monopole qui fait généralement autour d'un quart à un huitième de longueur d'onde et est encapsulée dans un radôme. À basse fréquence, la taille de la lame devient suffisamment grande pour introduire du bruit, augmenter la traînée aérodynamique de l'antenne et causer des dommages suite à une collision avec des équipements au sol lors de l'entretien et le service de l'aéronef. Par conséquent, et afin d'améliorer l'aérodynamisme des avions commerciaux efficaces, il devient nécessaire de disposer d'antennes conformes, à hauteur réduite et multifonctionnelles. Dans les avions commerciaux performants, l'aluminium est graduellement remplacé par un matériau composite à base de fibres de carbone. Ce matériau a l'avantage d'offrir une résistance meilleure que celle de l'aluminium pour un poids équivalent et aussi de réduire les coûts d'enretien et de réparation.

Dans cette thèse, quatre différents concepts d'antenne sont suggérés afin de réduire la hauteur d'une antenne, comparée aux antennes disponibles sur le marché pour des bandes de communications à Très Hautes Fréquences (VHF Comms 118-137 MHz), du système d'alerte de trafic et d'évitement de collision (TCAS 1.03-1.09 GHz) et du système d'équipement de mesure de distance (DME 0.96-1.22 GHz). Deux des concepts proposés sont basés sur le l'antenne en T avec des broches de court-circuit et des tronçons parasites pour rendre l'antenne à profil bas. Les deux autres concepts utilisent le chargement d'un monopole avec un matériau magnéto-diélectrique (MMD) et le chargement d'une antenne planaire avec un conducteur magnétique artificiel (CMA) pour rendre l'antenne à profil bas.

Le premier design consiste en une antenne bi-bande couvrant à la fois les bandes Comms TCAS et VHF. Une antenne VHF d'un dixième à l'échelle physique a été étudiée précédemment dans notre groupe de recherche, se basant sur le concept de monopole en T avec broches de court-circuit et tronçons parasites. Dans ce travail, l'antenne VHF est optimisée et modifiée pour une bande de

fréquence VHF à pleine échelle. Une plaque d'interface est ajoutée à la structure de l'antenne afin qu'elle puisse être facilement placée sur toute plate-forme appropriée pour d'éventuels tests ou utilisations futures. Une nouvelle approche est adoptée pour alimenter l'antenne TCAS placée sur l'antenne de la bande VHF. Ce concept présente l'avantage d'avoir une couverture bi-bande tout en utilisant l'empreinte d'une antenne à la surface de l'avion. La hauteur électrique de l'antenne TCAS est de 0.04λ et de 0.03λ pour la VHF, λ étant la longueur d'onde à la fréquence de fonctionnement la plus basse. La performance de l'antenne est mesurée lorsqu'elle est montée sur des plans de masse en aluminium et en composites. Un bon accord entre mesures et simulations est observé au niveau des propriétés de pertes de retour et de diagramme de rayonnement pour les deux types de plan de masse. En raison de la non disponibilité de systèmes de mesures de rayonnement en champ éloigné pour la bande VHF, des mesures de champ électrique en zone rapprochée sont effectuées dans une Chambre de Compatibilité Électromagnétique (CEM) du *Centre de Recherche Industrielle du Québec* (CRIQ) et comparées à une simulation similaire à l'installation.

Le deuxième concept concerne la bande DME. Le prototype réalisé est mis à une échelle égale à 4 fois la fréquence de fonctionnement réelle. Dans cette antenne, une antenne micro-ruban planaire excite des motifs métalliques circulaires formant un CMA et une antenne à large bande conforme ayant une hauteur de 0.07λ et des caractéristiques de rayonnement similaires à celles de l'antenne monopole sont proposées. Cette conception est inspirée de la littérature mais est modifiée pour une bande passante fractionnelle plus grande (BPF) d'environ 30% par rapport à 6%. Il met également l'emphase sur les problèmes liés aux effets d'espaces d'air lors de la mise en place du matériau diélectrique sur le plan de masse.

Dans le troisième concept d'antenne pour la bande DME, une méthode bien connue de chargement de matériau a été utilisé. Un MMD est d'abord testé pour sa permittivité (ε_r) et sa perméabilité (μ_r) à l'aide d'un équipement de test de matériaux. Le MMD ayant des valeurs élevées de permittivité et de perméabilité relatives d'environ 10 a été placé de manière unique en tant qu'élément de chargement sur une antenne monopôle standard d'un quart de longueur d'onde. Le matériau est placé sur la pointe sous forme de disque et en bas sous forme d'anneau pour perturber les propriétés électriques et magnétiques du monopôle avec la permittivité et la perméabilité d'un MMD, respectivement. La hauteur du monopôle chargé est considérablement réduite de 29.5% tout en conservant de bonnes propriétés de rayonnement par rapport à un monopôle non chargé.

Le quatrième concept se rapporte à la bande DME. Une antenne cadre sectorielle couplée (CSLA) est utilisée à partir de la littérature, en tant qu'élément rayonnant et un nouveau concept de plan de masse rainuré est utilisé pour améliorer la directivité de l'antenne à l'horizon ($\theta = 90°$), comme exigé par le système DME. La directivité à l'horizon est améliorée par le concept de boucle de courant magnétique équivalente en utilisant un plan de masse rainuré. À la fréquence de bande DME la plus basse, la hauteur électrique de l'antenne proposée est de 0.11 λ et son diagramme de rayonnement est similaire à celui d'un monopôle. Il présente toutefois l'avantage d'une réduction de hauteur de 0.25λ à 0.11λ. Comme les essais en soufflerie n'étaient pas disponibles, le calcul de la traînée aérodynamique du modèle proposé a été effectué à l'aide de formules empiriques et comparé à celui d'antenne DME de type lame standard.

Les quatre nouvelles conceptions d'antenne proposées dans cette thèse ont été simulées à l'aide d'un simulateur de structure haute fréquence (ANSYS HFSS), puis des prototypes ont été fabriqués et mesurés. La spécification du système requise pour chaque antenne proposée en termes de perte de retour, de diagramme de rayonnement et de bande passante est atteinte. La hauteur de chaque antenne est considérablement réduite, tout en conservant de bonnes caractéristiques de rayonnement similaires à celles des antennes lames utilisées sur le marché dans les quatre modèles, ce qui en fait de bons candidats pour les applications avioniques des aéronefs.

ABSTRACT

In aircrafts, antennas are used for communications as well as for different navigation systems ranging from 30 MHz to 4 GHz and more. The placement of antenna on the aircraft is critical to avionic system of an aircraft. Typically blade antennas have been used in the aircraft for various communication systems. Blade antenna is basically monopole of height usually about a quarter of a wavelength to one-eighth of a wavelength and encapsulated in a radome. At low frequency the size of blade becomes large enough to introduce the acoustic noise and increase the parasitic drag of the antenna and do mechanical damage and collision with ground equipment during aircraft maintenance and service. Hence to improve the aerodynamics of efficient commercial aircrafts there is a need of reduced height, conformal and multifunction antennas. In efficient commercial aircrafts aluminum has been replaced by composite material, other than being expensive it has advantage of such as weight reduction, more strength than aluminum and has fewer maintenance and repair costs.

In this dissertation four different antenna designs are proposed to reduce the height of an antenna as compared to commercially available antennas for Very High Frequency Communications (VHF Comms 118-137 MHz), Traffic Collision Avoidance System (TCAS 1.03-1.09 GHz) and Distance Measuring Equipment (DME 0.96-1.22 GHz) bands. Two of the designs proposed here are based on the concept of top-loaded antenna with shorting pins and parasitic stubs to make the antenna low-profile. The other two use the loading of a monopole with magneto-dielectric material (MDM) material and loading of a patch antenna with artificial magnetic conductor (AMC) to make the antenna low-profile.

The first design is a dual-band antenna covering both TCAS and VHF Comms bands. Previously in our research group a physically scaled one-tenth of VHF antenna has been investigated, which uses the concept of top-loaded monopole with shorting pins and parasitic stubs. In this work the VHF antenna has been optimized and modified for full-scaled VHF frequency band. An interface plate has been added to the antenna structure so that it can easily be placed on any platform suitable for future testing or use. A novel approach has been used to feed the TCAS antenna placed over the VHF band antenna. Such design has an advantage of having dual-band coverage while using footprint of one antenna on the surface of an aircraft. The electrical height for TCAS antenna is 0.04λ and for VHF its 0.03λ where λ is the wavelength at lowest frequency of operation. The

antenna performance has been measured for both aluminum and composite ground planes and good comparison has been seen in the return loss and radiation properties with both ground planes. Due to the unavailability of far field radiation measurements for VHF band, near electrical field measurements were done in *Centre de Recherché Industrielle du Québec* (CRIQ), electromagnetic compatibility (EMC) chamber and compared with the similar simulation setup.

The second design is for the DME band, but it is scaled to 4 times of the actual operating frequency. In this antenna a microstrip patch antenna excites the circular AMC cells and a conformal broadband antenna with height of 0.07λ and radiation characteristics similar to monopole antenna is proposed. This design is inspired by literature but has been modified for larger fractional bandwidth (FBW) of approximately 30% as compared to 6%. It also highlights issues related to the effects of air gaps while placing dielectric material on the ground plane.

In the third antenna design for DME band, a well-known concept of material loading has been used. The MDM is first tested for permittivity (ε_r) and permeability (μ_r) using Keysight material testing equipment. The MDM with high ε_r and μ_r values of approximately 10 has been uniquely placed as a loading element on a standard quarter wavelength monopole antenna. The material is placed at the tip as a disc and at the bottom as ring to disturb the electric and magnetic properties of monopole with the permittivity and permeability of MDM respectively. The height of loaded monopole is considerably reduced by 29.5% while keeping good radiation properties as compared to unloaded monopole.

The fourth design is for DME band. A coupled sectorial loop antenna (CSLA) is used from the literature, as a radiating element and a new concept of grooved ground plane is used to enhance the directivity of antenna at horizon ($\theta=90°$) as required by the DME system. The directivity at horizon is improved by the equivalent magnetic current loop concept with the use of grooved ground plane. At the lowest frequency of DME band the electrical height of the proposed antenna is 0.11λ and it has a radiation pattern similar to that of a monopole, but it has the advantage of height reduction from 0.25λ to 0.11λ. As wind-tunnel testing wasn't available, aerodynamics drag calculation of proposed model has been done using empirical formulas and compared with that of off-the-shelf DME blade antenna.

All four novel antenna designs proposed in this thesis have been simulated using high frequency structure simulator (ANSYS HFSS), fabricated and measured. The required system specification

for each proposed antenna in terms of return loss, radiation pattern and bandwidth has been achieved. The antenna height is considerably reduced while keeping good radiation characteristics similar to commercially used blade antenna in all the four models, which makes them good candidates for the aircraft avionics applications.

TABLE OF CONTENTS

LIST OF TABLES

LIST OF FIGURES

LIST OF SYMBOLS AND ABBREVIATIONS

AMC   Artificial Magnetic Conductor

ATC   Air Traffic Control

AUT   Antenna Under Test

CLAS   Conformal Load Bearing Antenna Structure

CRIQ   Centre de Recherché Industrielle du Québec

CSLA   Coupled Sectorial Loop Antenna

DAB   Digital Audio Broadcasting

DF   Direction Finding

DME   Distance Measuring Equipment

DO   DME Operating

DVB-H   Digital Video Broadcasting-Handheld

EBG   Electromagnetic Band gap

EMC   Electromagnetic Compatibility

EMI   Electromagnetic Interference

FAA   Federal Aviation Administration

FBW   Fractional Bandwidth

GPS   Global Positioning System

HF   High Frequency

LAN   Local Area Network

LTE   Long Term Evolution

MDM   Magneto-Dielectric Material

PEC   Perfect Electric Conductor

PMC   Perfect Magnetic Conductor

PLGS	Patch Loaded Ground Slab
RadAlt	Radar Altimeter
RAs	Resolution Advisories
RTCA	Radio Technical Commission for Aeronautics
SIW	Substrate Integrated Waveguide
SWA	Surface Wave Antenna
TAs	Traffic Advisories
TCAS	Traffic Collision and Avoidance System
T-DMB	Terrestrial-Digital Multimedia Broadcasting
TE	Transverse Electric
TEM	Transverse Electromagnetic
TM	Transverse Magnetic
UAV	Unmanned Aerial Vehicle
UHF	Ultra High Frequency
UWB	Ultra-Wideband
VHF	Very High Frequency
VOR	Very high frequency Omni-directional Range
VSWR	Voltage Standing Wave Ratio
WWAN	Wireless Wide Area Network
XRD	X-ray Diffraction

LIST OF APPENDICES

CHAPTER 1   INTRODUCTION

1.1   Aircraft antenna

In a wireless communication system, the antenna is one of the very important components. It provides an interface between the wireless electronics systems to the outside world. All antennas, regardless of their applications are characterized by common features such as operational frequency, Fractional Bandwidth (FBW), radiation pattern, Voltage Standing Wave Ratio (VSWR) or return loss (S11), efficiency, directivity, gain, polarization, etc. In aircrafts, antennas are used for communications as well as for different navigation systems ranging from 30 MHz to 4 GHz and more. These navigation systems provide a number of functions for the operation of the aircraft, such as Direction Finding (DF), Distance Measuring Equipment (DME), Global Positioning System (GPS), Microwave Landing System (MLS), Radar Altimeter (RadAlt) etc.

Figure 1-1 [1] lists different communication and navigation systems used by an aircraft along with respective antenna placement location. Large aircraft duplicate essential systems like Very High Frequency Communication (VHF Comms) system, Traffic Collision Avoidance System (TCAS) and Air Traffic Controller (ATC) system. They use more than one antenna for redundancy and safety reasons.
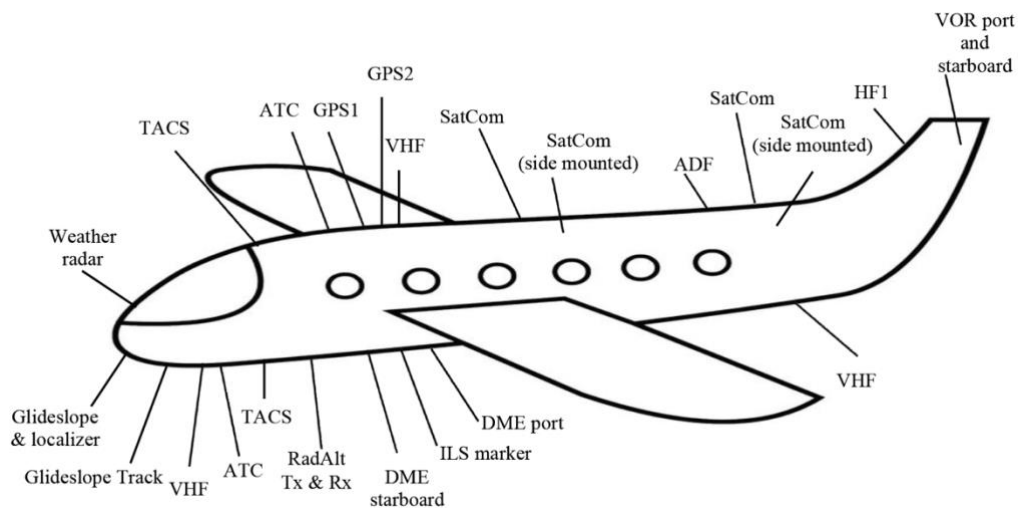
Figure 1-1: Antenna placement on a passenger aircraft for various communication systems [1].

1.2 Requirements for an aircraft antenna

The antennas used in an aircraft system are required to meet minimal operational performance standards. Radio Technical Commission for Aeronautics (RTCA) has developed technical performance standards in close partnership with FAA. For example, for DME the standard is documented as DO-189 [2], for VHF band it is DO-186B [3] and for TCAS the standard is documented as DO-185B [4]. The compliance of DME, TCAS and VHF aircraft antenna to these standards ensure that the equipment will perform adequately for the given operation. The test requirements of DME antenna are stated below:

1. The antenna should be placed at the center of a flat circular ground plane with diameter of 1.2 m (1200 mm).
2. The antenna VSWR should be less than 2 for the DME frequency band.
3. The average radiation field strength of antenna in the azimuthal plane should be equal to radiation field strength of a matched resonant quarter-wavelength vertical monopole.
4. The difference between the maximum and minimum radiation field strength in the azimuthal plane should not exceed 6 dB.
5. The elevation field strength of antenna should be equal or greater than that of a standard monopole antenna placed in the center of a ground plane at the same frequency with VSWR <1.2.

Similarly, the test requirements of a VHF antenna are following:

1. The antenna should be placed at the center of a flat square ground plane with size of 4 ft x 4 ft. (1219.2 mm x 1219.2 mm).
2. The antenna VSWR should be less than 3, for the VHF frequency band.
3. The average radiation field strength of antenna in the azimuthal plane should not be less than 6 dB as compared to radiation field strength of a matched resonant quarter-wavelength vertical monopole antenna.
4. The difference between the maximum and minimum radiation field strength in the azimuthal plane should not exceed 6 dB.
5. The elevation field strength of antenna should be equal or greater than that of a standard monopole antenna placed in the center of a ground plane at the same frequency with VSWR <1.2.

In general, the aircraft antenna requirements for various communication and navigation systems are listed as following:

1. Antenna location and placement: It is very important to establish the location of an antenna to be used in avionic systems as it can alter the stringent aerodynamic design requirements of the aircraft.

2. Dimensions: Size and weight are important factors that must be considered when selecting an antenna for a particular application. Size and weight also restrict the locations where the antenna can be installed.

3. Reliability: The candidate antenna must be capable of withstanding prolonged exposure to harsh environment conditions during the aircraft operation.

4. Maintenance: An antenna should be designed such that it requires a minimal repair and replacement time if it fails to operate.

1.3   Problems associated with aircraft antennas

Currently, large airplanes rely on blade and whip antennas as shown in Figure 1-2[1] [5] which are highly visible, obtrusive and prone to damages. Blade antenna is a quarter-wavelength monopole antenna encapsulated in a radome. Some of the problems associated with currently employed aircraft antennas are as follows:

Figure 1-2: Blade and whip antenna placed on an aircraft [5].

---

[1] Permission granted for the use of image.

Size and maintenance: In aircraft, for the aerodynamics and the mechanical stability, external antennas are a sensitive factor [6] . When the frequency of operation is low, the wavelength becomes large which makes the physical antenna size prohibitively large for most applications and unacceptable for platforms such as airplanes. A large external antenna has a greater tendency to collide and get damage with the ground equipment especially during aircraft maintenance and service.

Aerodynamics drag: During flight, airstream flows around an antenna. The physical interaction of the antenna with the air medium around causes an aerodynamics drag and generates aerodynamics noise [7]. The improper placement of antenna, additional weight and size of an aircraft antenna can increase the aerodynamics drag, which negatively effects the flying ability of an aircraft, such as increasing fuel consumption which eventually puts limitation on the speed of aircraft.

1.4 Motivation and context for new antenna design

There has been a great interest in the research and development of next generation energy efficient aircraft and avionics systems. The Canadian aerospace industry with the support of government of Canada is working on projects to improve aircraft operations, aircraft noise reduction and on additional topics targeted towards the development of greener aircraft for future. These projects also include work on composite materials i.e. to investigate materials that can be developed by reusing uncured aerospace grade pre-impregnated materials. All these activities mentioned above are a part of the green aviation research and development network (GARDN) [8] projects.

The work presented in this dissertation is a part of two academia-industry projects. The first project is partnered with École Polytechnique de Montreal (POLY), École de Technologie Supérieure (ETS), Concordia University, Bombardier Aerospace (BA) and MacDonald Dettwiler and Associates (MDA Corporation). The main contribution to the project is to make low-profile DME band antenna. The second project is Electromagnetic Platform for lightweight Integration/Installation of electrical systems in Composite Electrical Aircraft (EPICEA) and the collaborators are from Canada and europe, Axessim (France), Bombardier Aerospace (BA), École Polytechnique de Montreal (POLY), Ingegnerai dei sistemi (Italy) and Onera (France). Whereas, in this project, one of the objectives is to design low-profile dual-band (VHF & TCAS) antenna for aircraft communication system, which is a major contribution of this dissertation.

1.4.1 Objective and background

The objective of this dissertation is to design low-profile, conformal and multifunctional antennas that can work for both aluminum and energy efficient composite planes and can help to improve aerodynamics properties of commercial aircrafts. The following discussion explains the challenges and advantages of this work.

By making the antenna low-profile, it come very close to the metal body of an aircraft. Reducing the height of an antenna degrades its operational performance such as return loss, operating bandwidth and radiation pattern [9] .Therefore, it is required to investigate new designs, techniques and materials for low-profile antennas that can advantageously possess good radiation characteristics.

As mentioned earlier poor antenna placement can degrade the flying qualities of an aircraft and impact the performance of the avionics system. The compact and conformal antenna helps to find an installation location within the boundary layer especially if the antenna is added after the aircraft shape was frozen, i.e. normally a case where an additional installation or an upgrade to the aircraft electronics communication system is performed. A boundary layer is defined as a very thin layer of air flowing on the surface of aircraft. It gives an effective shape to any surface, which is slightly different from the actual physical shape. The details of the flow within the boundary layer are very important to understand the skin friction drag of an object. As any object protruding outside the boundary layer can produce a large drag force on the aircraft and cause turbulence [10].

The main advantage of combining two or more functions in one antenna results in the reduction of the total number of antennas required on an aircraft. This helps to minimize the overall aerodynamic drag, reduce number of service repairs or replacements due to corrosion and foreign object damage and reduce the number of structural holes needed to install the antenna. However, if a multifunctional antenna fails it can cause failure of more than one service thus additional measures are required to maintain reliability.

1.5 Contributions to research

This dissertation aims to design aircraft antennas, in compliance to the specific bands of communication and navigation systems used in an aircraft. Most of the research in this area is within the industry and commercially available antennas are usually blade antenna. Below are the

contributions made in this dissertation in the area of the aircraft antenna design. These novel, low-profile proposed designs are optimized, simulated, fabricated and tested. Both simulated and measured results are presented, which are in close agreement to each other and to the system requirements.

1. For the first time a dual-band antenna that covers both VHF Comms and TCAS band is presented. This antenna uses two separate antenna feeds and can be simultaneously used for both VHF and TCAS systems. The impedance matching and radiation characteristics of this antenna meet the system specifications and the presence of VHF antenna has minimal impact on the performance of TCAS antenna or vice-versa. The measured FBW of TCAS antenna is 5.6% and for VHF antenna its 14.9%. The height of TCAS and VHF Comms is 0.04λ and 0.03λ, where λ is the free space wavelength at lowest operating frequency of TCAS and VHF respectively. An interface plate has been integrated in the design for an easy assembly on any platform. The antenna performance was tested with both aluminum and composite ground planes to see the compatibility with both types of platforms.

2. A surface wave antenna (SWA), physically scaled by a factor of one-fourth for DME operating band is proposed. The antenna has been investigated for broad bandwidth by loading the patch antenna with circular artificial magnetic conductor (AMC) cells. The proposed design has 31% FBW (simulated). The height of antenna is 0.07λ and it shows radiation characteristics similar to those of a vertical monopole antenna.

3. A magneto-dielectric material (MDM) is used on a monopole at strategic positions to lower the resonant frequency. Without compromising the bandwidth of the antenna, the antenna height is reduced by 29%. The average measured efficiency of the antenna is ~ 60% for the DME band due to lossy nature of magnetic material.

4. For the DME band, a novel grooved ground plane is proposed with a well-known Coupled sectorial loop antenna (CSLA) [11]. The grooved ground plane is placed underneath the CSLA and by using the concept of dual loop antenna, maximum radiation at horizon is generated, which is one of the system requirements for DME band antenna. The drag coefficient for the proposed design is calculated by using empirical formula to get an estimate while comparing with a state-of-art blade antenna.

1.6 Thesis outline

In this dissertation four different designs of low-profile aircraft antennas for three different communication systems (VHF Comms, TCAS, and DME) are proposed. The outline of thesis is as follows.

In Chapter 2, general theory, state-of-art antennas and literature review is provided. A dual-band antenna for VHF Comms and TCAS system has been discussed in Chapter 3. Chapter 4 explains the design of SWA for DME band. Chapter 5 includes the discussion about the use of MDM for reducing the height of monopole antenna for DME band. Chapter 6 is the design of DME antenna with maximum directivity at horizon by using grooved ground plane and estimates the drag for the proposed design. Chapter 7 summarizes the thesis work with concise conclusion and gives some directions for the future research.

CHAPTER 2   LITERATURE REVIEW

This chapter covers the basic theory about aircraft communication systems, their working principles and state-of-the-art antennas currently used on aircraft. There is also a discussion about the advantages and disadvantages of composite and aluminum aircraft. This is followed by the literature review of aircraft antennas and the theory and techniques used in the design of four different proposed antennas.

2.1 TCAS system

Any passenger and cargo aircraft with a seating capacity of 10 or more are required to use TCAS navigation system as mandated by the Federal Aviation Administration (FAA) [12]. TCAS is an airborne system, which operates by interrogating the transponder of an approaching aircraft. This system helps the pilot to determine the presence of near-by aircrafts to avoid mid-air collisions. The distance between the aircrafts, which is defined as the range is determined from the time required to receive the reply, and the altitude is extracted from the information encoded within the reply signal. In a complete TCAS system, a pair of directional and omnidirectional antennas is used. The directional antenna determines the bearing to the approaching aircraft and an omnidirectional antenna yields only the range and altitude of an intruding, near-by aircraft [13]. However complete TCAS system is not explored here instead only an omnidirectional antenna is considered. The design specifications of omnidirectional TCAS antenna are given in Table 2-1. TCAS operates at two frequencies, 1.03 GHz is used for transmission i.e. to interrogate and 1.09 GHz frequency is to receive the transponders reply. This system is not intended to replace the

Table 2-1: TCAS antenna design specifications.

Frequency	1.03 – 1.09 GHz
Bandwidth	5.6%
VSWR / S11	<2 / -10 dB
Radiation Pattern	Omnidirectional
Polarization	Vertical

existing ground-based air traffic control (ATC) system. However, TCAS augments the ATC capabilities and reduce its work load and thus improve the overall level of flying safety. The latest version of TCAS is TCAS-II, which offers pilot aural and visual warnings, as well as resolution advisories (RA) [14]. These traffic advisories (TAs) help the pilot to perform visual search for the intruding aircraft and also prepare the pilot for a potential maneuver using resolution advisories (RAs). TCAS-II helps to avoid mid-air collision by establishing communication to other aircraft and asking one aircraft to climb up and the other to descend.

2.2 VHF system

Air traffic controller uses the VHF communication system for its operation. VHF airband covers 108 MHz to 156 MHz, where Very high frequency Omnidirectional Range (VOR) is between 108 MHz to 118 MHz and VHF Comms has a frequency band of 118 MHz to 137 MHz. In this dissertation VHF Comms will be discussed and going forward VHF Comms will be written as VHF.VHF system is employed in all types of aircraft. This allows the pilot to request information and landing instructions from air traffic control centers and the control towers. For redundancy, two or more VHF antennas are installed on an aircraft [15]. They are usually installed along the lower and upper fuselage as shown previously in Figure 1-1. The location of the receiving station is not always the same or known, therefore the signal is transmitted in all directions using an omnidirectional antenna with a vertical polarization. Due to the nature of radio-wave propagation at VHF frequencies, the system is limited to line-of-sight distances. One advantage of VHF communication is that the transmitted signals are often less distorted by static or other interferences. Table 2-2 lists the design specification of a VHF antenna.

Table 2-2: VHF antenna design specifications.

Frequency	118 – 137 MHz
Bandwidth	15.7%
VSWR / S11	<3 / -6 dB
Radiation Pattern	Omnidirectional
Polarization	Vertical

2.3 DME system

DME navigation system is used to track the nearest ground station ahead on the route during the flight. DME antenna is usually installed at lower forward fuselage. This system continuously displays information about the aircraft's distance from the ground station. This is determined via sending two communication signal (pulses) from the aircraft to the nearest ground station ahead and once these pulses are received at the ground station, the ground station in return transmits the paired pulses toward the aircraft and the distance is calculated by the on-board DME transceiver module. As shown in Figure 2-1 the distance (slant range) changes with the height of the aircraft. Therefore, it is required to have maximum directivity of the DME antenna for θ above 60° to 90° depending upon the height of the aircraft. The DME antenna needs to be compliant with DO-189 standard as explained in Chapter 1. The specification for DME antenna is given in Table 2-3.
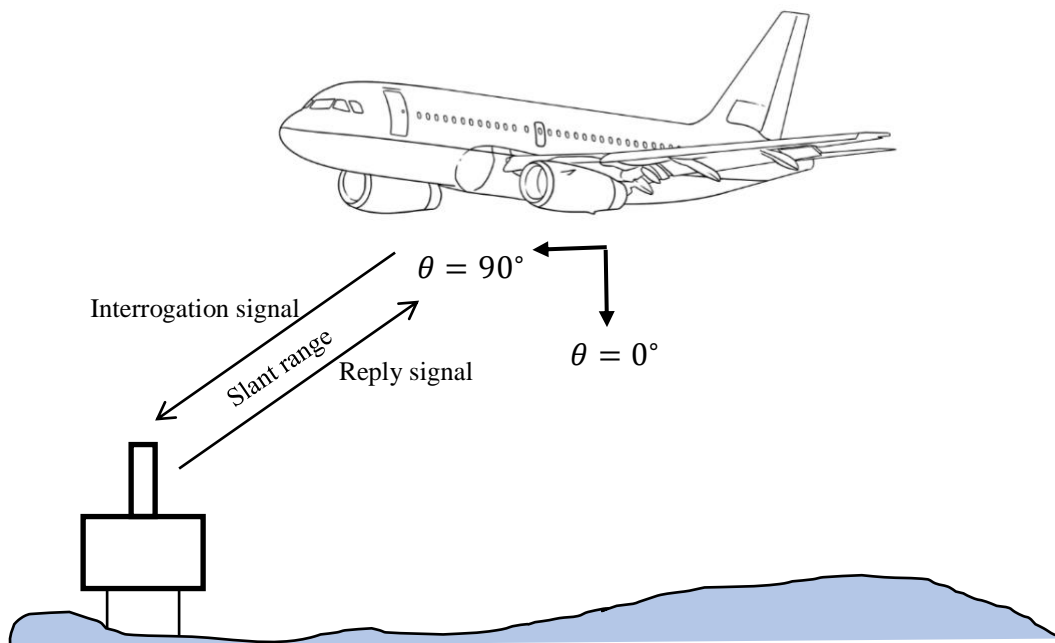
Figure 2-1: DME navigation system.

Table 2-3: DME antenna design specifications.

Frequency	0.96 – 1.22 GHz
Bandwidth	23%
VSWR / S11	<2 / -10 dB
Radiation Pattern	Omnidirectional with max directivity at horizon
Polarization	Vertical

2.4 Composite and aluminum aircraft

For most of the antennas placed on the aircraft, the skin of the aircraft works as a ground surface. Although the aircraft fuselage is cylindrical, the surface is usually very large and acts like a flat ground plane for an antenna. Hence the material with which the ground plane is made up of is significantly important for the antennas attached to it. In the past, aluminum was solely used to make the aircraft body but in last few years, composite aircraft has gained markets attention and is a replacement to the aluminum material. The main advantage of using composite material for an aircraft is the weight reduction and improved material strength as compared to aluminum material. Composite materials are mechanically stronger than aluminum, for equal weight, and can provide smooth finish on to the surface. The aircraft shows a better fuel economy, if weight is reduced which is possible with the use of composite materials. Composite material are more resistant to corrosion as compared to aluminum and therefore have low maintenance and repair cost associated to them [16]. For the case of aluminum body if a damage such as, dent or puncture happens, it can be repaired and can maintain its mechanical properties, however for such a damage to a composite material, requires the whole entire pieces to be replaced [17]. The composite material does not break easily as compared to aluminum, which can easily bend and dent after the damage. So, it is harder to find the internal structural damages in composite. Advancements to composites material technology has enabled to engineer high-temperature-resistant composite materials that can be used for high performance economical aircraft [18]. Unlike aluminum, the reduced conductivity of composite structure do not make them a good candidate for electromagnetic shielding such as in-

case of lightning strike [17]. Composite materials are expensive due to complex fabrication process. Efficient planes like Boeing's 787 Dreamliner and Airbus's A350 are made up of more than 50% of lightweight carbon fiber composites [19]. In an aircraft manufactured by using composite materials, antenna grounding is performed by using an aluminum sheet under the antenna and feed [20].

2.5 State-of-the-art antennas for aircraft communications

Aircraft antennas are used in both commercial and military aircrafts. Companies like Sensor systems, Honeywell, EDO Corp, Chelton and Rockwell Collins, manufacture these blades and whip type antennas.

2.5.1 Blade antenna

The most common type of antenna used in an aircraft for TCAS, DME and VHF systems is a blade antenna. Figure 2-2 displays examples of a blade antenna used in an aircraft [21-23]. A blade antenna is primarily a monopole encapsulated in a covering. Covering serves to protect the antenna form external environmental damage as well as its shape provide aerodynamic properties as needed by the aircraft. The blades can have several octaves of bandwidth and shaped in a way to deliver broadband performance.

TCAS Sensor Systems
S65-5366-735, height 2.45in

DME Sensor Systems
S65-5366-7L, height 2.2in

VHF Sensor Systems
S65-8280-10, height=11.85in
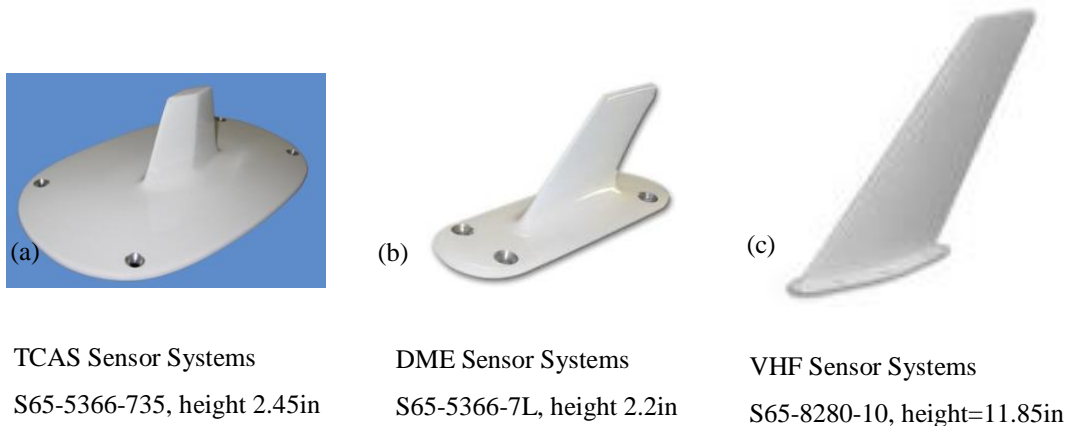
Figure 2-2: Commercial blade antennas from Sensor Systems [21-23].
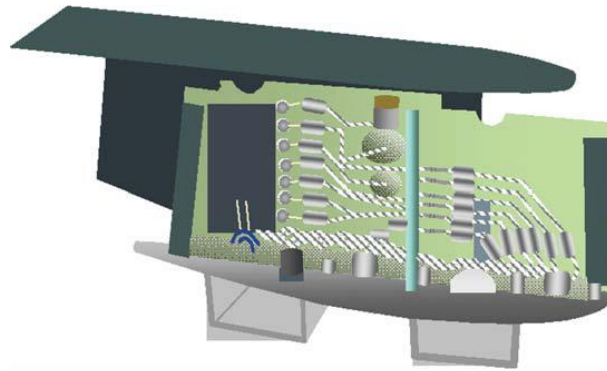
Figure 2-3: A UHF blade antenna showing the complex circuitry on the printed circuit element – manufactured by Chelton [24].

A passive blade can be used as an active antenna and its bandwidth performance can be improved by using a tuning circuit. An active UHF (225- 400 MHz) antenna is shown in Figure 2-3 [2] [24]. As previously discussed in Chapter 1, at low frequencies, the size of the quarter wavelength blade becomes significantly large enough that it can introduce acoustic noise, increase the parasitic drag of the antenna and be prone to mechanical damage and collision during aircraft maintenance and service. One of the best possible way a blade antenna could be used advantageously without introducing extra drag is when placed at vertical or horizontal stabilizer or winglets, (winglet is a wing tip on the wings of an aircraft) [25].

2.6 Literature review for low-profile antenna

Study and design of low-profile antenna has always been actively explored at industrial research platform. The increase in the volume of on-board communication system and compact design requirements has made it a challenging research topic for the aircraft communication manufacturing industry. The literature reviewed in this section begins with the discussion about the fundamentals of a small antenna. Further, section 2.6.2 gives the overview of research work

---

[2] Permission granted from Wiley.

conducted relevant to low-profile aircraft antennas and section 2.6.3 review the techniques used in the antenna designs proposed in this dissertation.

2.6.1 Small antenna

Defining the size of an antenna small has always been an interesting question. The definition of a small antenna can be somewhat ambiguous. However, if the size or volume of antenna including any ground plane image is less than $\frac{\lambda}{4}, \frac{\lambda}{8}$ or $\frac{\lambda}{10}$, it is considered as a small antenna. Wheeler defined the small antenna as one, whose maximum dimension is a fraction of one radiansphere [26], where radiansphere is a spherical region of radius $\frac{\lambda}{2\pi}$ around an antenna. The size or volume of a small antenna can be defined mathematically using the product of free space wavenumber (k) and radius of a sphere circumscribing the maximum dimension of antenna (a) as shown in Figure 2-4 (a). Where k, is given as $k = \frac{2\pi}{\lambda}$. If the size of the ground plane is significantly large and the impedance of antenna remains the same even if placed on an infinite ground plane, then the size of the ground plane is not required to be included in the definition of a as shown in Figure 2-4 (b). According to Wheeler, for an antenna size to be considered small the product of ka must be less than or equal to 0.5 i.e. $ka \leq 0.5$. In case of standard monopole of quarter-wavelength height, ka is equal to 1.57.
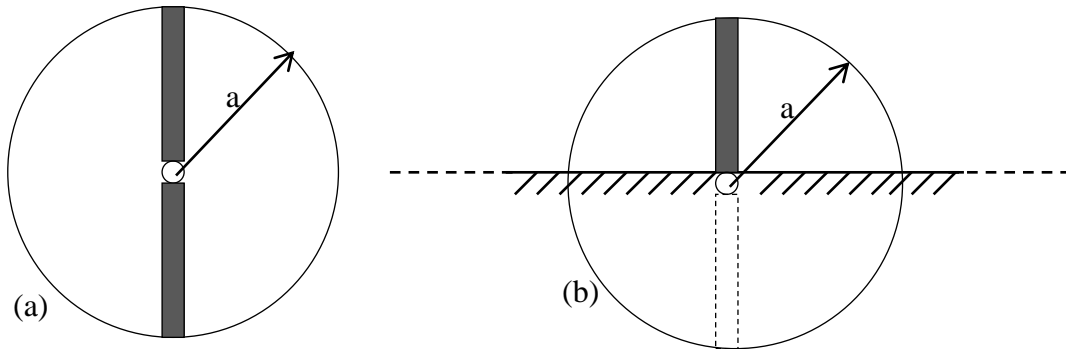
Figure 2-4: Definition of (a) Radius of a free-space dipole, (b) Radius of an imaginary sphere circumscribing the maximum dimension of a monopole on a ground plane.

$$ka = \frac{2\pi}{\lambda} \times \frac{\lambda}{4} = \frac{\pi}{2} = 1.57$$

Which implies that a standard monopole of quarter-wavelength height does not qualify to be a small antenna. In order for a monopole to qualify as a small antenna the maximum length of the monopole placed over infinite ground plane has to be approximately less than $\frac{\lambda}{12.5}$ or 0.08 λ. After Wheeler, L. J. Chu, has defined fundamental limits and the parameter trade-off for the size of the antenna versus frequency of operation, matched bandwidth and gain [9]. The fractional bandwidth for matched VSWR/S11 is defined as $FBW = \frac{w_+ - w_-}{w_0}$ where w_+ and w_- are the frequencies above and below the center frequency w_0. The upper bound of FBW for small antennas is given by equation (2-1) [27], where s is the VSWR and η is antenna efficiency.

$$FBW_{ub} = \frac{1}{\eta}\left[\frac{1}{ka} + \frac{1}{(ka)^3}\right]^{-1}\frac{s-1}{\sqrt{s}} \qquad (2\text{-}1)$$

Where the quantity in brackets is the quality factor given by $Q = \frac{1}{ka} + \frac{1}{(ka)^3}$. For small antennas, the product of bandwidth and efficiency is inversely proportional to Q and it is usually high. High quality factor means the ratio of energy stored in the antenna to the total power (radiated and dissipated) is high.

2.6.2 Antennas for aircraft applications

Designing low-profile aircraft antenna is challenging, especially when meeting the requirements of bandwidth, matching, and radiation characteristics. Following literature review shows that most of the designs compromise on one or the other factors as listed before.

A wide band omnidirectional antenna for VHF/UHF band is presented in [28]. The antenna is composed of a broadband gradually tapered exciter placed between two metallic sheets. It is matched for S11<-10 dB for a broad frequency band of 470 MHz to 6 GHz. The height of antenna is 0.094λ at the lowest operating frequency but the radiation pattern shows many ripples in the azimuthal plane due to the shape of the exciter.

A conical antenna radiator is loaded with capacitive disc and connected with parallel shorting post is presented in [29]. This antenna has a radiation pattern similar to a monopole for frequency 500 MHz to 1000 MHz. The antenna dimensions are $0.25\lambda \; x \; 1\lambda \; x \; 1\lambda$, whereas the height is comparable to a standard monopole and becomes large for low frequencies and thus does not qualify to be a low-profile antenna.

A conformal load-bearing antenna structure (CLAS) is proposed in [30] for UHF and TCAS systems. It consists of a log-periodic antenna covered with magneto-dielectric material. The antenna is made of multilayered structure to reduce its size and weight. The height is approximately 0.02λ at the lowest frequency 200 MHz and the VSWR is less than 3.5 for 200 MHz to 400 MHz. The VSWR achieved in this design is above the specifications of UHF antenna system.

A very thin, Substrate Integrated Waveguide (SIW) antenna designed for C band (4.78-4.88 GHz), with bandwidth of 100 MHz is presented in [31]. The radiation pattern of this antenna is highly directional and is employed for a missile communication system.

In [32] a monopole antenna matched for frequency band of 112 MHz to 130 MHz is proposed. The antenna does not use any matching circuit. The height of antenna is 68 cm which is 0.25λ for lowest operating frequency. This antenna has less bandwidth and the height is comparable to that of a standard monopole antenna.

A monopole antenna coated with magneto-dielectric material is presented in [33] for High frequency (HF) applications. The electrical size of antenna is reduced by uniformly placing metallic posts around it. The antenna height is only reduced by 10% as compared to bare monopole for a resonant frequency of 27 MHz with a very narrow bandwidth. The literature review presented above covers only a small sample showing typical designs for low frequency aircraft antennas.

2.6.3 Techniques to make low-profile antenna

This section explains the techniques reported in the literature to reduce the height of an antenna, without sacrificing the main electrical properties such as matched bandwidth, efficiency and radiation pattern.

2.6.3.1 Top-loaded monopole antenna with shorting pin

Top-loaded monopole with shorting pins makes the antenna compact and reduces the height for low-profile characteristics. A short bare monopole has low impedance as compared to standard monopole. Adding a top disc element can make the antenna impedance capacitive. While adding shorting pins creates a short-circuited transmission line in parallel to the feed. The shorting pins counter the negative reactance of top disc element and make the antenna to resonate at a reduced height.

In 1976, Goubau [34] presented a top-loaded low-profile antenna of h=0.07λ (4.3 cm) and diameter 0.2λ (12.3 cm) for the frequency band of 450-900 MHz and VSWR <3 as shown in Figure 2-5. This antenna consists of four interconnected electrically conductive small elements. This structure is called as "diakopted", meaning it is sliced into smaller sub-structures and each structure is separated from its immediate neighbor and each sub-structure can be assigned individual port where voltage and current can be defined individually.

A low-profile cylindrical monopole antenna, top-loaded with a shorted circular patch is shown in Figure 2-6 [35]. It is designed for existing mobile wireless communication systems operating at ~2 GHz. It has an impedance bandwidth greater than 14% with height of 0.07λ and diameter of 0.27λ.

Top loaded monopole antenna can be used to shape the antenna beam. A conical beam antenna resonating at 10 GHz with height 0.1λ, diameter 1.2λ and FBW of 7 % is presented in [36] and shown in Figure 2-7.
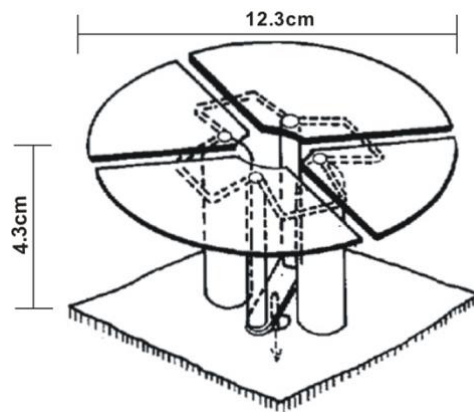
Figure 2-5: Broadband multi-element antenna © 1981 IEEE [34].
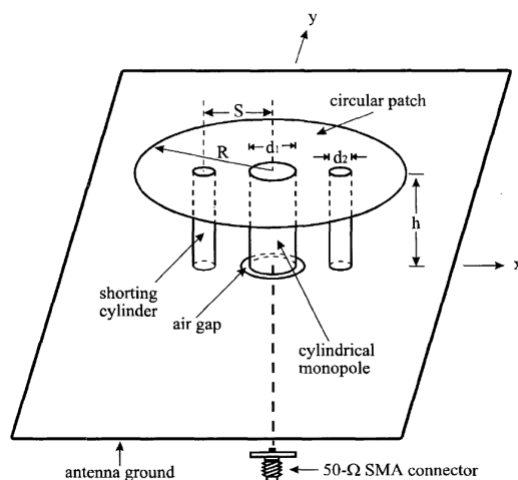
Figure 2-6: Cylindrical monopole antenna with shorted circular patch © 2001 IEEE [35].
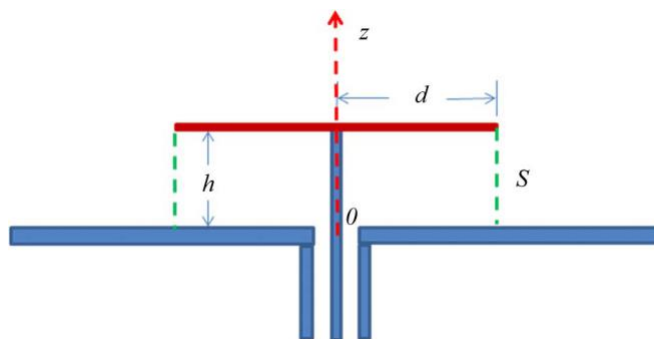
Figure 2-7: Top-loaded conical beam monopole antenna © 2011 IEEE [36].

A simulation model of top-loaded fat monopole antenna with four shorting posts is presented in [37]. The antenna has a simulated bandwidth of 18.5% and VSWR <1.5 and shown in Figure 2-8. The diameter of antenna is 0.24λ, height is 0.1λ and the diameter of ground plane is 0.72λ.

In [38] a simulation model of top-cap monopole antenna with wide bandwidth of about 95% and VSWR<3 is achieved by using genetic algorithm optimization for the frequency range from 250 MHz to 700 MHz. The height of antenna is 0.12λ and the diameter of antenna is 0.16λ as shown in Figure 2-9.

A top-loaded monopole antenna with a triangular feed and oblique shorting post is presented in [39]. As shown in Figure 2-10, this antenna has a side wall which generates the second resonance and gives broadband characteristics of 33% FBW. The height of antenna is h = 0.1λ and diameter is 1.1λ.
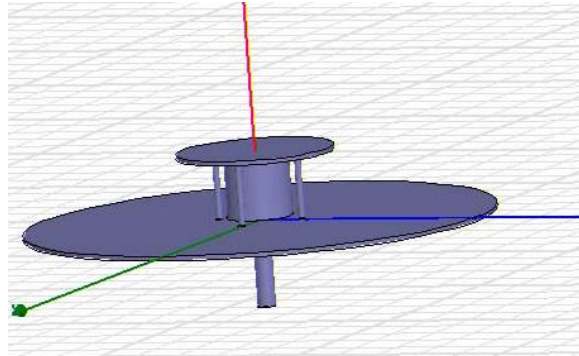
Figure 2-8: Top loaded monopole antenna with shorting posts © 2000 IEEE [37].
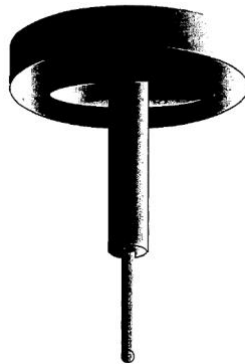
Figure 2-9: Top-cap monopole antenna © 2004 IEEE [38].

Figure 2-10: Fabricated prototype of top-loaded monopole antenna © 2009 IEEE [39].
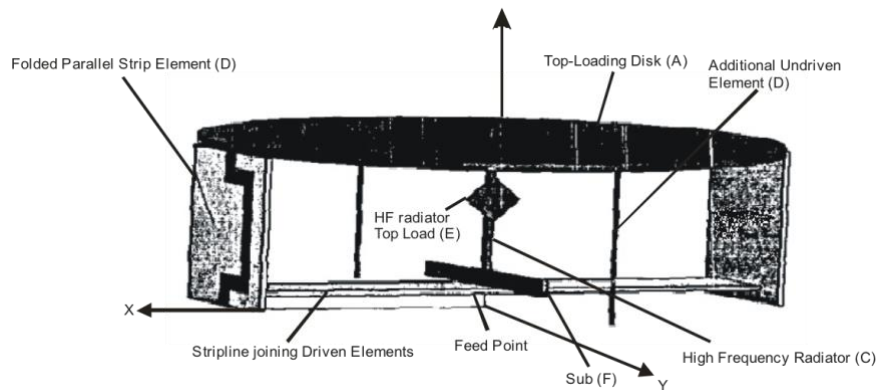
Figure 2-11: Modified Goubau antenna model © 2004 IEEE [40].

In [40] a modified form of the Goubau antenna [34] is presented and shown in Figure 2-11. Unlike Goubau's antenna, it has an undivided top disc. The antenna is feed through folded parallel strip vertical elements with dielectric loading and has a HF radiator under the top disc. It has bandwidth of 380 - 1530 MHz for VSWR<2 with a height of 0.08λ and diameter equal to 0.23λ, where λ is 789 mm at 380 MHz.

Based on the criteria discussed in section 2.6.1, few of the antennas presented above are categorized as small antenna as per Wheeler criteria. These antennas find applications in mobile communications systems, such as satellite navigation systems, cellular systems and wireless LAN. In Table 2-4 summary of top-loaded, low-profile antenna in this literature review is presented. These designs have one or more limitations such as, complicated antenna design, not a significant antenna height reduction, high VSWR, unsymmetrical radiation pattern or ripples in the radiation pattern. Some of these designs include only the simulation models and does not discuss about the impact of size of the ground plane. Based on this discussion it can be inferred that an optimally designed top-loaded monopole antenna can be a good candidate to be used in avionics communication system.

2.6.3.2   Surface wave antenna

In a Surface Wave Antenna (SWA), surface waves propagate along the antenna surface and radiate into free space at discontinuities in the antenna structure and ground plane. This occurs when the structure supports leaky modes, or also when a surface wave gap is produced.

Table 2-4: Summary of different low-profile, top-loaded antennas in literature.

Reference	Frequency/ bandwidth	Height of antenna in wavelength (lowest frequency)	Diameter of antenna	Radiation pattern	S11 (dB)	Geometry features
[34]	450-900 MHz	0.07λ	0.2λ	omni	-6	Top-plate multi-element
[35]	2 GHz	0.07λ	0.27λ	omni	-10	Top-loaded with two shorted pins
[36]	10 GHz	0.1λ	1.2λ	omni	-10	Top-loaded
[37]	0.94-1.2 GHz	0.1λ	0.72λ	omni	-14	Top-loaded with four shorting posts
[38]	250-700 MHz	0.12λ	0.16λ	omni	-6	Top-cap
[39]	1.5-2.1 GHz	0.1λ	1.1λ	omni	-10	Top-loaded with four oblique shorting posts and triangular feed
[40]	380-1530 MHz	0.08λ	0.23λ	omni	-10	Undivided top-plate with two shorting posts and one HF radiator

A cylindrical SWA offers a low-profile structure and can produce a monopole like radiation pattern but most of SWA are linear and produce a pencil beam or fan beam.

In [41], a SWA is presented with 5.9% FBW for S11<-10 dB and height of 0.05λ. A center-feed patch used as transducer with S11<-6 dB and generate surface waves on a thin artificial ground, which improves the matching of patch antenna. The fundamental mode TM_{11} in circular patch antenna and higher modes like TM_{12} radiate in the boresight, while modes like TM_{21} and TM_{41} can radiate conical beams. The TM_{01} mode produces an equivalent monopole like radiation pattern.

In [42] a horizontal dipole is placed over two dimensional periodic Patch-Loaded Grounded Slab (PLGS). Such a structure has low-profile features. This antenna has a radiation pattern similar to that of a vertical monopole. Furthermore, in [43] it is explained that this radiation does not come from the dipole itself. Instead, it is coming from a classic T-shape antenna due to unbalanced feed of dipole antenna. Figure 2-12 shows a vertical wire, which is used to model the unbalanced feed of dipole. The radiation pattern and E –field polarization was similar to a vertical monopole. It was investigated that common-mode currents in the vertical wire are larger than the horizontal dipole current. Hence the radiation from unbalanced dipole is dominated by the feed and it operated like a classic T antenna. A wide band ceramic slab SWA producing unidirectional surface waves is presented in [44]. The antenna has a wide operational bandwidth, from 6.1 to 18 GHz, with a thickness of 0.12λ at the center frequency.
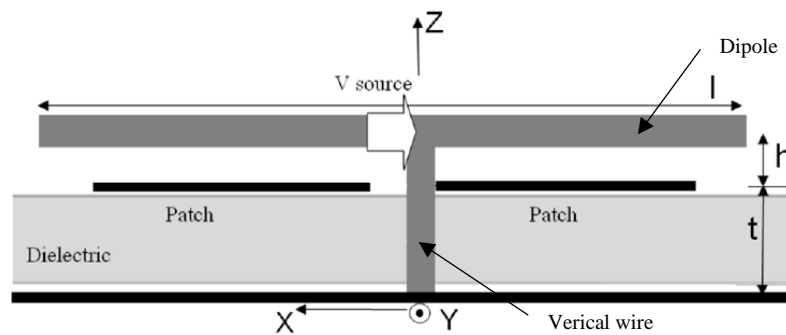
Figure 2-12: Unbalanced short dipole placed on 10x10 PLGS © 2007 IEEE [42].

2.6.3.3 Antenna with magneto-dielectric material loading

The use of magneto-dielectric material (MDM) is reported in literature in the past. With the advancement in the material technology and more flexibility over the control of magnetic and

electrical properties, customized materials have found their way in many applications related to antenna design.

MDM placed on Perfect Electric Conductor (PEC) ground can help to make ultra-wideband (UWB) antenna with good radiation characteristics. In [45], it is shown that having the same relative permittivity and permeability, or having higher relative permeability and lower relative permittivity produces an in-phase reflection of plane wave on an infinite material interface similar to that of a Perfect Magnetic Conductor (PMC). Using an Artificial Magnetic Conductor (AMC) instead of a metallic ground plane helps horizontally polarized antennas to keep good radiation characteristics, even if placed very close to the AMC ground plane. A L-band stacked patch antenna using MDM is presented in [46]. Thin ferromagnetic films are used on top of polymer to implement the MDM. By using GA to optimize the stacked patch antenna significant miniaturization of antenna size up to 60% and large operating bandwidth of 20% has been achieved. In [47-49] MDM has been used as a replacement of a dielectric substrate for handset devices for Long term evolution (LTE)/ Wireless wide area network (WWAN)/ Global positioning system (GPS) applications. For Digital Audio Broadcasting (DAB) and Terrestrial Digital Multimedia Broadcasting (T-DMB) meandered line antenna is designed using ferrite $\mu_r = 5 \sim 6$ composite material and ferrite film [50]. This antenna is 30% more compact as compared to a dielectric-only material loading based antenna.

In [51], a comprehensive analysis is conducted to evaluate the behavior of coated monopole antenna with different magnetic, dielectric and MDM. In Figure 2-13, a monopole with material cladding is shown. The cladding creates a quarter-wavelength resonant cavity effect and the annular slots near the feed on the ground plane transforms the input impedance. The best overall antenna performance in terms of bandwidth and efficiency is obtained for equal values of relative permittivity and permeability, rather than employing purely dielectric material or alternatively purely magnetic material.

In [52], a 3D inverted F antenna is investigated for DVB-H applications. The use of lossy MDM enhances the impedance bandwidth, so for the purpose of realistic comparison lossless MDM and
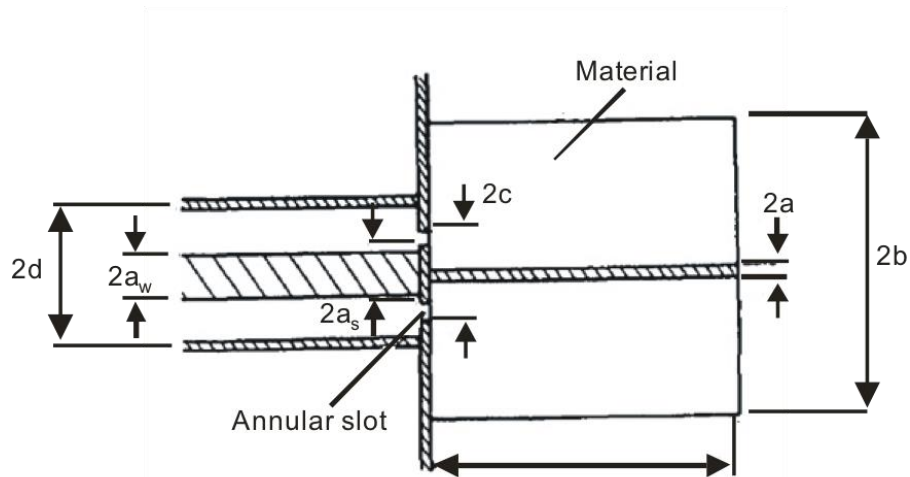
Figure 2-13: Sectional sketch of antenna showing coaxial feed (left), annular excitation slot in ground plane (middle and material-coated monopole (right) © 2005 IEEE [51].

lossless dielectric materials are studied. Again, it is found that MDM exhibits the property of enhancing the bandwidth as compared to dielectric only materials.

2.6.3.4 Antenna with grooved ground plane

The presence of a grooved ground plane in different shapes has been studied for the control of antenna radiation characteristics. The presence of groove on the ground plane changes the edge diffraction as compared to a conventional flat ground plane. A monopole with a grooved ground plane can favor radiation at a lower elevation angle over the simple ground plane [53].

A low-profile shorted circular patch ring antenna of 1.3% FBW is presented in [54]. This antenna consists of a center-feed patch antenna coupled to annular rings, which are shorted with pins in order to produce an omnidirectional radiation pattern with more than 3 dB of gain. The antenna radiation pattern has ripples of around 2 dB or more. A grooved ground plane using deep grooved metal structure acting as choke rings is presented in [55]. It is used to enhance the gain in the broadside of a patch antenna on electrically large flat ground plane. The gain is improved by 10 dB. A microstrip annular ring antenna is designed for wireless LAN communication at 450 MHz in [56]. The antenna is very low-profile with the use of shorting pins and has its maximum gain at

horizon. However, the bandwidth is very narrow and is not covering the whole WLAN band. In [57] a V-shape groove is presented to reduce the ripples in the radiation pattern of a monopole with small ground plane. Diffractions and reflections at the edge of the finite ground affect the radiation pattern of antenna and causes ripples. In [58], a radiation configuration is designed for a recessed monopole antenna surrounded with a negative index material. This antenna is placed on the ground plane and mapped by a negative index material block to a virtual location above the ground to get the radiation pattern of monopole. A non-protruding and conformal antenna is presented in [59] for DME band. On a finite ground plane, the antenna radiation pattern at horizon is less than that of a standard monopole. Different techniques have been studied in literature review to provide broadband impedance bandwidth with omnidirectional radiation pattern. However, some of those designs give asymmetrical radiation patterns, some have maximum radiation tilted higher from the horizon in elevation and few have gain fluctuation over the band, which is undesired feature for practical systems such as DME.

2.7 Conclusion

An overview about VHF, a DME and TCAS antenna used in aircraft communication and navigation systems is presented in the chapter. The literature reviewed here covers a wide range of examples of different techniques used to make antennas compact and low-profile. These existing solutions and techniques to reduce the antenna size can be applied to the aircraft antennas, to obtain a low-profile antenna and radiation characteristics similar to that of a monopole antenna. The following chapters, Chapter 3, Chapter 4, Chapter 5, and Chapter 6 explain all proposed designs, having background linked to the techniques citied in this chapter.

CHAPTER 3   DUAL-BAND ANTENNA

In this chapter we have presented a novel dual-band antenna design for the aircraft communication system. The antenna is designed to function at two frequency bands used in aircraft systems, which are VHF communications and TCAS. The work presented in this chapter includes requirement of VHF and TCAS system, individual antenna design, a dual-band antenna design, its fabrication and discussion of results.

3.1 Functionality of the TCAS antenna

In a complete TCAS system, pair of directional and omnidirectional antennas is used to determine the presence of a nearby aircraft. However, the scope of this work is to explore a simplified version of TCAS system using only omnidirectional antenna. An omnidirectional antenna is used to yield the range and altitude of an intruding/approaching aircraft [14]. For redundancy more than one antenna are used. One antenna is installed at the upper fuselage and one is installed at the lower fuselage location. The front of the aircraft is where it is more likely that a collision can happen, and it is where TCAS coverage is most essentially required. The use of omnidirectional antenna covers the required zone for TCAS system. Figure 3-1 elucidates the placement of TCAS antenna on the aircraft whereas Table 3-1 shows the specifications for TCAS band.
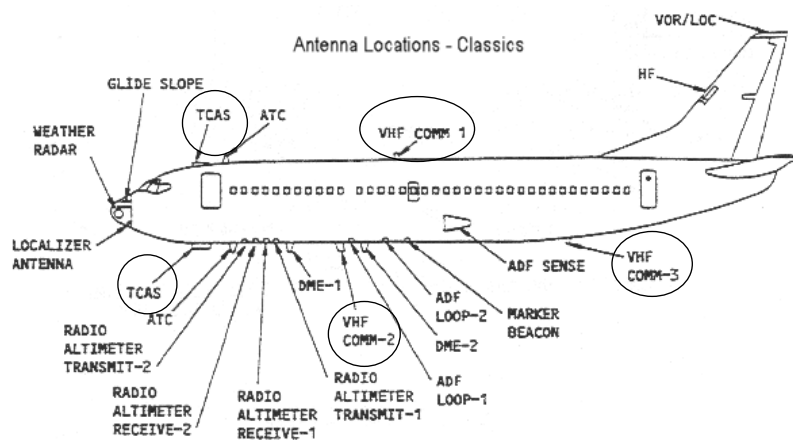
Figure 3-1: Placement of TCAS and VHF antenna on the aircraft [60].

Table 3-1: TCAS antenna design specifications.

Frequency	1.03 – 1.09 GHz
Bandwidth	5.6%
VSWR / S11	<2 / -10 dB
Radiation Pattern	Omnidirectional
Polarization	Vertical

3.2 Commercially available TCAS antennas

Commercially available TCAS omnidirectional antennas are a streamlined blade antenna made of aluminum alloy cast material. Blade antennas are quarter-wavelength monopole antennas, encapsulated in a radome for improved mechanical strength and hence they are rugged. For TCAS band the height of the blade ranges from 70 mm to 34 mm as shown in Figure 3-2.

Figure 3-2: TCAS antenna (a) Cobham 2442-88 [61], (b) Sensor Systems S65-5366735 [21].

3.3 Design of a low-profile TCAS antenna

TCAS requires a vertically polarized omnidirectional antenna. Conventional low-profile printed patch antennas are not suitable for TCAS system whereas reduced height monopole antenna can be a suitable fit. The most important challenge with these reduced height or low-profile monopole antennas is impedance matching. The impedance of electrically small antenna ($<< \lambda/4$) has more reactance and very small radiation resistance. To improve the antenna impedance, a short monopole can be loaded with a top disc. A very popular top-loaded monopole antenna presented by Goubau's [34] is a good example as discussed in chapter 2, section.2.6.3.1. This antenna consists of four

interconnected electrically conductive small elements. Where each sub-structure is assigned an individual port and the voltage and current can be controlled individually on these ports. This proposed multi-element structure has a bandwidth of 450-900 MHz and height is reduced to 0.07λ and the diameter of antenna is 0.2λ.

3.3.1 Top-loaded monopole antenna

The design of the proposed TCAS antenna includes the study of loading a bare quarter-wavelength monopole with a top disc and adding shorting pins and other features to antenna to make it low-profile. The first half of this section discusses the general design of a top disc monopole and the second half explains the proposed design for TCAS antenna.

A bare wire monopole of diameter 1.3 mm and height of quarter-wavelength at 1 GHz is fed by a 50-ohm coaxial line placed on an infinite ground plane. The monopole is simulated using High Frequency Structural Simulation tool (HFSS), as shown in Figure 3-3 (a). The diameter used for wire monopole is same as that of the diameter of inner conductor of SMA connector. The simulation result indicates the resonant frequency of monopole at height h=70 mm is 1 GHz. If the height of the monopole is reduced by 60 mm i.e. from $h = 70\ mm$ to $h_1 = 10\ mm$, as shown in Figure 3-3 (b), the resistance of antenna decreases and the reactance of the antenna also increases but on the negative side, i.e., becomes more capacitive with increase in series resonance frequency. A circular disc made of thin substrate having copper on one side is placed on the top of monopole and is used as a top disc. The substrate used is Rogers 5880 with ε_r=2.2 and a thickness of 31 mils or 0.787 mm. The use of substrate can help in making any design changes in the later steps of antenna design. The disc with diameter b is placed on the monopole of height h_1 is shown in Figure 3-3(c). The diameter b is selected to compensate the negative reactance of reduced height monopole and to bring the imaginary part of impedance close to zero at ~1 GHz. Figure 3-4 shows the impedance plot, for the three cases, 1) the bare monopole of height h, 2) bare monopole of height h_1, and 3) the top-loaded monopole of height h_1. The real impedance or resistance of top disc antenna is very small, and it has poor impedance match as can be seen in Figure 3-4. Here the reference impedance is 50 Ω, i.e. the characteristic impedance of the coaxial line.
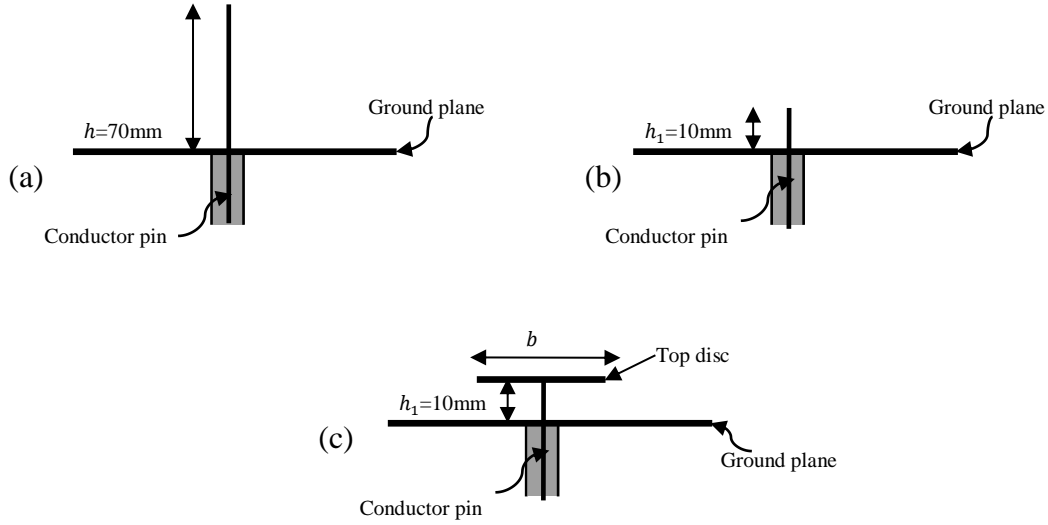
Figure 3-3: (a) Bare monopole with height h on ground plane, (b) Bare monopole with height h_1 on ground plane, (c) Monopole with height h_1 and top disc.
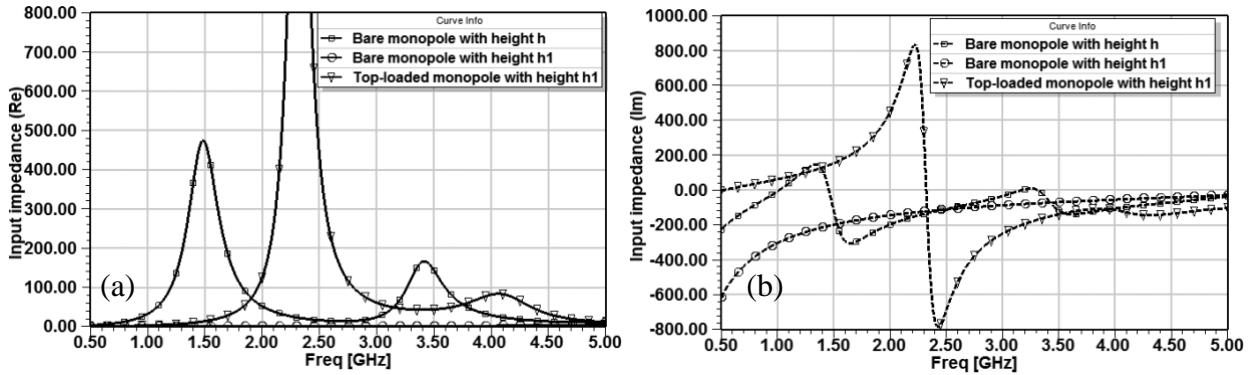
Figure 3-4: Simulated impedance comparison of bare monopole and top-loaded monopole (a) Real part of impedance, (b) Imaginary part of impedance.

3.3.2 Top-loaded monopole antenna with shorting pins

The use of top disc has compensated the reactance of reduced height monopole but still the antenna does not resonate at the required frequency of 1 GHz as shown in Figure 3-5. Next a shorted pin of
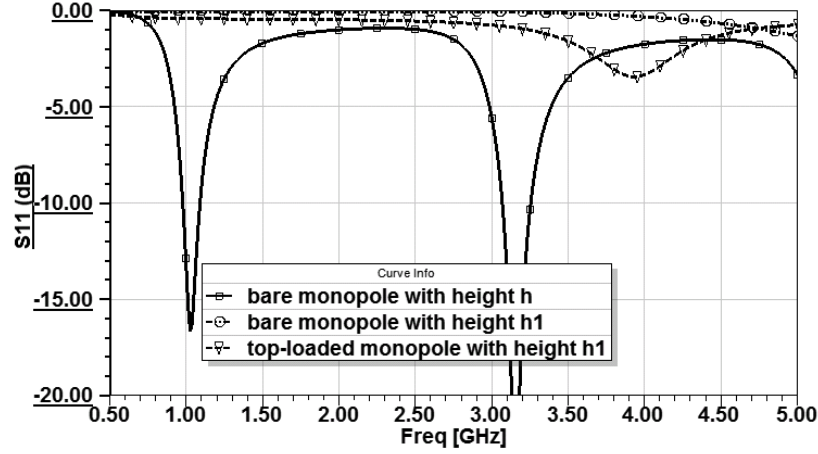
Figure 3-5: Simulated S11 of bare and top-loaded monopole antenna.
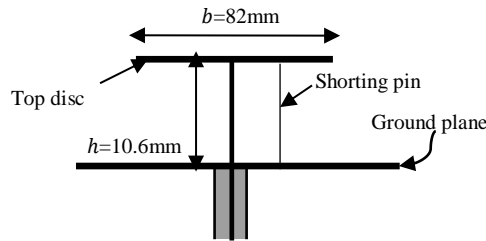
Figure 3-6: Top-loaded monopole with one shorting pin.

diameter 1.5 mm is introduced between the top disc and the ground plane, as shown in Figure 3-6. Shorting pin acts like a parallel inductance and the resonance frequency drops down significantly. Here the diameter of shorting pin is selected based on standard diameter of pin available. The distance of shorting pin from the center pin is adjusted using parametric study in simulations that will be discussed in next section 3.3.3. To further increase the resonant frequency, more pins are added to the design. Figure 3-7 shows the impedance plot for three cases for which the height of the top disc is set to 10 mm, and the diameter of the top disc is fixed at 82 mm. The "no pin" case is the simple top-loaded monopole with height h_1 as shown in Figure 3-3 (c). Second case uses the same antenna but augmented with a shorting pin. Adding a shorting pin creates a short-circuited transmission line in parallel with the feed which introduces a new strong parallel resonance between 0.5 and 0.75 GHz as shown in Figure 3-7. This also moves the series resonance to lower frequencies with no noticeable effect on the upper parallel resonance near 2 GHz. These results

suggest that the addition of shorting pin can lead to a shift to the resonance, thus providing a mean to control the reactance curve above the lower series resonance frequency. To illustrate this, to the above design four shorting pins were added and the results are given in Figure 3-7. The use of four pins in parallel has a reduced antenna's equivalent inductance, and consequently increases the new resonance frequency near 1.25 GHz. At this frequency, the antenna radiates more efficiently, and the rate of reactance variation is significantly reduced. However, these results indicate the input impedance is not 50 Ω at the TCAS operating frequencies. One other aspect of using more pins is added symmetry in the current distribution, which is a desirable feature in omnidirectional antennas. The above results indicate that the strategy to achieve good impedance matching at the TCAS frequencies consists of modifying the equivalent inductance of the shorting pins in such a way that the negative reactance range of the pin's parallel resonance cancels the reactance of the top-loaded monopole at the frequency of interest.

3.3.3 Top-loaded monopole antenna with shorting pins and CPW

As presented above for the four-pin case given in Figure 3-7, higher inductance is required to lower the resonance frequency from 1.2 to 1 GHz. Reducing the number of pins could be one solution to address this issue, however it would diminish the azimuthal symmetry of the radiation pattern. Alternatively, using thinner shorting pins could be one solution however the fabrication of thin pins with very accurate diameter could become a challenge. The other solution includes the use of longer pins, but that would increase the height of the antenna and thus defeat the goal of having a low-profile design.
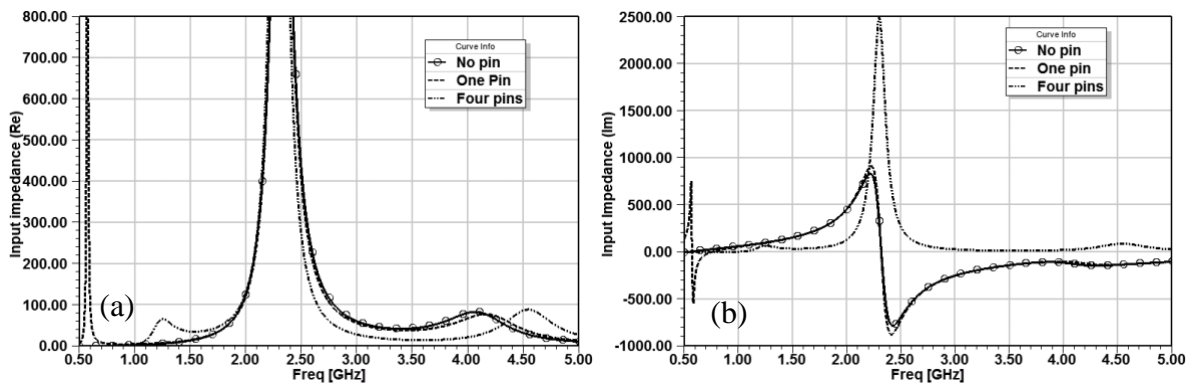
Figure 3-7: Impedance comparison of no pin, one pin and four pins (a) Real, (b) Imaginary.

As an alternate, the proposed solution here consists of increasing the pins inductance by adding inductance in the plane parallel to the top disc. This can be achieved by inserting short printed line segments at the connection point between the vertical pins and the top disc. In practice, a shorted Co-Planar Waveguide (CPW) line is etched on the top plate of a monopole, which acts as a series inductance (L_s) to each pin's inductance (L_p). As illustrated in Figure 3-8 where a top disc, the pin connection points and the layout of the CPW lines etched on the disc are shown. The equivalent circuit model of the antenna is given in Figure 3-9. In the equivalent circuit R_s, L_s, C_s are the resistance, inductance and capacitance of top-loaded monopole and L_{p1}, L_{p2}, $L_{p3,}$ and L_{p4} are inductance of shorting pins and L_{s1}, L_{s2}, L_{s3} and L_{s4} are series inductance of CPW line. Figure 3-10 and Figure 3-11 show the effect of adding the CPW segments on the antenna's S11 and impedance (real and imaginary) respectively. The result shows that the total inductance is increased, and the resonant frequency is shifted from 1.2 GHz to 1.04 GHz, while the physical size of the antenna remains unchanged. This S11 response is sensitive to antenna geometry parameters such as discussed later in the parametric study.
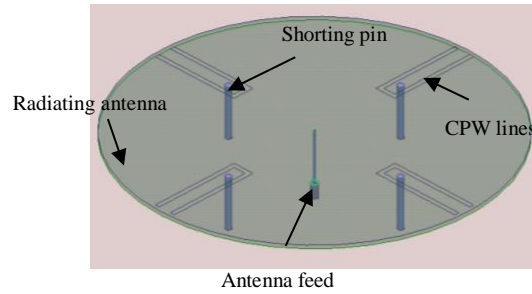
Figure 3-8: Simulated TCAS antenna model with shorting pins and CPW.
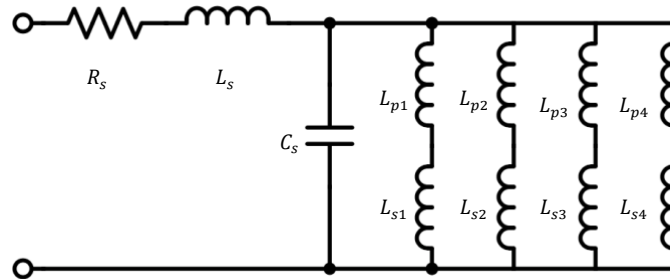
Figure 3-9: Equivalent circuit of TCAS antenna.

The proposed design is a reduced height monopole and the use of shorting pins and CPW has made it possible to get the matched impedance bandwidth of TCAS band. The height of the antenna is 0.04 λ and the width is 0.28 λ for the lowest resonant frequency of 1.03 GHz. The antenna physical parameters like the length of CPW line ($line\_length$), distance of CPW line from the center (pos), thickness of CPW ($line\_width$) has been optimized in the simulations by doing parametric study of these variables. The distance between shorting pin and edge of CPW line (d_1) is kept at 4 mm and the gap between the CPW line (g) is kept at 5 mm for ease in fabrication.
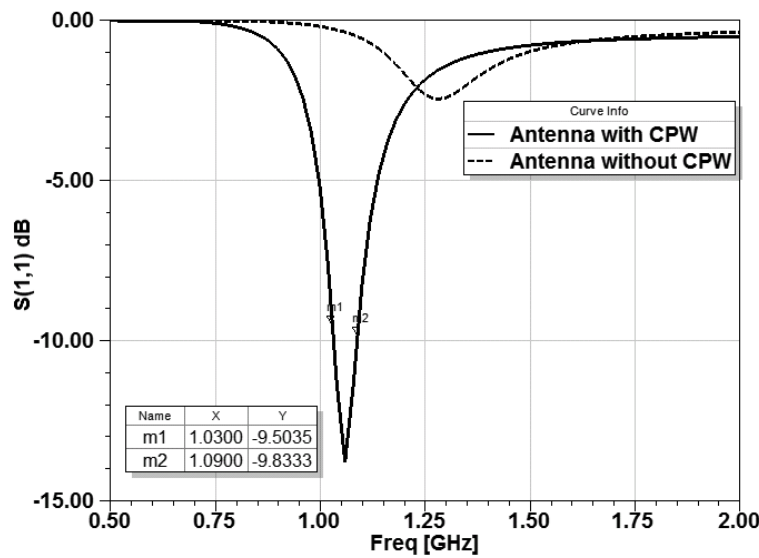
Figure 3-10: S11 comparison of antenna after including the CPW.
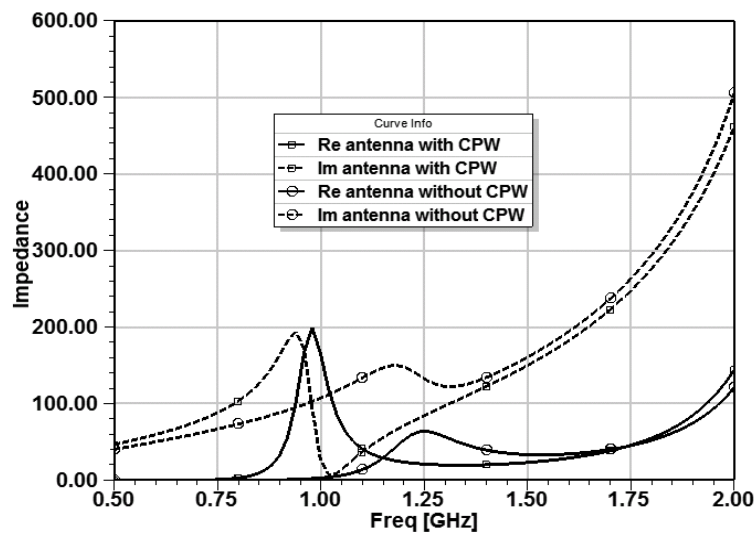
Figure 3-11: Impedance of antenna with and without CPW.

Figure 3-12 shows the top side of TCAS antenna with the above-mentioned parameters. The parametric study results on $line\_length$, pos and $line\_width$ are shown in Figure 3-13, Figure 3-14 and Figure 3-15. These results indicate that by decreasing the CPW line length, the resonant frequency is decreased. By decreasing the distance of CPW and shorting pin from the center pin of antenna, i.e., decreasing the value of pos, the resonant frequency decrease. Also, with the increase in the $line\_width$ of CPW line, the resonant frequency is decreased. Based on the above design parameters the optimized version of TCAS antenna model with both top and side view is given in Figure 3-16. The new height of antenna is 11.46 mm, which also includes the thickness of the top substrate and the thickness of microstrip line substrate (Rogers 5880) that will be used to feed the antenna. The need for a microstrip line will be discussed in the next subsection 3.3.4.
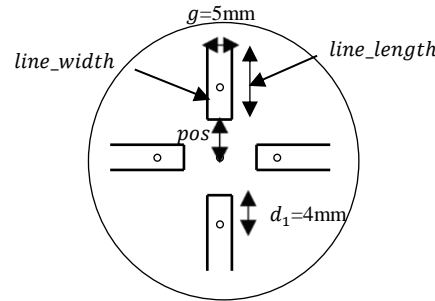
Figure 3-12: TCAS antenna parameters.
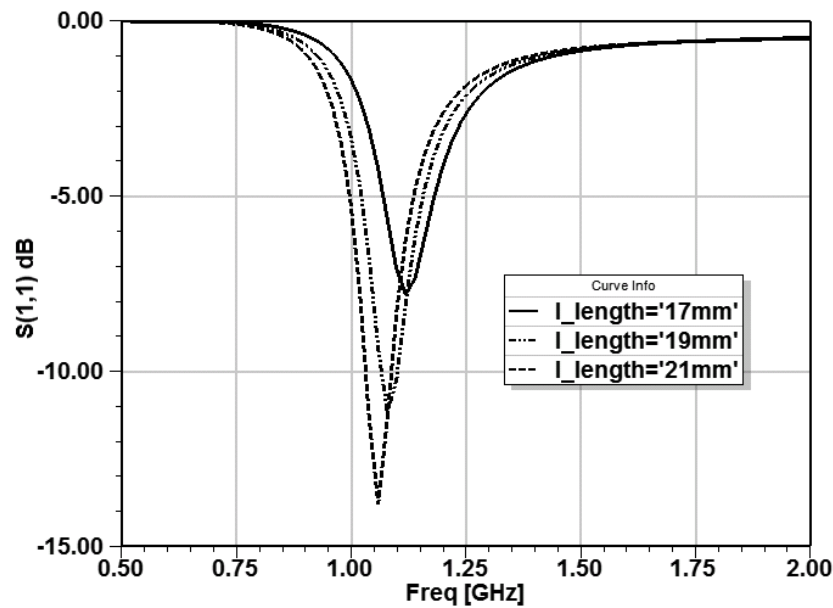
Figure 3-13: Parametric study on CPW line length.
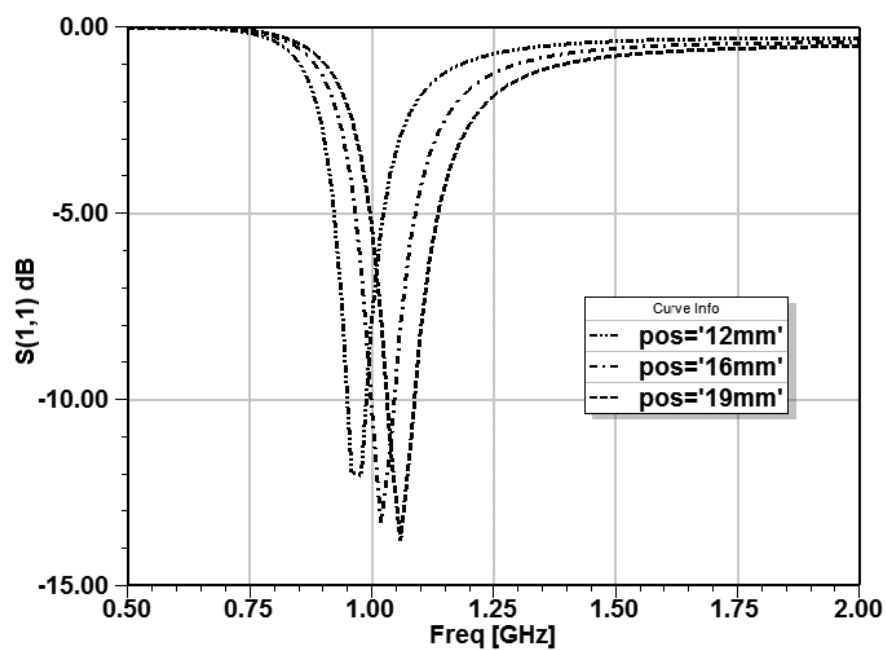
Figure 3-14: Parametric study on position of CPW line from the center
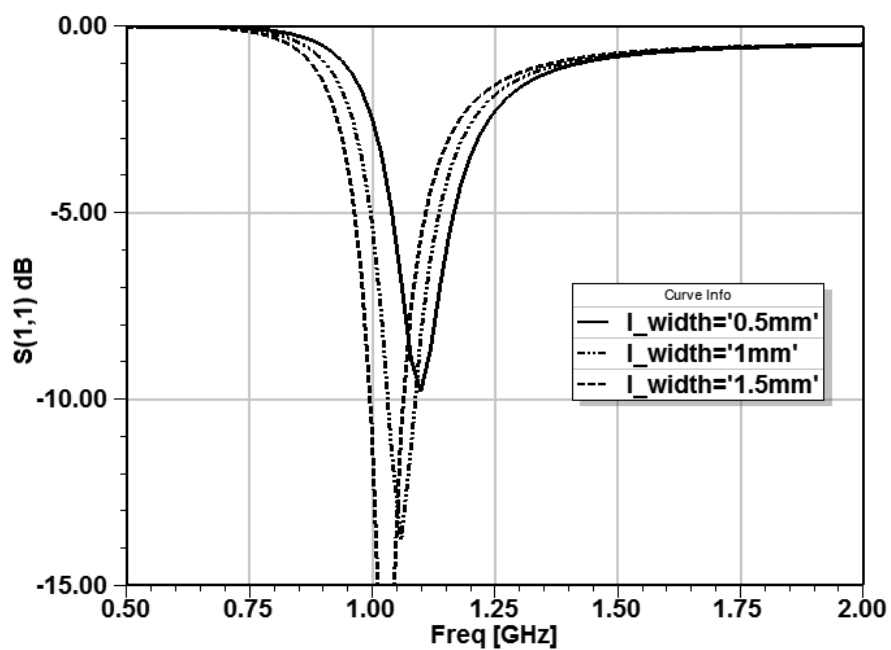
Figure 3-15: Parametric study on CPW line width.
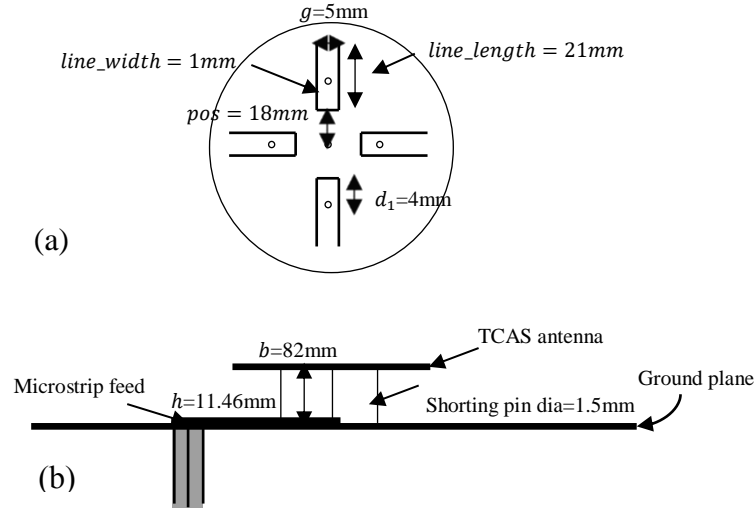
Figure 3-16: TCAS antenna model (a) Top view, (b) Side view.

3.3.4 Microstrip line feed to the TCAS antenna

The use of microstrip feed will be discussed here. As the TCAS antenna will be placed on the structure of the VHF antenna, and to keep the geometrical symmetry of antenna, microstrip feed is used. The antenna is feed at the center however through a microstrip line whose one end is connected to the coaxial cable. This cable will be hidden in a structural part of the VHF antenna, as we will discuss later in section 3.10. The isometric view of simulation model of TCAS antenna is shown in Figure 3-17 (b).

3.4 Fabrication and testing of the TCAS antenna

The fabricated prototype of TCAS antenna is shown in Figure 3-18. The TCAS antenna was placed on the circular aluminium ground plane of diameter 602.5 mm. This ground plane is actually the top-plate of VHF antenna to be discussed in detail in section 3.10 for the dual-band operation. Return loss and radiation characteristics of this antenna is tested. The simulated and measured S11 of TCAS antenna is given in Figure 3-19. The measured results have S11<-10 dB at 1.03 GHz but S11<-9 dB at 1.09 GHz. This small shift in S11 at 1.09 GHz can be tuned by changing the optimized parameters of antenna such as length of CPW.
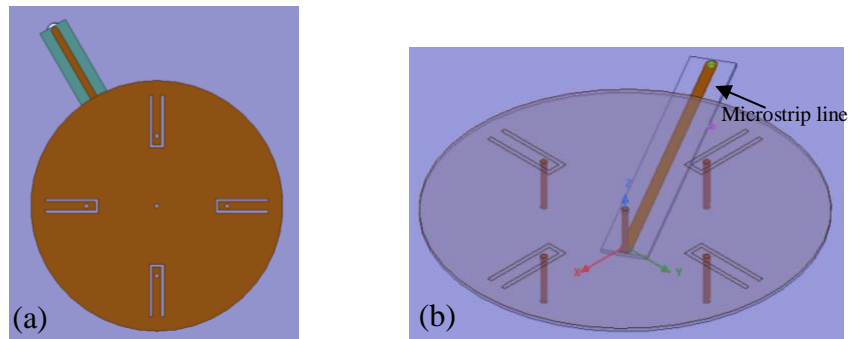
Figure 3-17: Simulated model of TCAS antenna with microstrip line (a) Top view, (b) Isometric view.
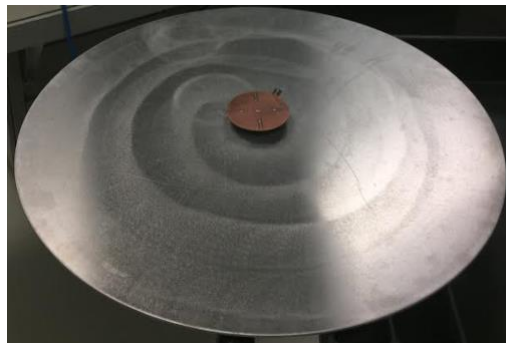
Figure 3-18: Fabricated prototype of TCAS antenna.
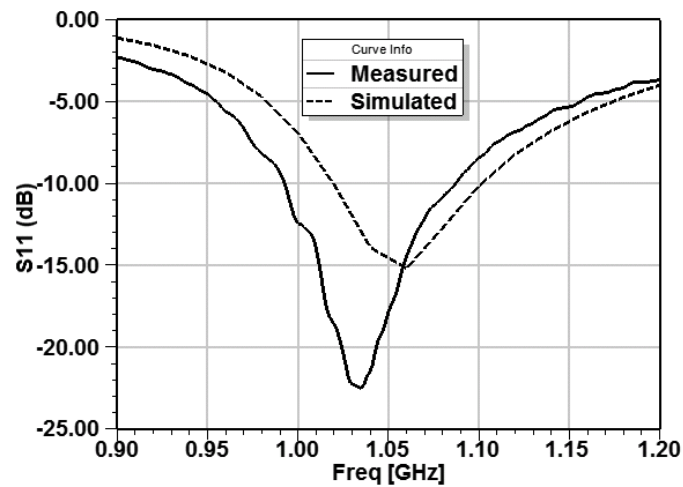
Figure 3-19: Simulated and measured S11 of TCAS antenna.

The realized gain value for both simulated and measured cases are compared. Both azimuthal and elevation planes show a very good agreement and are given in Figure 3-20(a) and (b) respectively. A small shift of the null near $\theta = 0°$ is expected because the microstrip feed is at an angle and distance from the center of antenna. Also, it could be due to error in fabrication, i.e. the fabricated structure may not be perfectly symmetric. For the proposed antenna S11 result covers the TCAS band of operation, the radiation pattern is omnidirectional and with almost no ripples in azimuthal plane. Further the proposed antenna is low-profile, with monopole like radiation pattern thus a good candidate for TCAS band operation.
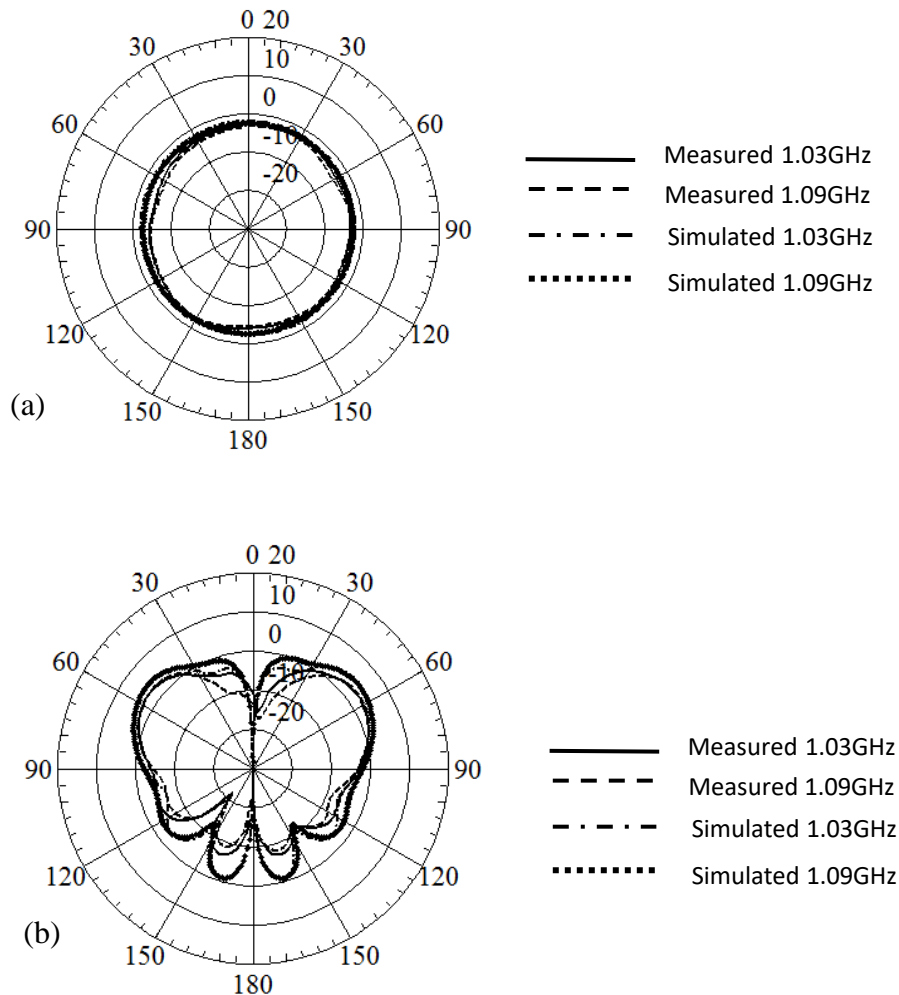
Figure 3-20: Realized gain of TCAS antenna both simulated and measured (a) Azimuthal (H) plane, (b) Elevation (E) plane.

3.5 Functionality of aircraft VHF communication antennas

The VHF communication system is employed in all types of aircrafts for air traffic control. The pilot uses this system to receive information and directions from air traffic control center. It is usually installed along the longitudinal/vertical plane of the symmetry of the fuselage as shown in

Figure 3-1. As the location of the receiving station is not always the same or known, the signal must be sent in all directions therefore it is required that the antenna should be omnidirectional with vertical polarization. The specifications of VHF antenna are shown in Table 3-2.

Table 3-2: VHF antenna design specifications.

Frequency	118-137 MHz
Bandwidth	14.9%
VSWR / S11	<3 / -6 dB
Radiation Pattern	Omnidirectional
Polarization	Vertical

3.6 State-of-the-art technology-VHF

The monopole and its variants are the most commonly used vertically polarized VHF aircraft antennas. Typical length for VHF blade is from $\frac{\lambda}{4}$ to $\frac{\lambda}{10}$. Commercial companies like Cobham, Sensors Systems and Cooper antenna are designing antennas, featuring lightweight and covers large bandwidth. Digitally-tuned blade antenna covering large bandwidth for UHF/VHF bands (30 MHz to 500 MHz) has been reported in [62]. Advanced microprocessor technology is used to accomplish fast, automatic frequency tuning. The frequency setting information can be transmitted to antenna from the radio via a multi-pin connector. Figure 3-21 shows an off-the-shelf VHF extended blade antenna designed to cover frequency range of 118 to 156 MHz [63] . The height of this blade antenna is 11.42 inches (290 mm) or 0.11 λ where λ is wavelength at 118 MHz.

Figure 3-21: VHF blade antenna Cobham 2448-88-00.

3.7 Previous design of scaled VHF antenna

One-tenth scaled version of a low-profile VHF antenna [64] covering the band 1.17 to 1.37 GHz was previously presented by our research group. This antenna uses the concept of a top-loaded monopole with several shorting pins, an inductive loading stub and is feed by semi-rigid coaxial cable. The outer conductor of the coaxial cable is shorted to the middle plate as shown in Figure 3-22. This middle disk of diameter W_m=52 mm and thickness 0.5 mm is acting as a radial stub and creates the inductive loading. The circuit model of this antenna is shown in Figure 3-23. Where, R_s, L_s and C_s are resistance, inductance and capacitance of top-loaded antenna respectively and R_i, L_i, C_i are due to the shorted inductive loading and C_c is due to the capacitive coupling between top plate and middle plate.
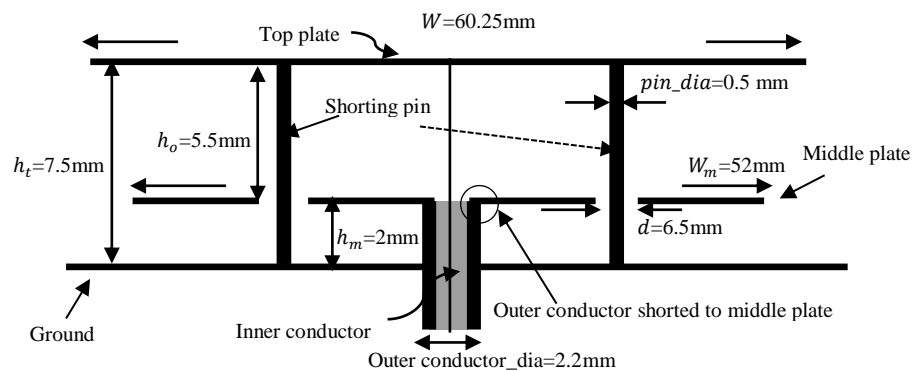
Figure 3-22: Model of one-tenth scaled VHF antenna.
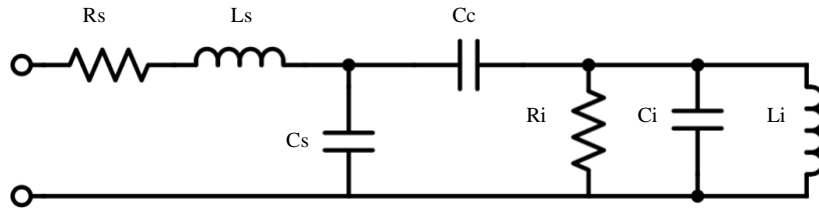
Figure 3-23: Equivalent circuit of VHF antenna model.

Both the measured and simulated results are shown in Figure 3-24. From there we can see that the first resonance is around 1.16 GHz which is due to the top-loaded monopole and the second resonance is around 1.39 GHz, due to inductive stub [64].

3.7.1 Limitation to the scaled VHF antenna

The antenna presented in [64] offers limitations to both operation and fabrication, e.g. when comparing the simulated and measured results. In the measured return loss the second resonance is shifted to lower frequency, as shown in Figure 3-24 [64]. It was observed that the height h_m as shown in Figure 3-22 is a sensitive parameter and with a very small change in its value from 2 mm to 2.1 mm or 2.2 mm can cause the second resonance to shift. In addition, the intent of this design is to work for VHF frequency band therefore it is important that the full-scale VHF design should be physically rigid enough to prevent any errors in measurements. Scaling this antenna geometry to 10 times also implies scaling of the semi-rigid coaxial feed line, which is practically not possible.

As seen in Figure 3-22, the outer conductor of coaxial feed is shorted to the middle plate to make a short circuit stub. Since scaling semi-rigid coaxial line is practically difficult rather impossible, therefore there is a need to adapt and redesign the feed structure. So that it can still fulfill the design requirements along with the use of standard coaxial feed line and is practically possible to fabricate. In addition, scaling the thickness of the middle and top plates 10 times makes it 5 mm. The use of such thick non-standard metal sheets will add unnecessary weight to the antenna.
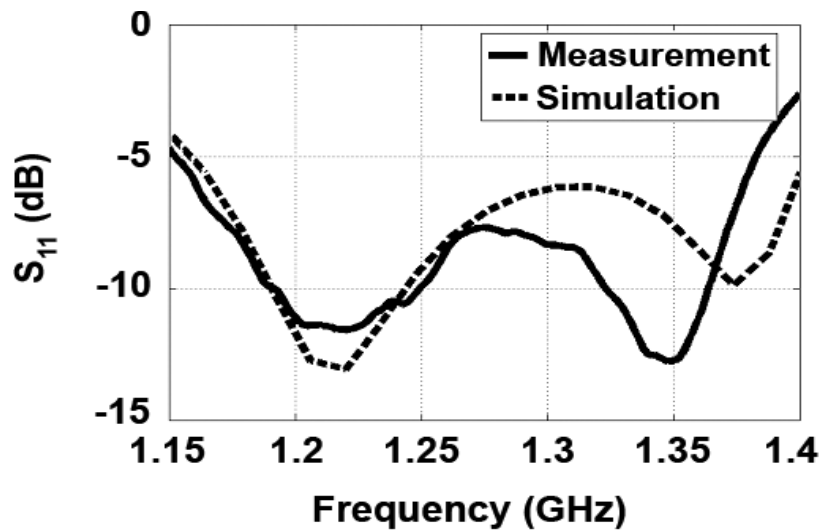
Figure 3-24: Simulated and measured S11 for one-tenth scaled VHF antenna © 2011 IEEE [64].

Finally, this antenna will be placed on an aircraft, where the aircraft body will act as the ground plane for the antenna. Hence there is a requirement to have an interface or a fastening plate that can be part of the antenna and can be used to connect the antenna to either aluminum aircraft body or composite or a barrel (which is a cylindrical surface to imitate the shape of aircraft) for future testing. All these design challenges discussed above are addressed step by step in the next section.

3.7.2 Design of the full-scaled VHF antenna

The full-scaled VHF antenna is shown in Figure 3-25 where all the geometry parameters are scaled to 10 times. Figure 3-26 shows the simulated S11 of full-scaled antenna where S11< -6 dB from 118 to 137 MHz. Following sub-section details about the improvements made step by step in the design to have full-scaled VHF antenna.

.
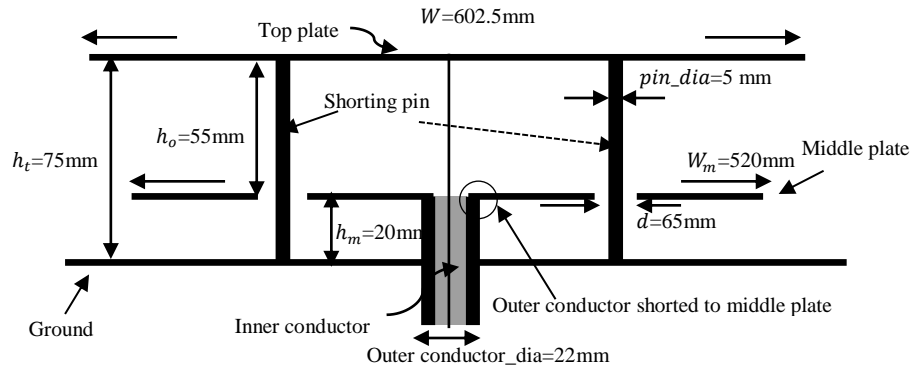
Figure 3-25: Full-scaled VHF antenna (all dimension x10 of Fig.3-22).
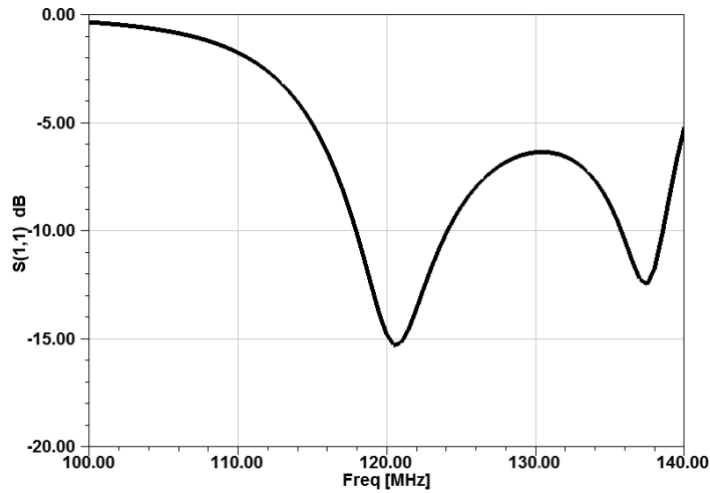
Figure 3-26: Simulated S11 of full-scaled VHF antenna.

3.7.2.1 Thickness of plates

The first improvement is to change the thickness of top and middle plates from 5 mm to 2 mm to address the weight concerns. Instead of using a 5 mm thick plate, an aluminum plate of 2 mm is used while keeping h_m, h_t and h_o same. This change of the thickness of plate changes the inductance and the S11 response shifted towards high frequency side as shown in Figure 3-27 and Figure 3-28. This change in the plate thickness has a very small effect on S11 but its advantageous in terms of being less weight.
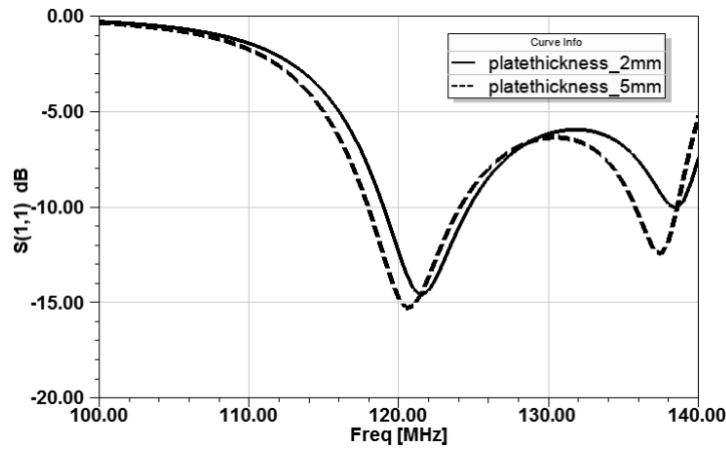
Figure 3-27: Simulated S11 with different plate thickness.
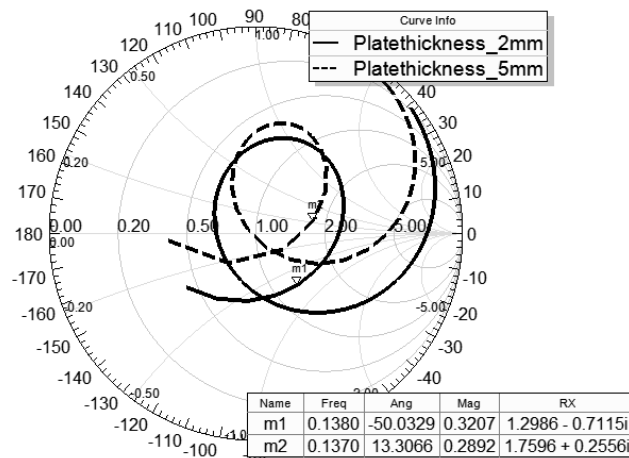
Figure 3-28: Simulated S11 with different plate thickness on smith chart.

3.7.2.2   Change in coaxial feed

As discussed earlier the outer conductor of the coaxial feed is connected to the middle plate forming a short circuit stub between the middle plate and the ground plane, as shown in Figure 3-25. This generates the second resonance around 137 MHz. Since this surface is actually shorting the middle plate to ground, the antenna matching near this frequency becomes very sensitive to the outer diameter of the coaxial line. If the feed is changed to standard coaxial feed as shown in Figure 3-22, the outer conductor diameter becomes 2.2 mm instead of 22 mm, which in turn changes the length of short circuit stub. As the second resonance is due to stub consequently the S11 performance deteriorates as shown in Figure 3-29.
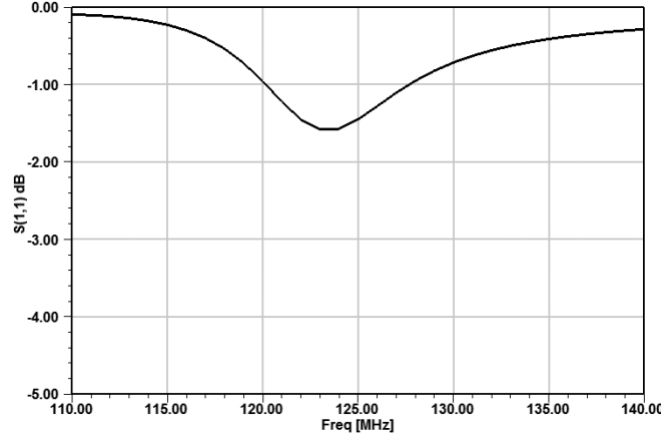
Figure 3-29: Simulated S11 of full-scaled VHF antenna with 50 Ω coaxial feed.

Therefore, it is much needed that the antenna feed should be redesigned in such a way that, the outer conductor diameter is large enough for the stub length to have the second resonance at 137 MHz, the cable dielectric and inner conductor diameters are of standard dimensions, and the 50 Ω impedance is kept the same. In order to implement the above requirements, a metallic cylinder with outer diameter 22 mm and inner diameter of 4.1 mm is placed between the ground plate and the middle plate. A standard SMA connector with Teflon diameter $b = 4.1$ mm and inner conductor diameter $a = 1.3$ mm is used to feed the antenna. From the basic theory we know that the characteristic impedance of a coaxial line is given by equation (3-1).

$$Z = \frac{\eta}{\sqrt{\varepsilon r}} * \frac{1}{2\pi} * \ln\left(\frac{b}{a}\right)$$
(3-1)

Where $\varepsilon_r = 2.1$ for Teflon. Using will give impedance of $Z = 47.6$ Ω. The new geometry of antenna feed is shown in Figure 3-30. Simulated S11 of new geometry of antenna feed and full-scaled antenna, are shown in Figure 3-31 and Figure 3-32. The S11 of antenna with standard feed and aluminum cylinder of diameter 22 mm is not < -6 dB for the VHF band. Looking at Figure 3-31 the marker m2 shows that the impedance of antenna is inductive. One solution to address the VHF band coverage is to make the antenna impedance close to m1, which is achieved by reducing the size of outer diameter of aluminum cylinder. A parametric sweep of the diameter (dia_oc) is shown in Figure 3-33 and Figure 3-34. We can see here that if the diameter of outer conductor, dia_oc=18 mm, S11 is better than -6 dB over the band of 116-137 MHz.
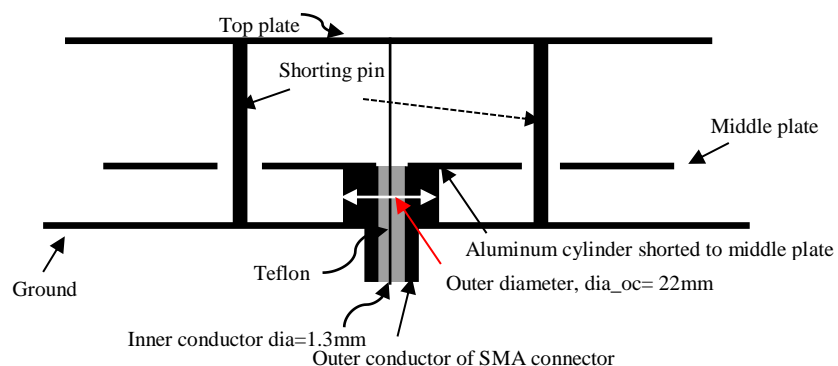
Figure 3-30: Full-scaled VHF antenna with aluminum cylinder and 50 Ω coaxial feed.
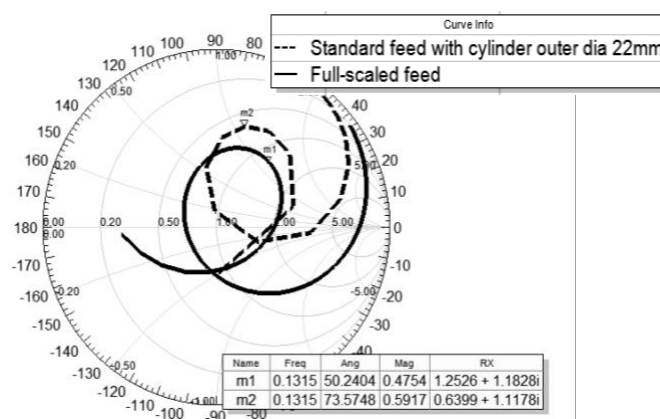
Figure 3-31: Smith plot of comparison of S11 of full-scaled VHF antenna and modified feed antenna.
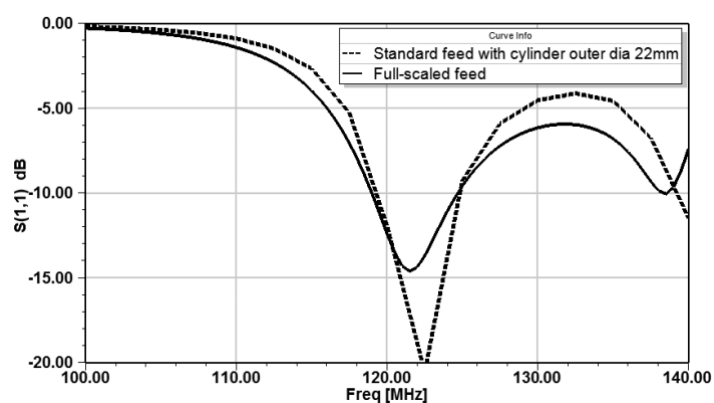
Figure 3-32: Comparison of S11 of full-scaled VHF antenna and modified feed antenna.
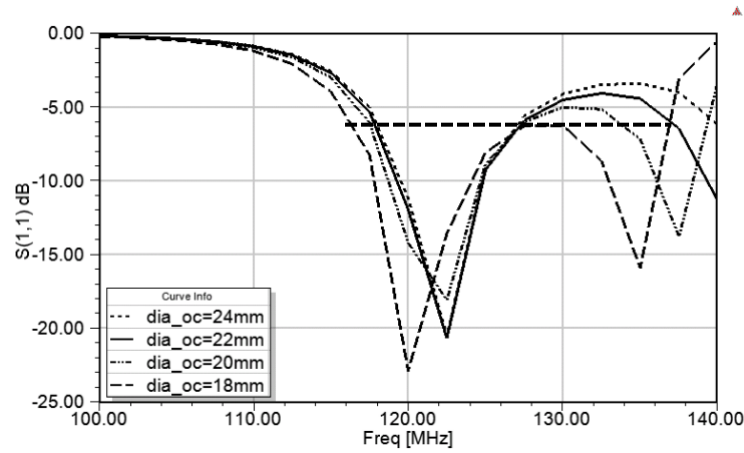
Figure 3-33: Parametric sweep of dia_oc.
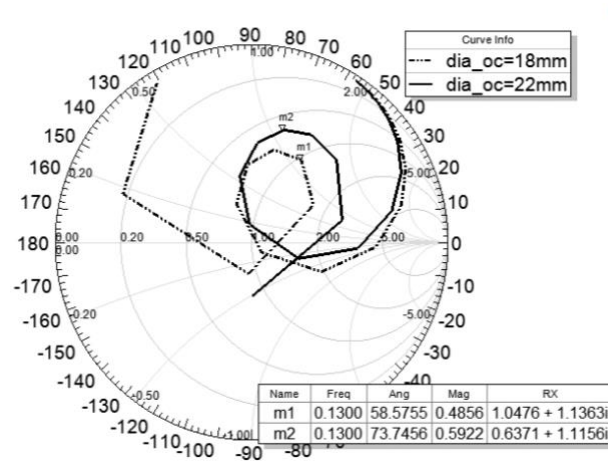
Figure 3-34: Smith plot of parametric sweep of dia_oc.

3.7.2.3   Changing the middle plate diameter

In addition to the above changes to the antenna shown in Figure 3-29, the diameter of the middle plate W_m was changed from 520 mm to 518 mm. This shifted the S11 response towards the higher side of frequency. This adjustment is made to maintain a safe margin of S11<-6 dB around 136 MHz as shown in Figure 3-35.
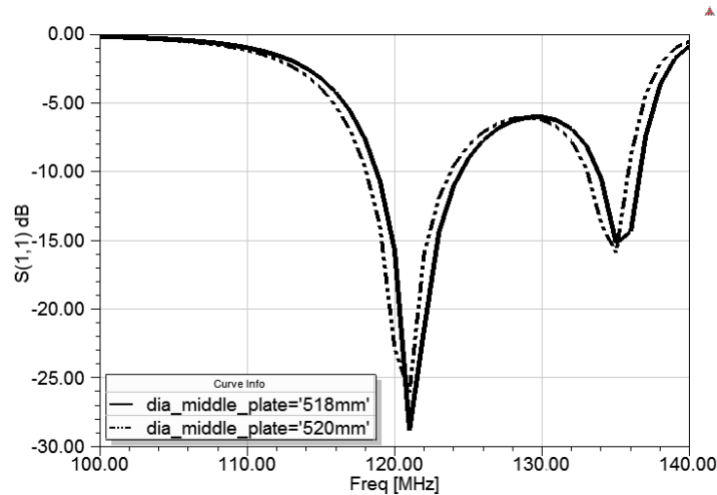
Figure 3-35: S11 comparison of diameter of middle plate.

3.7.2.4 Addition of interface plate to the antenna

A barrel will be used to test the antenna performance as it can imitate the shape of aircraft body. This barrel is cylindrical shape and can accommodate multiple antennas on it. To make an easy installation of the antenna on the aircraft or barrel for the testing purposes, an interface plate of respective length, width and thickness equal to 200 mm x 200 mm x 6.35 mm has been attached to the antenna structure and to ground plane while keeping same $h_m = 20\ mm$. These dimensions were a requirement by industry partners involved in this project. Figure 3-36 schematically describe the new antenna model. The use of interface plate as part of the VHF antenna also allows us to easily assemble it for testing with aluminum ground plane and composite ground plane separately. With this new arrangement, the S11 changes and the second resonance disappears for dia_oc=18 mm, as shown in Figure 3-37. As the length of current path towards the edges of the ground plane increases, so it is required to adjust the dia_oc such that the inductance decreases and the S11<-6 dB over the band. It has been shown in Figure 3-38, that antenna starts to have good impedance bandwidth with the decrease in dia_oc from 22 mm to 12 mm. Adjusting the outer conductor diameter has rectified the problem caused by the inclusion of the interface plate.
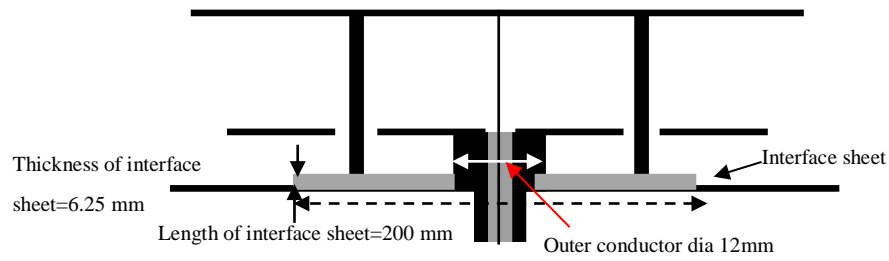
Figure 3-36: VHF antenna with interface plate.
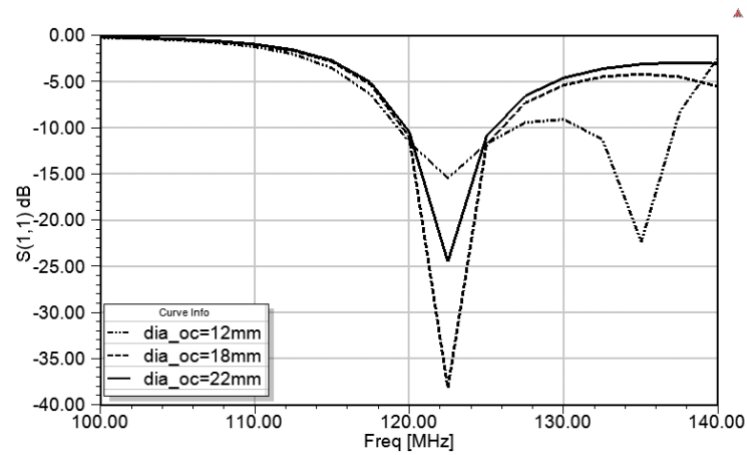
Figure 3-37: S11 of VHF antenna with interface plate for various dia_oc.
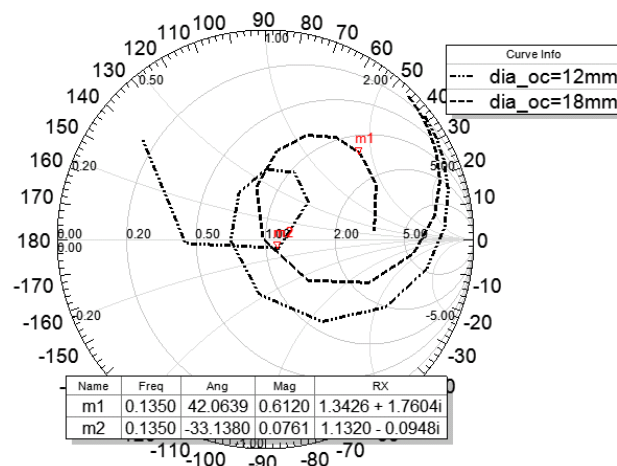
Figure 3-38: Smith chart comparison of S11 for different values of dia_oc.

Figure 3-38 shows that for frequency 131.5 MHz, as given by m1, by changing the dia_oc to a value of 12 mm the imaginary part of impedance value is close to zero. Above improvements, discussed in section 3.7.1 have resulted in achieving relevant solutions and the final simulated model for VHF antenna is shown in Figure 3-37 with dia_oc=12 mm. This VHF antenna has reduced height as compared to standard VHF blade antenna. The total height of the proposed design is 75 mm as compared to sensor system VHF blade which has height of 290 mm. The simulation shows that our designed antenna covers the full operational band of VHF communication and it has a rigid structure. The fabrication and testing of this antenna will be discussed in detail in section 3.11.

3.8 Need for a multiband antenna on an aircraft

Conformal and multiband antennas have an important impact on communication and navigation applications especially for aircraft, ships and other vehicles. Multi-functional antennas that operate over broad frequency bands or multiple independent bands have also evolved with the expansion of wireless systems. One way to encompass different communication systems is to employ a separate antenna for each system. An advantage of this approach is that it meets the specific needs of each communication system. But for platforms such as an airplane, ship or automobile, which require the use of many communication systems, this approach has several problems such as space, cost and electromagnetic compatibility/interference (EMC/EMI). Therefore, there is significant interest in antennas that are smaller in size as well as multi-functional. In addition, by installing fewer antennas, installers will save both time and money. The aircraft companies will appreciate the reduction in the number of antennas on their aircraft and reduced drag, resulting in fuel economy and even higher speeds.

3.9 Specification of a dual-band antenna

In this section the design of dual-band antenna is presented. The proposed design is based on the improvements and techniques as discussed in the previous sections 3.3 and 3.7.2. The desired dual-band antenna design specifications are given in Table 3-3.

Table 3-3: Dual-band antenna design specifications.

	TCAS	**VHF**
Frequency	1.03 – 1.09 GHz	118-137 MHz
Bandwidth	5.6%	14.9%
VSWR / S11	<2 / -10 dB	<3 / -6 dB
Radiation Pattern	Omnidirectional	Omnidirectional
Polarization	Vertical	Vertical

3.10 Design of dual-band antenna

A sketch of proposed dual-band antenna is shown in Figure 3-39 where a TCAS antenna is placed over the top plate of VHF antenna. One of the shorting pins of the VHF antenna is made of hollow cylinder to provide a path for the coaxial line to connect TCAS microstrip line. TACS antenna is feed by using a 50 Ω microstrip line, this allow us to keep the TCAS antenna at the geometrical center of VHF antenna and preserving symmetry as shown in Figure 3-39.

A comparison of simulated S11 of the VHF and TCAS antennas alone and as a dual-band antenna has been well depicted in Figure 3-40 and Figure 3-41 .When TCAS antenna is placed on the top plate of VHF antenna, the simulated VHF response shifts to higher frequencies as shown in Figure 3-40. This shift is due to the coupling of TCAS antenna. The simulated S11 response of TCAS also shifts to the lower frequencies due to the loading effect of VHF antenna as can be seen in Figure 3-41. The TCAS antenna can be tuned to get S11<-6 dB at 1.09 GHz by changing the CPW line parameters.
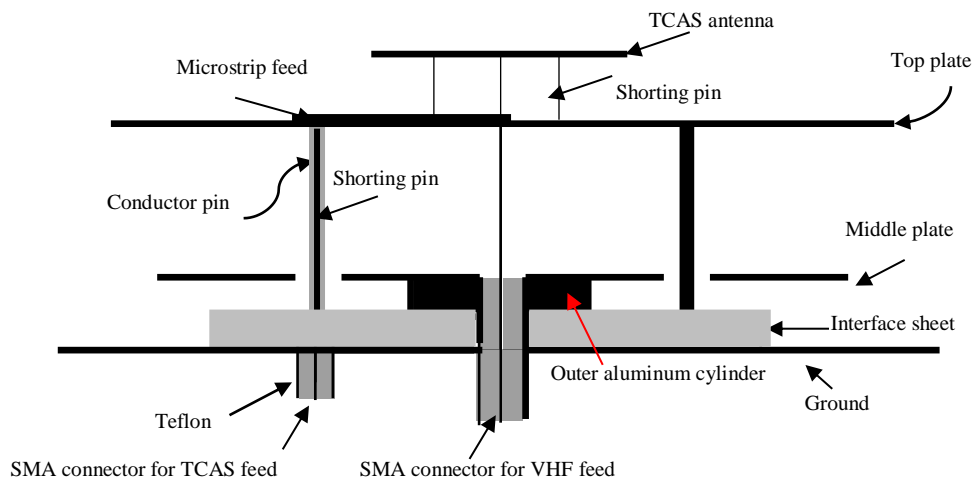
Figure 3-39: Full model of dual-band antenna.
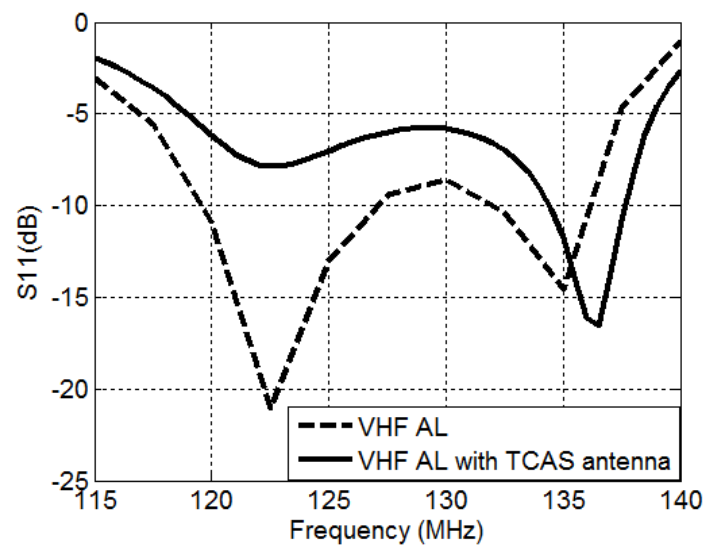
Figure 3-40: Comparison of simulated S11 of VHF antenna with aluminum ground and VHF antenna with TCAS antenna on aluminum ground.
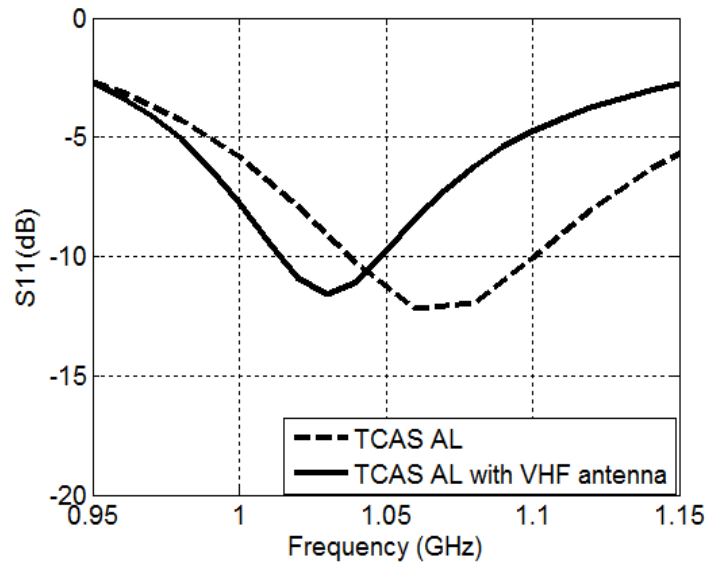
Figure 3-41: Comparison of simulated S11 of TCAS with aluminum ground and TCAS antenna with VHF antenna on aluminum ground.

3.11 Fabrication of the dual-band antenna

The VHF antenna is fabricated and the TCAS antenna was placed over the top plate of VHF antenna. Two SMA connectors were used to feed TCAS and VHF antenna. The SMA connectors were placed on the bottom side of interface sheet. The inner conductor of SMA connector has a diameter of $a =1.3$ mm. The inner conductor for TCAS SMA feed is extended by using a wire of similar diameter and the extension wire is connected to the microstrip line as shown in Figure 3-42 (c) .The conductor wire was passed through one of the shorting pin of VHF antenna, which is hollow cylinder of inner diameter $b=4.86$ mm, results in a change in the impedance as seen at connector port. Using equation (3-1) the change in the impedance is calculated as $Z = 79\ \Omega$, for $\varepsilon_r = 1$ for air, $b = 4.86$ mm, $a = 1.3$ mm. To make Z close to 50 Ω, a was changed from 1.3 mm to 2.2 mm which brings $Z = 48\ \Omega$ The extended wire now has diameter of 2.2 mm and a sleeve was put to solder it to the inner conductor of SMA connector.

Figure 3-42, Figure 3-43 and Figure 3-44 shows different steps for the assembly of dual-band antenna. Threaded holes are made on the periphery of the interface plate to allow installation on the ground plane on the aircraft skin. The three shorting pins of the VHF antenna are also connected to the interface plate. Three nylon screws are placed to give mechanical support to the middle plate. Figure 3-42 shows the installation of the middle plate over the interface plate. In the next step, the top plate with already build-in TCAS antenna is placed over the middle plate. The shorting pins for VHF antenna and three screws handle the weight of top plate for a stable mechanical structure. Figure 3-45 shows a closer view of antenna prototype from the bottom.
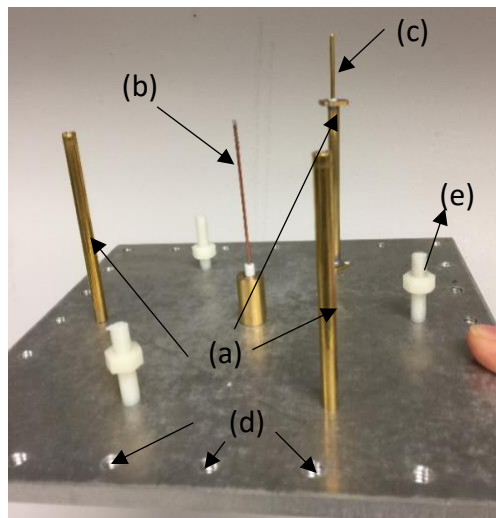
Figure 3-42: Step1: (a) 200 mm x 200 mm square interface plate with three shorting pins for VHF antenna, (b) Center pin for the VHF feed, (c) TCAS feed passing through one of the shorting pin, (d) holes for connecting the ground plane both aluminum or composite with the interface plate, (e) Nylon screws for holding the weight of middle plate.
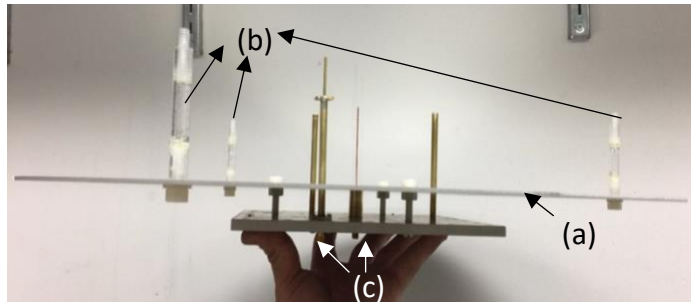
Figure 3-43: Step2: (a) Middle plate of VHF antenna has been placed on the top of interface plate, (b) Plastic screws are placed at strategic points to support the top plate, (c) SMA connectors.
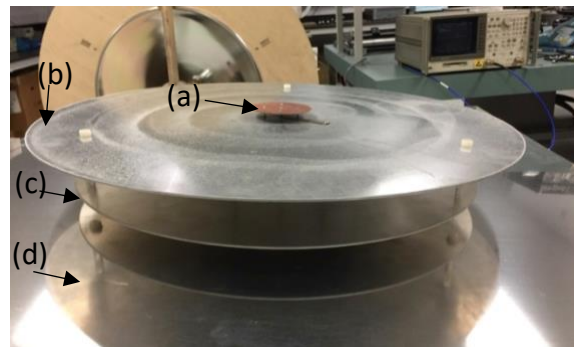
Figure 3-44: Step 3: (a) TCAS antenna, (b) Top plate of VHF antenna, (c) Middle plate of VHF antenna, (d) Aluminum ground plane.

Figure 3-45: Outdoor testing of the dual-band antenna.

3.12 Experimental characterization of the dual-band antenna

The dual-band antenna was tested with both aluminum and composite ground planes. The size, length x width of both ground plane is 3x4 feet or 914.4x1219.2 mm. For VHF testing, the size of antenna ground plane should be 4x4 foot according to DO-186B for VHF antenna testing standards. The size was selected 3x4 feet due to the manufacturer limitations for the composite ground plane. For simulations, the same size of ground plane was used in the HFSS software. Outdoor measurements were done as shown in Figure 3-46. The composite consists in a multilayer carbon fiber reinforced polymer, covered with a thin copper mesh acting as lightning protection. A 5-mils paint layer is then applied (gray aspect on Fig .3.46(b)).

In the simulations a composite conductivity of 3.5E4 Siemens/m was used. The comparison of measured and simulated S11 results with both ground planes and for both VHF and TCAS antennas are shown in Figure 3-47. The VHF antenna when measured outdoor has S11<-6 dB for 120-138 MHz for both aluminum and composite ground planes. Furthermore, the simulated S11 of VHF antenna is also very much similar to the measured results. As it has been discussed before the S11 of VHF antenna on aluminum ground alone was better than -6 dB at 118 MHz but when the TCAS antenna was placed on the top of it, the simulated S11 response was shifted 2 MHz towards higher frequencies. The same behavior was observed in the measured S11 of VHF antenna when loaded with the TCAS antenna.

Figure 3-46 : Outdoor measurements (a) Aluminium ground connected to the antenna, (b) Composite ground connected to the antenna.
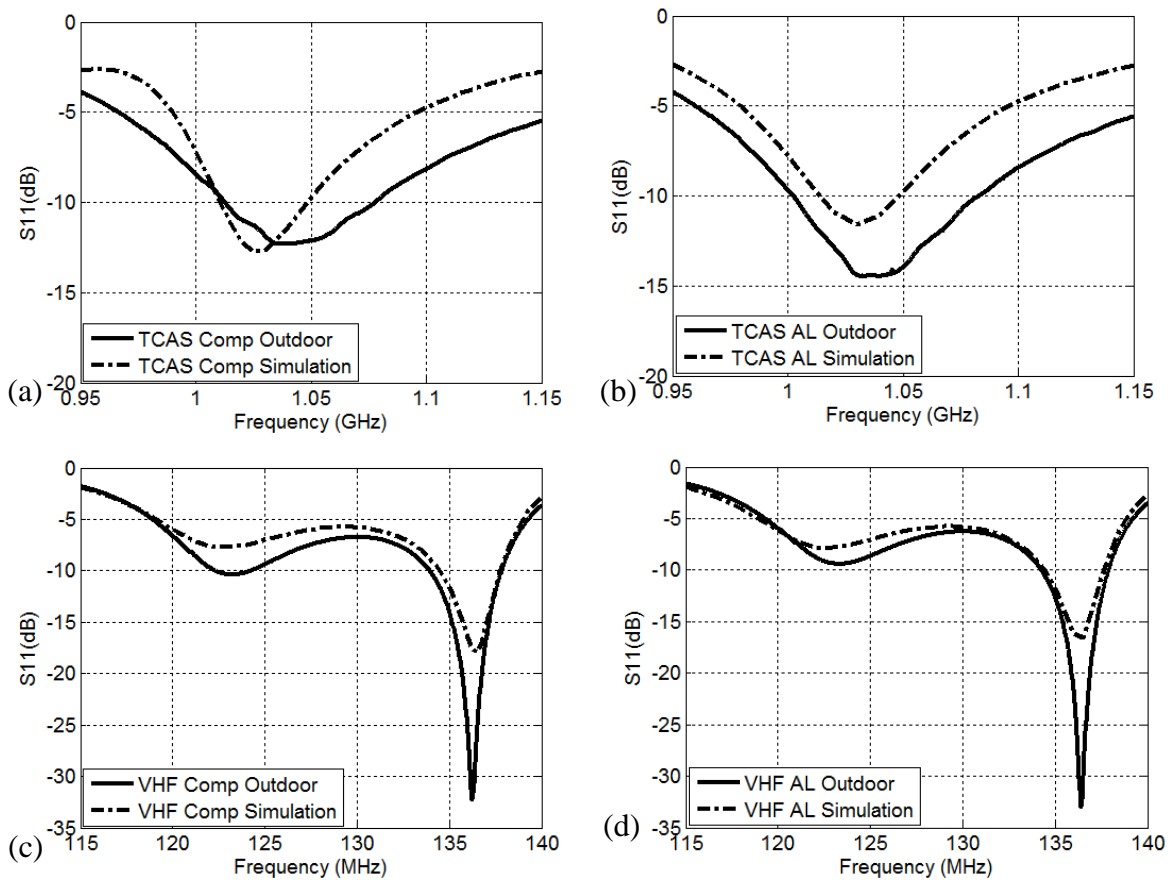
Figure 3-47: Simulated and measured S11 for VHF and TCAS for both aluminum (AL) and composite (Comp) ground.

Also, as shown earlier in Figure 3-41, the simulated S11 response of the TCAS was shifted to lower frequencies due to loading effect of VHF antenna. Instead of covering the TCAS band of 1.03-1.09 GHz with S11<-10 dB, it is covering 1.01 to 1.05 GHz. The simulated S11 responses of TCAS with both composite and aluminum ground plane are similar. However, the measured S11 with aluminum ground plane has 10 MHz more bandwidth at the lower edge of frequency band. In addition, the measured S11 response of the TCAS antenna can be tuned for S11<-6 dB at 1.09 GHz instead of -8 dB by changing the length of CPW line.

3.13 Near-field testing of the dual-band antenna

In Poly-Grames, the radiation pattern characterization facility is limited to operate only above 800 MHz frequencies. As per our knowledge there are no facilities in Canada to measure far-field antenna radiation patterns in the 100 MHz range. To investigate the radiation characteristics of the dual-band antenna in the VHF band, a possible alternative is to limit us to perform near-field measurements, which can then be compared with near-field simulations. VHF near-field emission measurements are done routinely in electromagnetic compatibility (EMC) compliance tests. The antenna was tested in the EMC chamber of the Centre de Recherche Industrielle du Québec (CRIQ) located in Montreal. Near electric fields with both aluminum and composite ground planes were measured. The results for the measurements are compared with the simulation results from the HFSS. The measurement setup in the EMC chamber is shown in Figure 3-48. The antenna under test (AUT) is used as a transmitting antenna and is placed on a rotating table platform, at a height of 0.9 m from the ground as shown in Figure 3-48(a). The platform rotates the antenna from 0 to 360° in the horizontal (azimuth) plane. The receiving antenna is a log-periodic dipole array (ETS-LINDGREN 3143B), which operates for 25 MHz to 1000 MHz. This antenna, shown in Figure 3-48(b), can be moved vertically on a 4 m tower. Combining this linear movement with the rotation of the AUT table allows generating cylindrical near-field scans. Figure 3-49 (a) shows the EMC chamber where the horizontal distance between the axis of rotation of the turntable and the position of the receive antenna is 4 meters.
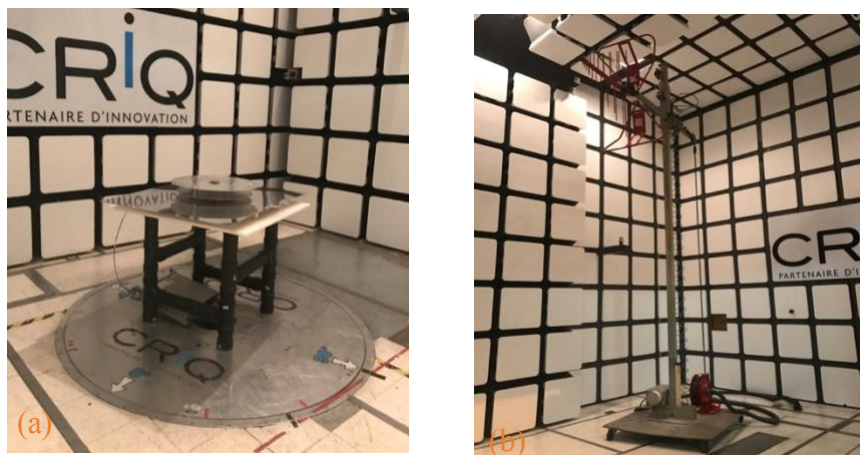
Figure 3-48: Near-field measurement setup (a) Antenna under test, (b) Receiving antenna.
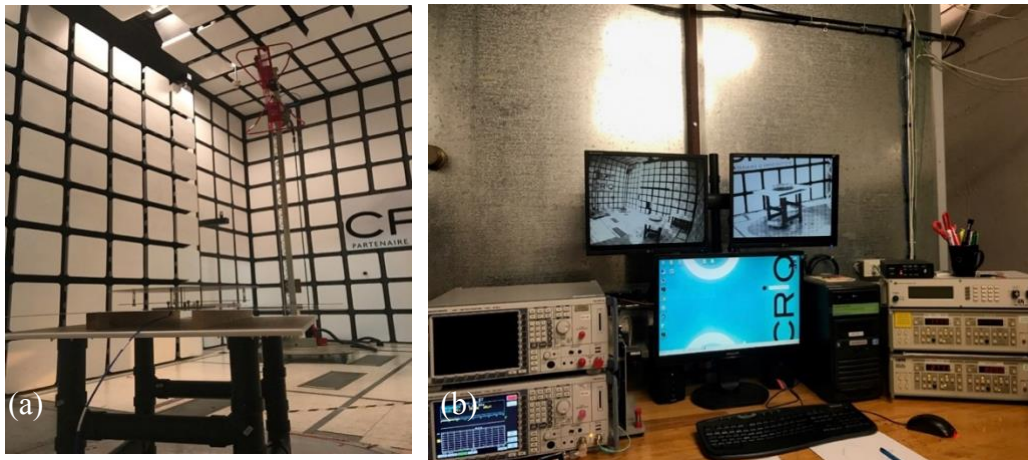
Figure 3-49: Near-field measurement setup in CRIQ (a) EMC chamber, (b) Operator room.

Figure 3-49 (b) shows the operator room where the EMC radiation data can be retrieved from software. As opposed to anechoic chambers, only the walls and ceiling of EMC test chambers are covered with absorbing materials. The floor is made of a good conductor and will therefore cause reflections, which is also taken into consideration in our simulation model used. For our tests, we positioned the receiving antenna at the following heights from the floor on the tower: 1 m, 1.5 m, 2 m, 2.5 m, 3 m, 3.5 m, and 4 m. At each height, the transmitting antenna is rotated at azimuth angles of 0°, 45° and 90° (other quadrants were not measured considering the symmetry of the structure). The transmitted power was set to -30 dBm. As shown in Figure 3-49 ,the electric fields are recorded from the operator room and antenna correction factor and cable losses are added to get the corrected value of electric field intensity in dBµV/m. In HFSS the antenna is simulated in near-field setup as shown in Figure 3-50. Three lines sources where each line has length of 4m is placed at $\phi = 0°, \phi = 45°$ and $\phi = 90°$. Each line has length of 4 meters, in order to simulate the measurement positions. The distance between the center of the DUT to the measurement lines is set equal 4 meters, similar to the test setup in the chamber as explained above.

Tests were done over at 120 MHz, 123 MHz and 137 MHz. The comparison of measured and simulated electric fields is shown in Figure 3-51, which shows a good agreement between simulated and measured results for all the frequencies of interest and at different angles for both aluminum (AL) and composite (Comp) ground planes. Azimuthal variations caused by the

rectangular shape of the AUT ground planes are similar on both cases of ground planes. A measurement versus simulation difference of approximately 12 dB consistently appear on all the tested cases, i.e. for all heights, angles and types of ground planes.

This systematic error, being independent of geometry is not likely to be related to a defect with the VHF antenna (in fact TCAS measurements in this test chamber, not shown here, revealed the same level of offset). It is most likely due to an error either in the handling of the chamber cable correction terms, in the generator setting, in the power setting of the simulation, or a combination of all these factors. The most important fact is that the same trends with angle and height were present in both sets of results, as well as the independence on the type of ground plane. Which concludes that the fabricated VHF antenna operated in accordance with simulation predictions.

Near-field line setup to get the strength of electric field at various points along the length

Antenna Under Test

$d = 4\ m$

$h_t = 1\ to\ 4\ m$

Ground Plane

$h = 0.9\ m$
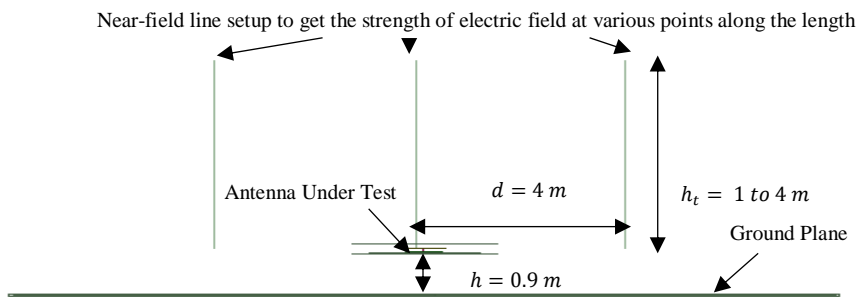
Figure 3-50: Simulation setup to analyze the one electric fields of the VHF antenna.
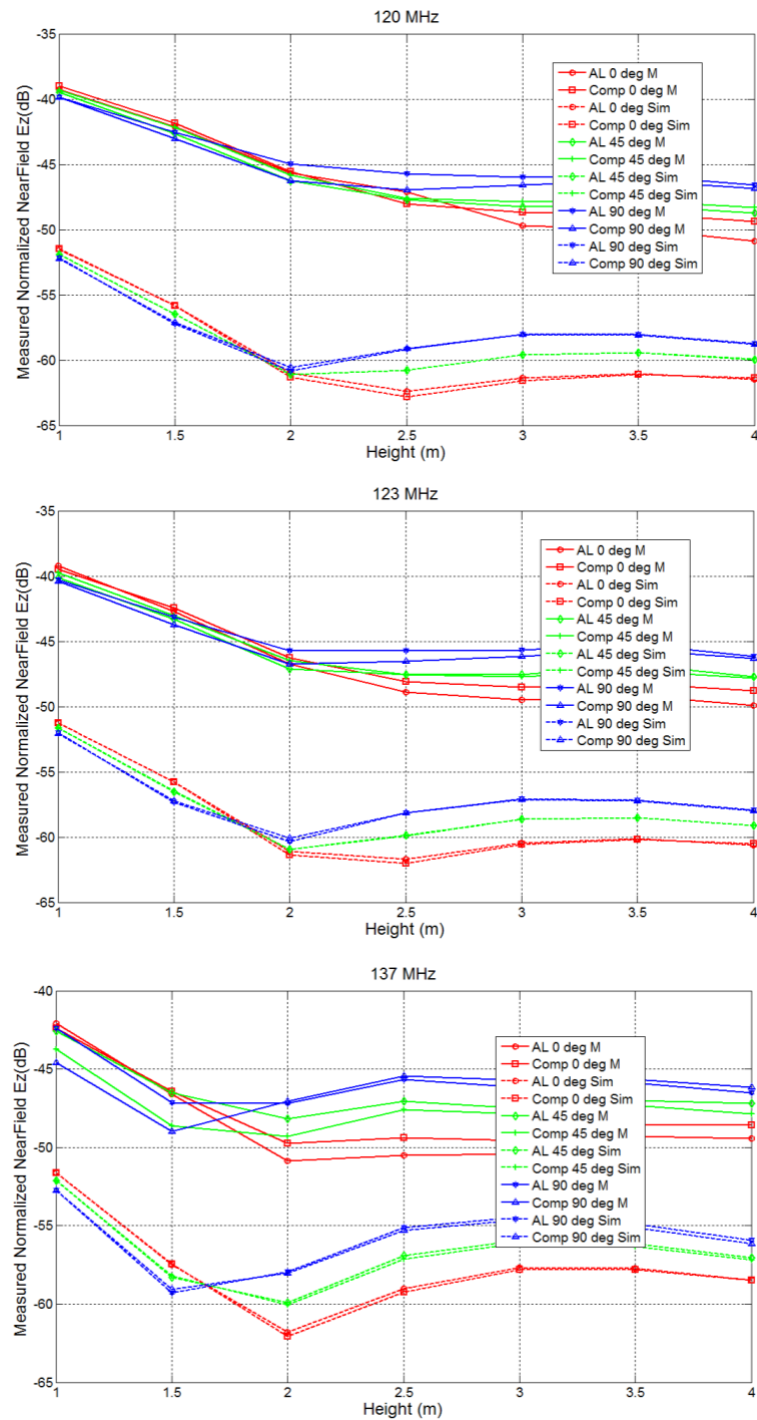
Figure 3-51: The comparison of simulated and measured electric fields at $\phi=0°$, $\phi=45°$ and $\phi=90°$ for both aluminum and composite ground plane for VHF band for 120 MHz, 123 MHz and 137 MHz.

3.14 Conclusion

In this chapter we have presented for the first time the design and fabrication of dual-band antenna, which can cover both TCAS and VHF systems. The use of top-loaded monopole with shorting pins and the use of shorted stub has helped to reduce the antenna height. The dual-band antenna has excellent characteristics and return loss nearly compliant with operating system requirements. The mechanical assembly of dual-band antenna was challenging, considering a large physical structure at VHF frequency. Different supporting posts were used to carry the weight of multiple plates. The placement of feed of TCAS antenna passing through one of the shorting pins of VHF antenna and accurate connection to the microstrip line was one of challenge. The VHF radiation characteristics were measured in near-field testing in an EMC test facility and compared with the simulation results. This testing has been quite helpful in validating the radiation performance of antennas, when antenna test ranges are not available for such low frequencies.

CHAPTER 4   SURFACE WAVE ANTENNA FOR DME APPLICATIONS

The work presented in Chapter 3 is intended to make low-profile dual-band antenna for TCAS and VHF frequency bands. In this chapter we are presenting a low-profile surface wave antenna (SWA) for DME communication system.

4.1 Functionality of DME antennas

The acronym DME stands for "Distance Measuring Equipment". The DME antenna that is usually a blade antenna is installed at the lower forward fuselage of an aircraft. This system continuously displays the information about the aircraft distance from the ground station. More details of DME operation can be found in Section 2.3.

4.2 Design of a DME surface wave antenna

The design of a low-profile SWA for DME band is presented here. In order to overcome the antenna size limitations of the antenna test facilities of the Poly-Grames Research Centre, the antenna design presented here is scaled down physically to a one-fourth factor. The proposed conformal antenna helps to improve the aerodynamics drag of aircraft and make it less susceptible to physical damages as compared to protruding blade antenna. The specifications of DME antenna are given in the Table 4-1.

Table 4-1: Specifications of DME antenna.

Frequency	Scaled	DME band
	3.84-4.88 GHz	0.96 – 1.22 GHz
Bandwidth	25%	23%
VSWR / S11	<2 / -10 dB	<2 / -10 dB
Radiation Pattern	Omnidirectional with max directivity close to horizon	Omnidirectional with max directivity close to horizon
Polarization	Vertical	Vertical

4.2.1 Surface wave antenna

The concept of surface wave antenna is very interesting for the low-drag aircraft antenna application because it leads to low-profile designs. However, most SWAs exhibit a narrow beam, which is in contradiction with the requirement of the DME system. A SWA with a radiation pattern similar to that of a monopole antenna with fractional bandwidth (FBW) of 5.6% for S11< -10 dB was reported by [65]. This antenna utilizes a circular patch antenna loaded with a lattice of 8 x 8 square artificial magnetic conductor (AMC) cells. The diameter of the ground plane was 2λ, and the size of antenna is also 2λ as the antenna operation depends on the size of the ground plane. The width of the square artificial magnetic conductor (AMC) cell was 0.1λ, and the height of the substrate was 0.04λ.

The proposed design presented here is inspired by [65] and is low-profile with large FBW equal to 30% by using circular shaped AMC cells. If we consider a standard quarter-wavelength monopole antenna operating at 3.8 GHz, it has a height of $20\ mm$. The total height of the proposed design is only 6.09 mm, which is ~ 70% less than a standard monopole. The radiation pattern of this antenna is highly symmetric and has less cross-polarization. However, the height of the proposed antenna is almost double as compared to [65] but with the advantage of larger bandwidth. Such design of a conformal antenna, that exhibits very low-profile can be almost flush-mounted on an aircraft. The next sub-section explains the theory of grounded dielectric slab, surface waves generation in the dielectric slab and in-detail design of SWA for its wide-band operation due to dual resonance.

4.2.2 Grounded dielectric slab

Both lossy and non-lossy dielectric materials can be used to guide electromagnetic waves. This material medium can be used as a transmission line or a waveguide. The electromagnetic wave when propagating in the dielectric slab may bounce back and forth between its upper and lower interfaces. A grounded dielectric slab is shown in Figure 4-1 , where the fields outside the slab is evanescent and part of the energy propagates in the substrate and part of it propagates in the air region, both in y-direction. There is no net power flow in the z direction in both regions.
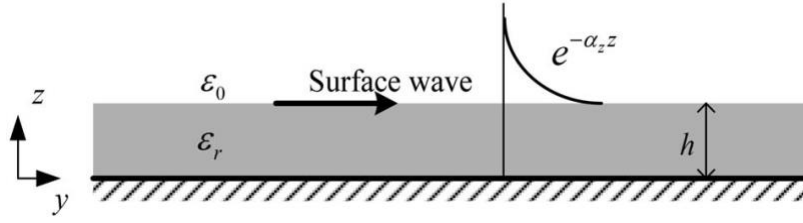
Figure 4-1: Surface waves on a grounded dielectric material.

Surface wave modes are supported by the grounded dielectric. The difference between dielectric slab/waveguide and grounded dielectric slab is that the later can only have TM (odd) and TE (even) modes. The cutoff frequency of TE or TM modes are a function of permittivity, permeability and thickness of dielectric slab and are given as equation (4-1) [66].

$$(f_c)_m = \frac{m}{4h\sqrt{\mu_d \varepsilon_d - \mu_0 \varepsilon_0}} \tag{4-1}$$

Where for TM (odd) m=0,2,4… and for TE (even) m=1,3,5… with dominant mode TM_0 of zero cutoff frequency.

4.2.3 Probe-fed dielectric slab

When a vertical metallic probe is placed in proximity to the center of a grounded dielectric slab Transverse magnetic (TM) surface waves are generated. These surface waves propagate along the antenna surface and radiate into free space at discontinuities caused by a ground plane and/or dielectric truncation [67]. One of the antenna requirements for DME communication systems is to have maximum directivity for low elevation angles, in the 60° to 90° range (near horizon). This is studied by changing the height and radius of substrate in which a probe is placed in the center and by looking into the directivity at horizon.

Figure 4-2 shows simulation model of the probe-feed grounded dielectric slab. The substrate is Rogers 6002, with ε_r=2.94, tan δ=0.0012 and is the same as used in [65]. The probe length in the dielectric is $\frac{sub\_h}{2}$, where sub_h is the thickness of the dielectric. The length and radius of the probe are 1.5 mm and 0.65 mm respectively, which are very small as compared to the wavelength in the dielectric $\lambda_d = \frac{\lambda_0}{\sqrt{\varepsilon_r}} = 39$ mm at the center frequency 4.4 GHz.
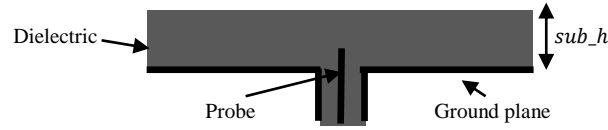
Figure 4-2: 50Ω coaxial probe feeding surface waves in a grounded dielectric substrate.

The substrate height sub_h is changed to 2 mm, 4 mm, 6 mm and 8 mm and the elevation pattern above an infinite ground plane is computed as shown in Figure 4-3. As can be seen in the Figure 4-3, the directivity at horizon increases with the increase in the height. We can also see that for sub_h of 6 mm and 8 mm there is a dip in the radiation pattern at $\theta = 40°$ and $45°$ respectively. This is due to the strong excitation of the surface wave mode which in turn gives rise to the diffracted field [68] and this increases the directivity at an angle close to horizon. The $sub\_h = 6$ mm is chosen for which the average directivity for the range $\theta = 60°$ to $90°$ is better than other cases. After the selection of height of the substrate, the diameter of substrate is studied next. The directivity at horizon for three cases is shown in Figure 4-4. For each diameter the diffracted field from the edge of the substrate has produced a dip at different angle.
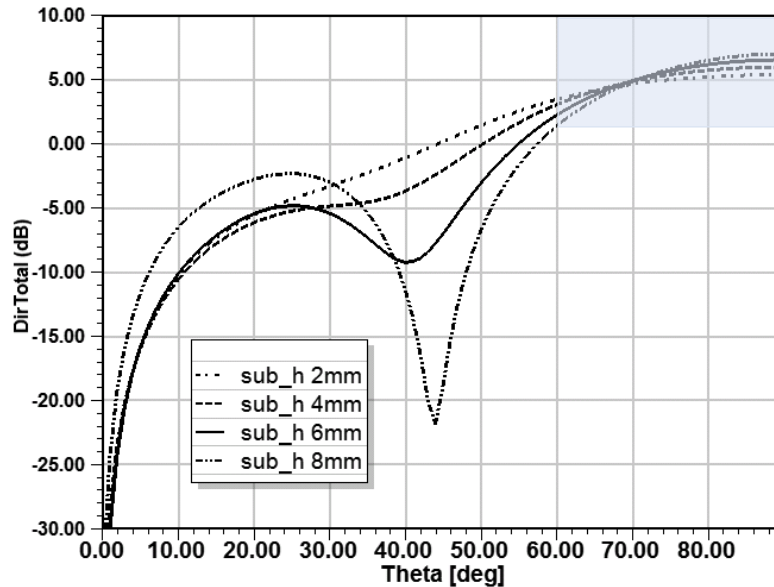
Figure 4-3: Simulated directivity of probe at horizon, $\theta = 89°$ for infinite ground plane.

The deeper is the dip the more directivity we get at the horizon. Substrate radius of 90 mm is selected to keep good directivity at horizon $\theta = 60°$ to $90°$ and less value of dip in the radiation pattern.

4.2.4 Patch-fed dielectric slab

As discussed in the previous section a short probe can increase the directivity at horizon for sub_h =6 mm, but impedance matching with the 50Ω feeding line is poor. As a next step, a circular patch with resonant frequency of 4.4 GHz (center of 3.84 GHz - 4.88 GHz) was placed on a dielectric sheet at $h = \frac{sub\_h}{2} = 3\ mm$. The patch size was determined using equation (4-2) [69].

$$f_{nm} = \frac{1}{2\pi\sqrt{\varepsilon_o\mu_o\varepsilon_r\mu_r}} \times \frac{X}{a} \tag{4-2}$$

Using above equation for $X = 3.817$ mm (zeros of Bessel function) and for $f = 4.4$ GHz, $\varepsilon_r = 2.94$, $h = 3$ mm, the radius of the patch calculated is $a = 23.8$ mm.
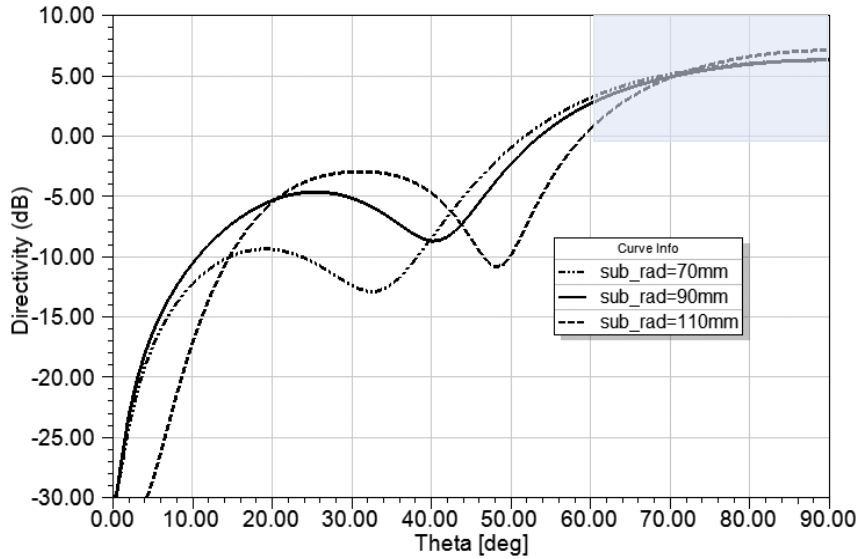
Figure 4-4: Simulated directivity of probe at horizon, $\theta = 89°$ for infinite ground plane with different substrate diameter.

Figure 4-5 shows the side view of patch antenna on Rogers's 6002 dielectric. The TM_{02} mode of the circular patch antenna has a strong electric field but weak magnetic field in the center of patch.

The feed location has been made in the center to have a symmetric radiation pattern and less cross-polarization. Figure 4-6 we can see that the patch has resonance at around 4.4 GHz however the matching of antenna is still not good. The following section explains the technique used to improve and enhance the patch antenna bandwidth.

4.2.5 Patch loaded with perfect electric conductor (PEC)

Figure 4-7 shows the patch with a dielectric superstrate. The total dielectric height is now the substrate height plus the superstrate height which is, $sub\_h = 6\ mm$. By adding a superstrate, the simulation result shows that the patch resonant frequency is moved to 4.2 GHz from 4.4 GHz as shown in Figure 4-9. If a Perfect Electric Conductor (PEC) boundary condition

Figure 4-5: Center feed circular patch over infinite ground plane.
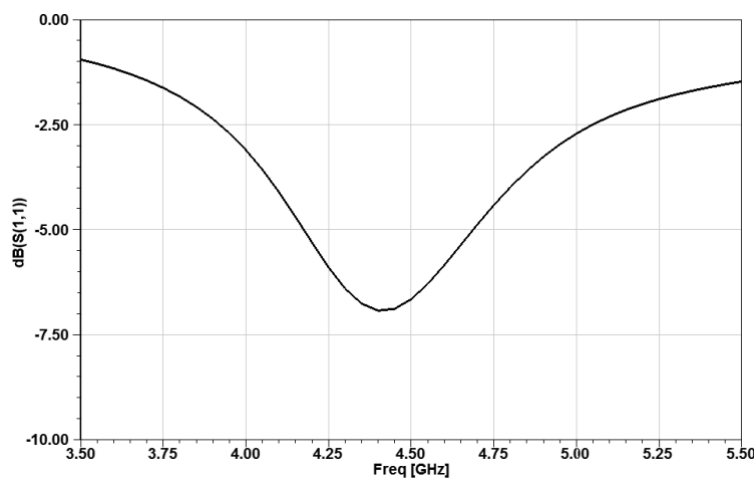
Figure 4-6: Simulated S11 of a patch antenna.

is applied on the top of dielectric surface, as shown in Figure 4-8. The structure forms a parallel plate dielectric waveguide with a patch in the middle producing another resonance at 5 GHz as

shown in Figure 4-9. This resonance at 5 GHz depends on the *sub_h* and size of the patch antenna. It should be noted here that the return loss in this case is not due to radiation in free space but rather due to power guided in the parallel plate modes.
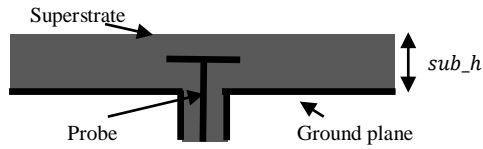
Figure 4-7: Center feed circular patch with dielectric superstrate.
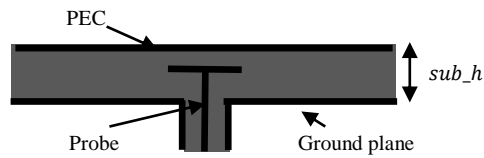
Figure 4-8: Center feed circular patch with PEC at the top.
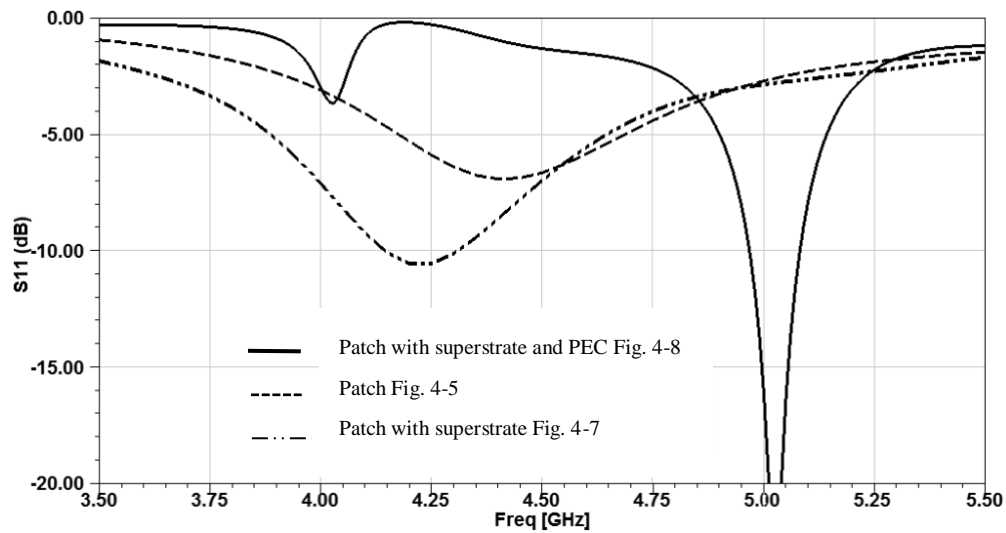
Figure 4-9: Simulated S11 comparison of patch, patch with superstrate, and patch with superstrate and PEC.

4.2.6 Patch loaded with artificial magnetic conductor (AMC)

The Electromagnetic Band-gap (EBG) surfaces, High Impedance Surface (HIS) or Periodic Band-gap structures (PBG) have two important characteristics, one is to suppress the propagation of surface currents, and second is reflection of electromagnetic waves with no phase reversal [70]. Figure 4-10 shows a periodic mushroom EBG structure. The unit cell consists of a square patch connected to the ground plane through a metal via. This structure acts like a two-dimensional electric filter and prevents the propagation of currents along the surface [71]. As the dimension of EBG unit cell is much smaller than the wavelength, it can be modeled using lumped elements. Using the lumped element model approach this structure can be represented as a parallel resonant LC filter, resonating at a frequency based on the value of capacitance and inductance.

The theoretical dimension of square AMC cell is calculated for a specific frequency by using equations (4-3), (4-4) and (4-5). These equations are derived in [72] for inductance and capacitance of HIS and the method is explained as below.

In high impedance surface the inductance is due to the conductive loop below the top metal layer which consist of vias and also due to the both metal sheets. A solenoid of current is used to imitate this geometry and calculate the sheet inductance in Henrys/square. The electric flux function for a pair of semi-infinite plates separated by a gap is used to imitate the geometry of HIS by limiting the plates to end at width of the patch. The capacitance calculated by this method is in Farads-square.

In Figure 4-10, L is the inductance and C is the capacitance of the equivalent circuit. Variable h is the height of AMC patch from the ground plane, w is the width of the AMC patch, g is the gap between the adjacent AMC patches.

These EBG surfaces have been successfully used as the ground plane for various antenna types to enhance the radiation efficiency with a low-profile configuration [73]. On the contrary, as discussed in [74], for the patch loaded grounded dielectric slab, since the vias suppressing the TM mode are not present, surface waves can propagate along the ground plane. This is the case we will be investigating by using AMC without vias as a superstrate on the patch antenna. Next the theoretical calculation of AMC geometry is discussed along with the simulation results for angle of reflection.
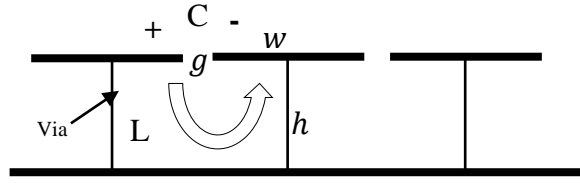
Figure 4-10: Mushroom type EBG structure.

$$L = \mu_o h \tag{4-3}$$

$$C = \left(\frac{w\varepsilon_o(\varepsilon_r + 1)}{\pi}\right) \cosh^{-1} \frac{w + g}{g} \tag{4-4}$$

$$f = \frac{1}{2\pi\sqrt{LC}} \tag{4-5}$$

Using above equations for Rogers 6002 substrate with $\varepsilon_r = 2.94$, $\varepsilon_o = 8.854 x 10^{-15}$F/mm, $\mu_o = 4\pi 10^{-10}$H/mm, $w = 14.5$ mm, $g = 1$ mm, $h = 3$ mm, the resonant frequency is $f = 3.5$ GHz for square AMC cell. The size of unit cell or periodicity of AMC cell is p, where $p = w + g = 14.5 + 1 = 15.5$ mm.

The square AMC cell was simulated in HFSS using driven mode with plane wave impedance, master-slave boundary conditions and Floquet ports as shown in Figure 4-11. The phase of reflection is calculated at the surface of the AMC cell by deembedding the port. The zero crossing of phase of reflection coefficient means that reflection of electromagnetic waves occurs without phase reversal. Here the AMC bandgap is defined as the frequency band for which the reflection phase is in the interval -90° to 90°.
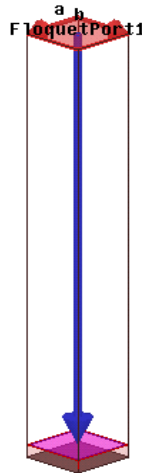
Figure 4-11: Unit AMC cell.

The square AMC cell and circular AMC cell are shown in Figure 4-12(a) and Figure 4-12(b) respectively. The phase of the reflection versus frequency is compared for both cases and is shown in Figure 4-12(c). Evaluating the results of Figure 4-12(c) we can see that the zero crossing for square AMC is at 3.6 GHz which is close to the above theoretically calculated value i.e. 3.5 GHz. The zero crossing for circular patch is higher than the square patch and is around 4.8 GHz. This can be illustrated using equation (4-4). As the capacitance between the adjacent circular AMC patches is less as compared to the square AMC patches, the resonant frequency f has increased. Moreover, as the square patch has more area (more metal sheet) and circular patch has less area (less metal sheet), inductance decrease and the frequency increases. Here it is worth mentioning that in both cases, there is no inductance due to the conductive loop as the vias are not present.

Furthermore, the slope of the phase curve (Figure 4-12(c)) in the interval from -90° to 90° is less steep as compared to the square AMC cells indicating that the circular AMC cells have more bandwidth. For -90° to 90° band the square patch has FBW of 22% and circular patch has 29%. Next, the performance of the patch antenna with an AMC superstrate is evaluated and is compared with patch antenna with PEC.
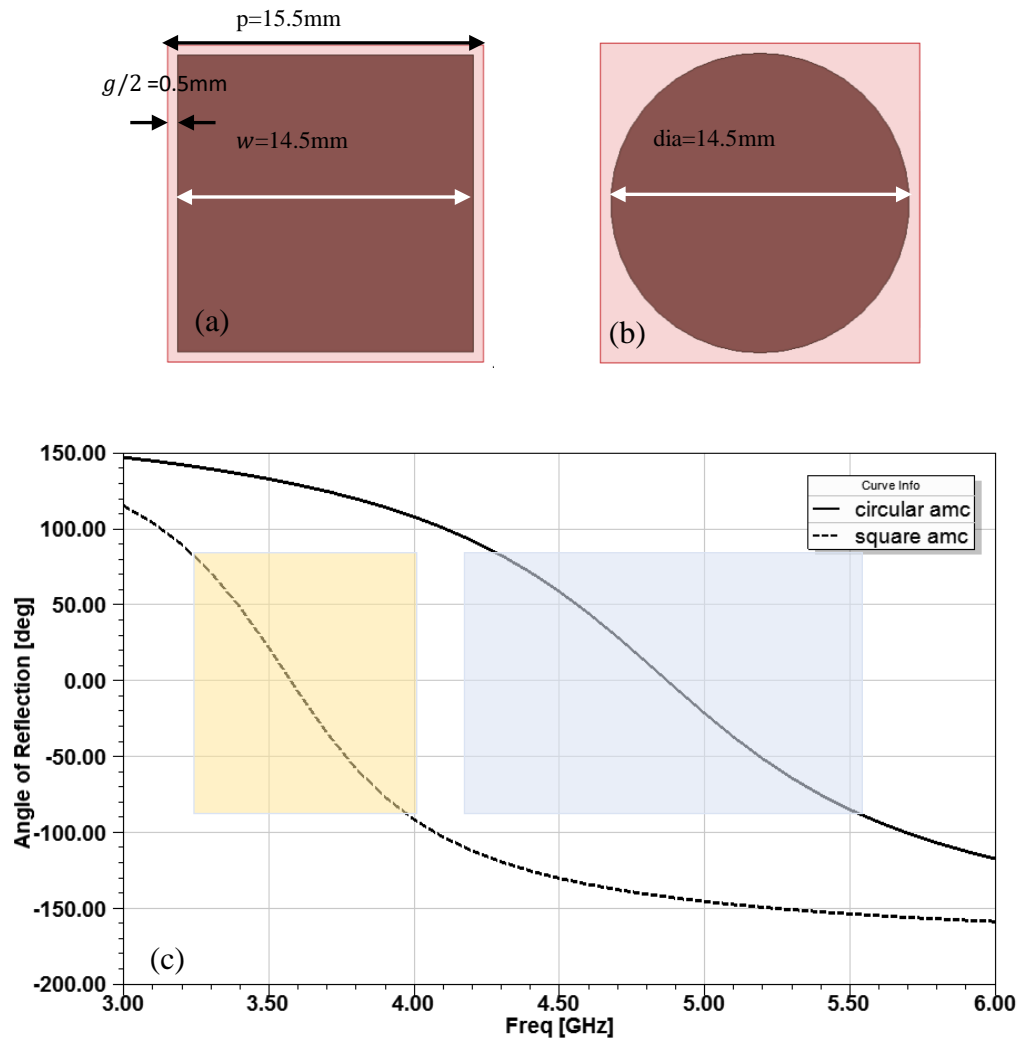
Figure 4-12: Comparison of phase of reflection coefficient of square and circular AMC cells.

Figure 4-13 shows the cross-sectional view of the simulation model for (a) PEC and (b) AMC metal layer placed over the patch antenna. The AMC surface successfully launch the surface waves by converting the electromagnetic fields under the patch and thus improves the radiation performance of antenna and impedance bandwidth. Figure 4-14 (a) and (b) shows the comparison of simulated impedance of patch with PEC and AMC cells. With PEC boundary condition the impedance is reactive, and energy is stored in the dielectric material. The placement of AMC cells facilitates the electromagnetic radiation to leak through the AMC surface, which lowers the imaginary part of the impedance.
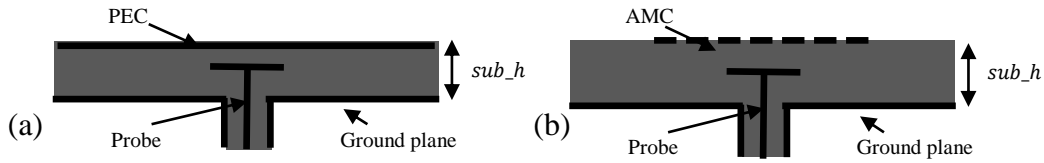
Figure 4-13: Simulation model of (a) Patch with PEC, (b) Patch with AMC.
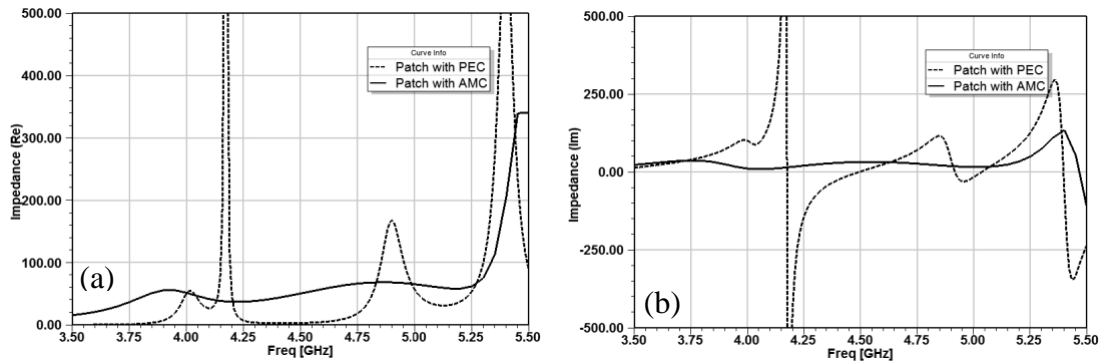
Figure 4-14: Comparison of simulated impedance of patch with PEC and AMC (a) Real, (b) Imaginary impedance

Next is the selection of number of AMC cells that was based on impedance matching and gain characteristics. Different number of arrays 5x5, 7x7 and 9x9 were simulated in square lattice arrangement using circular AMC cells as shown in Figure 4-15. The simulated S11 for (a), (b) and (c) case are compared in Figure 4-16. Evaluating the S11 for the above three cases it was seen that 7x7 is the best case where S11 < -10 dB for required frequency band.
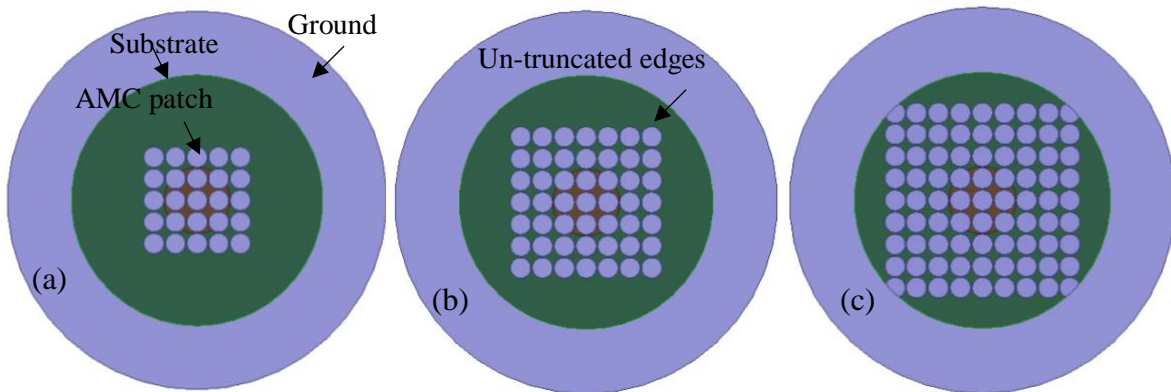
Figure 4-15: Square AMC layer (a) 5x5, (b) 7x7, (c) 9x9.
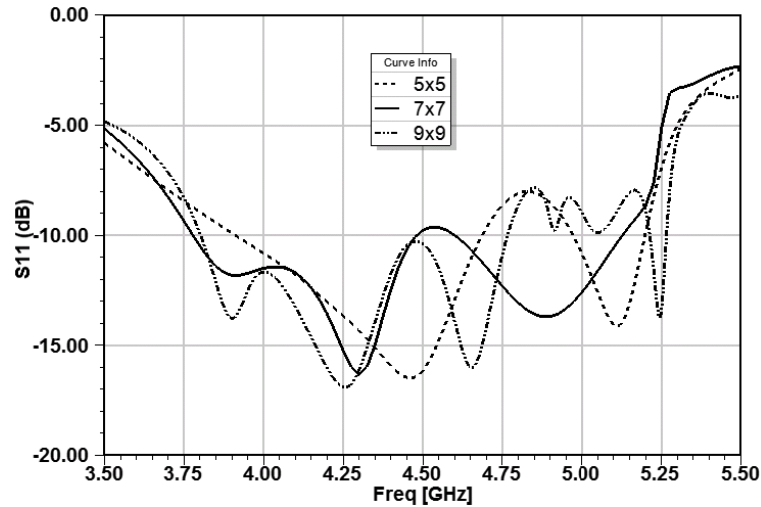
Figure 4-16: Simulated S11 of square AMC layers.

In the next step the corners of the square lattice of AMC array was truncated and shaped into circular circumference as shown in Figure 4-17 and same number of arrays 5x5, 7x7 and 9x9 are simulated. Simulation results indicate that for the case of 7x7 arrays is the best solution based on S11 criteria and has large bandwidth as given in Figure 4-18. The truncation of corner of square lattice has reduced the ripples in S11 and has improved the bandwidth as compared to square corners that can be seen by comparing Figure 4-17 and Figure 4-18 .The use of circular AMC cell vs square AMC cell, truncated edges of AMC layer and circular ground plane has helped to reduce ripples in the azimuthal radiation pattern which is one of the requirements of DME operating system.
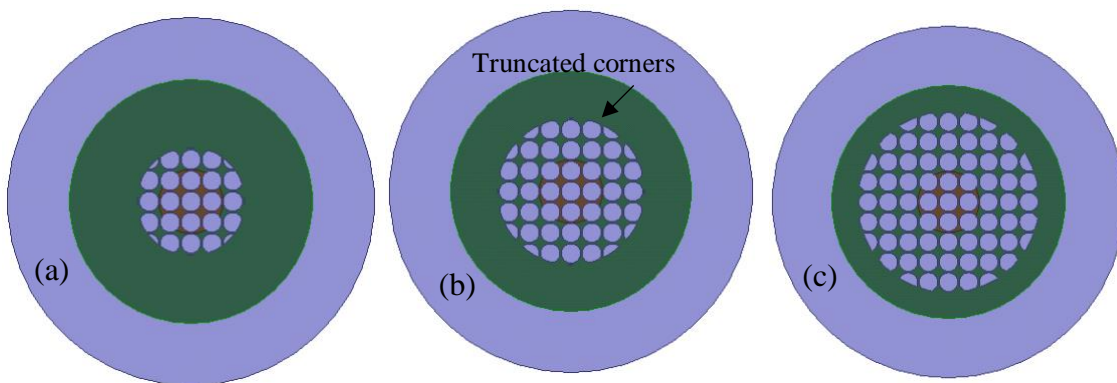
Figure 4-17: Truncated AMC layer (a) 5x5, (b) 7x7, (c) 9x9.
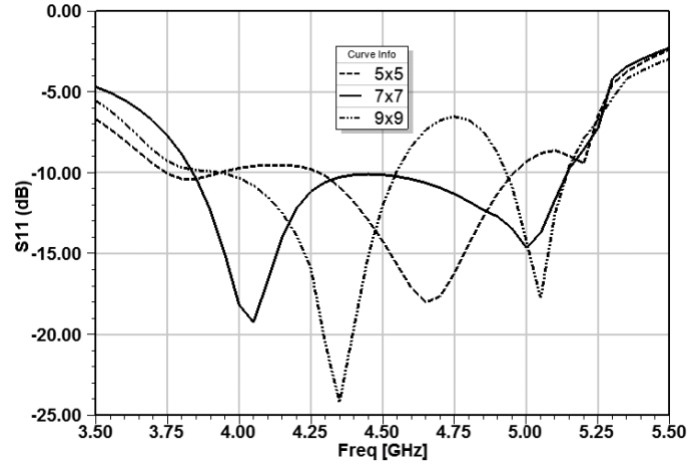
Figure 4-18: Simulation of truncated AMC layer.

Figure 4-19 (a) shows the first layer SWA antenna and Figure 4-19 (b) shows the AMC cells placed on the top of the patch antenna. Figure 4-19 (c) shows the side view of SWA antenna. The size of ground plane is based on DO-189 standards. According to DO-189 compliance for DME band, which is $4x\lambda_0$, where λ_0 is the free space wavelength at 1 GHz. As the proposed design is physically scaled one-fourth times of DME operating band i.e. 4.4 GHz will be the center
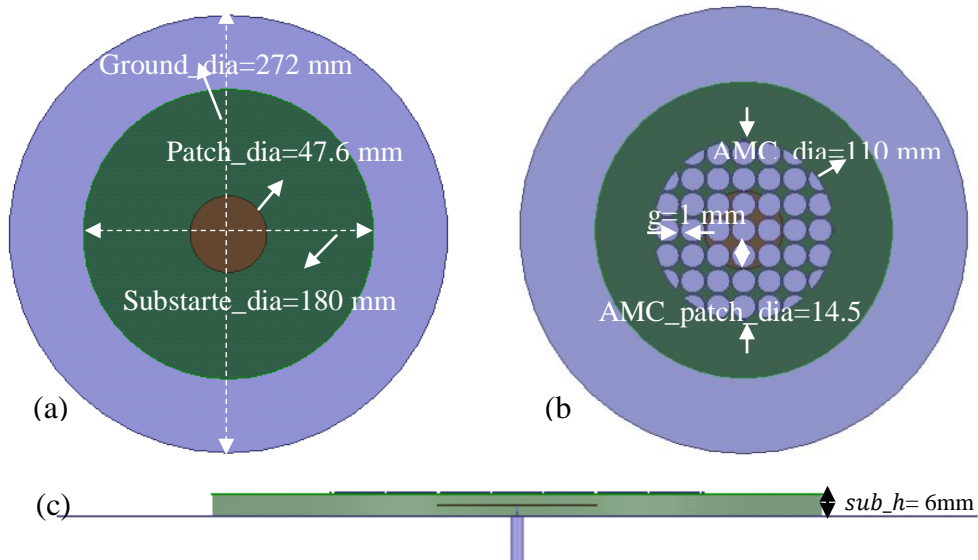
Figure 4-19: Simulation model of SWA (top view) (a) Patch only, (b) SWA, (c) Side view of SWA.

frequency. The size of antenna ground plane is $4x\lambda_0 = 272 \, mm$, where $\lambda_0 = 68 \, mm$ at 4.4 GHz. The simulated S11 for two cases are shown in Figure 4-20. The patch loaded with AMC also known as SWA shows dual resonance, one due to the patch and the other due to the AMC metallic surface. These two resonances are merged smoothly due to the broadband behavior of circular AMC cells.
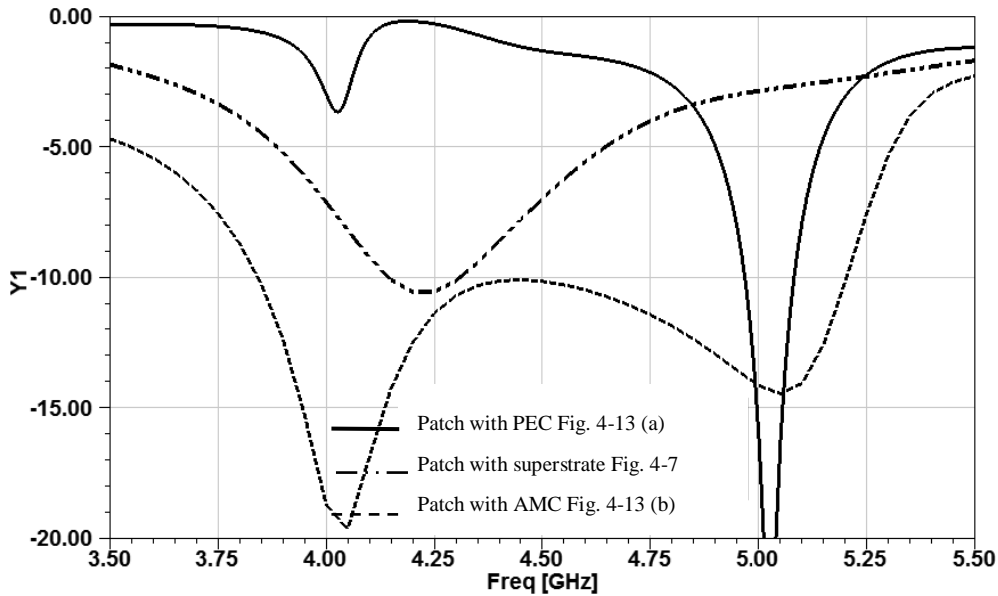
Figure 4-20: Simulated S11 for patch with superstrate, patch with PEC and patch with AMC.

The total height of antenna is 0.07λ and diameter of antenna, which is the diameter of substrate is 2.27λ, where λ=78 mm, is the free space wavelength for the lowest resonant frequency of 3.84 GHz. The simulated FBW for S11<-10 dB is from 3.85 GHz to 5.2 GHz, which is 30%. This is more than the required compliance as given in Table 4-1.

4.3 Fabrication of a SWA prototype

In this section, fabrication of SWA prototype is discussed. In the simulation model shown in Figure 4-19, two dielectric sheets are used. The lower layer is etched to form the patch antenna and the second layer has AMC patch array etched on it. As the design thickness is 3 mm, we were unable to find the substrate sheet large enough and suitable for diameter 180 mm from Rogers student sample program. Instead the prototype was fabricated using multiple parts. Two dielectric sheets of standard thickness of 3.05 mm, of diameter 140 mm were used, as shown in Figure 4-21(a). Three rings with inner diameter of 140 mm, outer diameter of 180 mm and of thickness 2.28 mm each, were placed on top of each other as given in Figure 4-21(b). Figure 4-21(c) shows the top

view of the SWA assembly. These subparts helped us to get the same diameter of the antenna however not the correct thickness. This simulation model is different from the original simulation model presented in Figure 4-19. The impact of this geometry on S11 will be discussed in Section 4.4.

Figure 4-22 shows views of the assembled antenna in different steps. First the patch antenna is etched on first layer of substrate with bottom copper etched away. Etching bottom copper removes the unwanted resonance due to capacitance with the ground plane. This patch antenna along with one outer ring was joined with compression on the aluminum ground plane. In the second step the AMC layer on the second sheet were etched and as a third step two more outer rings were joined to complete the assembly. The tape used to connect all the parts is 3M brand, model 9458, $\varepsilon_r = 3.21$ and thickness before compression is 1 mil and thickness after compression is reduced to 0.5mils. The holes were made for nylon screws to avoid the airgap between the dielectric sheets and to achieve a good contact to the ground plane.
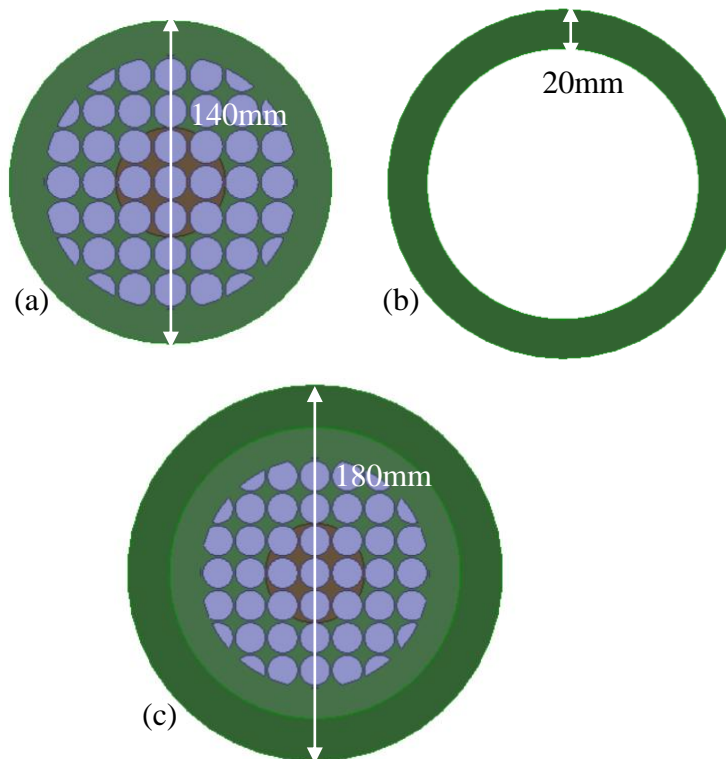
Figure 4-21: Top view of simulated model for the fabricated prototype of SWA, (a) Middle sheet with patch and AMC layer, (b) Outer rings, (c) Complete SWA assembly.
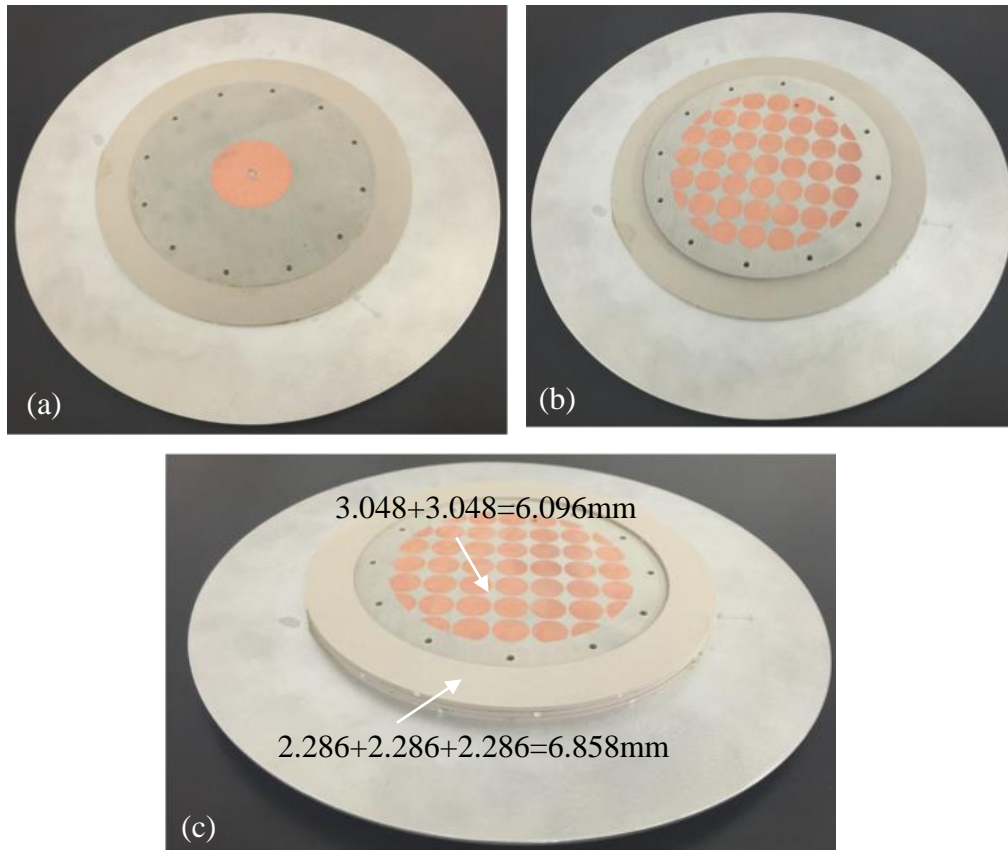
Figure 4-22: Fabricated SWA. (a) Patch layer, (b) Patch and AMC layer, (c) Addition of the outer rings.

4.4 Testing of the SWA

In this section the testing of the realized SWA prototype is presented. The antenna was tested for S11 and radiation pattern, and the results were compared with those of a standard quarter-wave monopole antenna.

4.4.1 S11 measurement

The simulated and measured S11 of the patch antenna, shown in Figure 4-22 (a) are given in Figure 4-23. A shift in frequency of almost 240 MHz can be seen in measured S11 as compared to simulated S11. The reason of this shift will shortly be discussed in the text. As the fabricated antenna was made using multiple dielectric sheets and rings, first the fabricated SWA as shown in Figure 4-22(c), is modeled. It is simulated and compared to initial simulated model as shown in

Figure 4-19 and to the measured S11 and given in Figure 4-24. It has been seen that S11 is changed with this new model which is using middle sheet and outer rings, as compared to original simulation model. However, still the measured results are different from the modified antenna model. Both measured S11 results of patch and SWA are further investigated to understand the reason behind the observed differences.

The patch antenna resonant frequency has a shift of 240 MHz from the simulated design results. A possible reason behind this shift is the presence of a gap between the dielectric sheet placed between the patch and the ground plane.

In the patch antenna simulations, when an air gap of 0.2 mm from the aluminum ground is introduced as shown in the new S11 matches very closely to the measured S11 response of the patch antenna, as given in Figure 4-26. This gap is therefore a possible reason for the mismatch between our simulated and measured results.
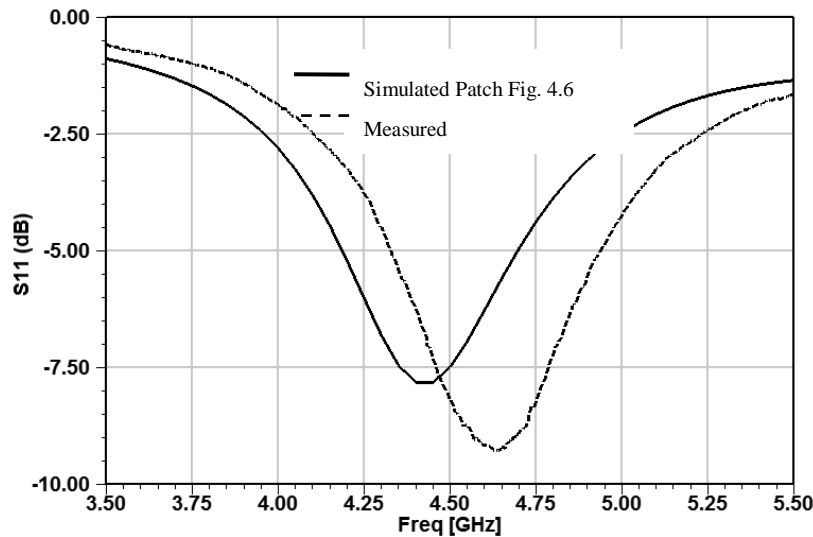
Figure 4-23: Comparison of simulated and measured S11 of patch antenna.
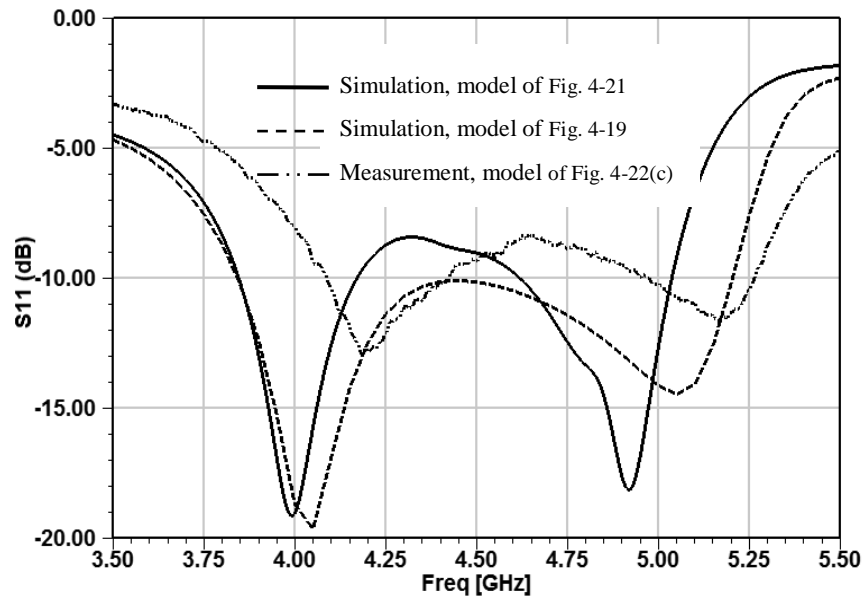
Figure 4-24: Comparison of simulated and measured SWA antenna.

Figure 4-25: Center feed circular patch with airgap=0.2 mm.
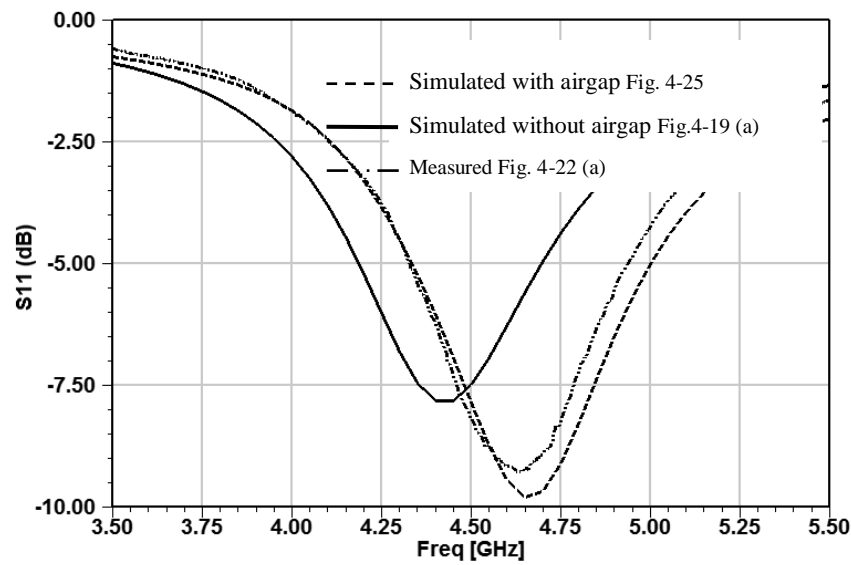
Figure 4-26: Comparison of S11 of patch antenna, simulated with air gap and measured.

By applying this same air gap in the simulation model of fabricated SWA as shown in Figure 4-27, we are able to obtain a better agreement between simulations and measurements, as shown in Figure 4-28. Hence the difference in proposed S11 and measured S11 can be partly attributed to the complex fabrication due to multiple dielectric sheets that yield to the air gaps and change in S11. Considering the measured S11 <8 dB (4.1 GHz to 5.3 GHz), the FBW is 25.5%. For DME the requirement of FBW is 23% for S11 <10 dB. The S11 of antenna can be improved by tuning the AMC cells or patch antenna for 3.84 to 4.88 GHz.

Figure 4-27: Side view of SWA with airgap.
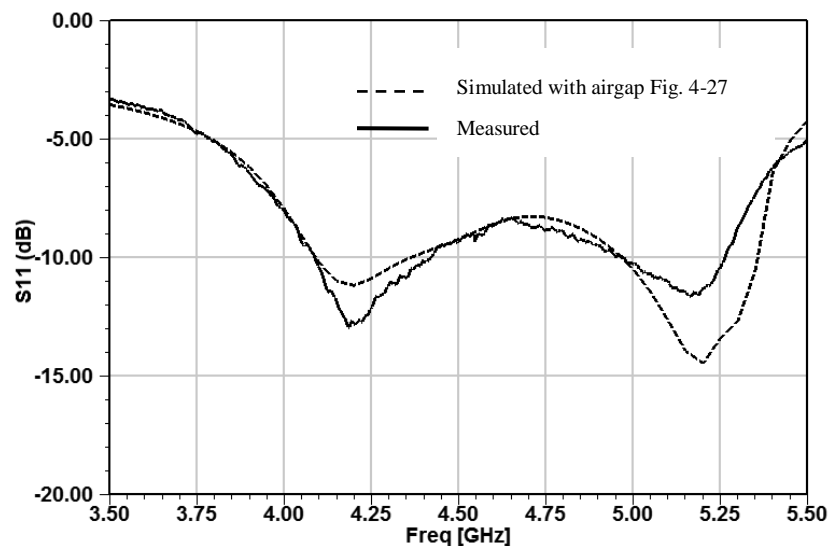
Figure 4-28: Comparison of simulated S11 for simulated SWA model with airgap and measured fabricated SWA.

4.4.2 Radiation pattern measurement

The radiation pattern of the antenna prototype was measured in a Satimo Starlab near-field setup.

The simulated realized gain is shown in Figure 4-29 (a), (b), (c), & (d) and Figure 4-30 (a), (b), (c), & (d) shows the measured gain for azimuth and elevation plane over a set for frequencies in the band of interest. For all these frequencies, the SWA exhibits omnidirectional radiation pattern.
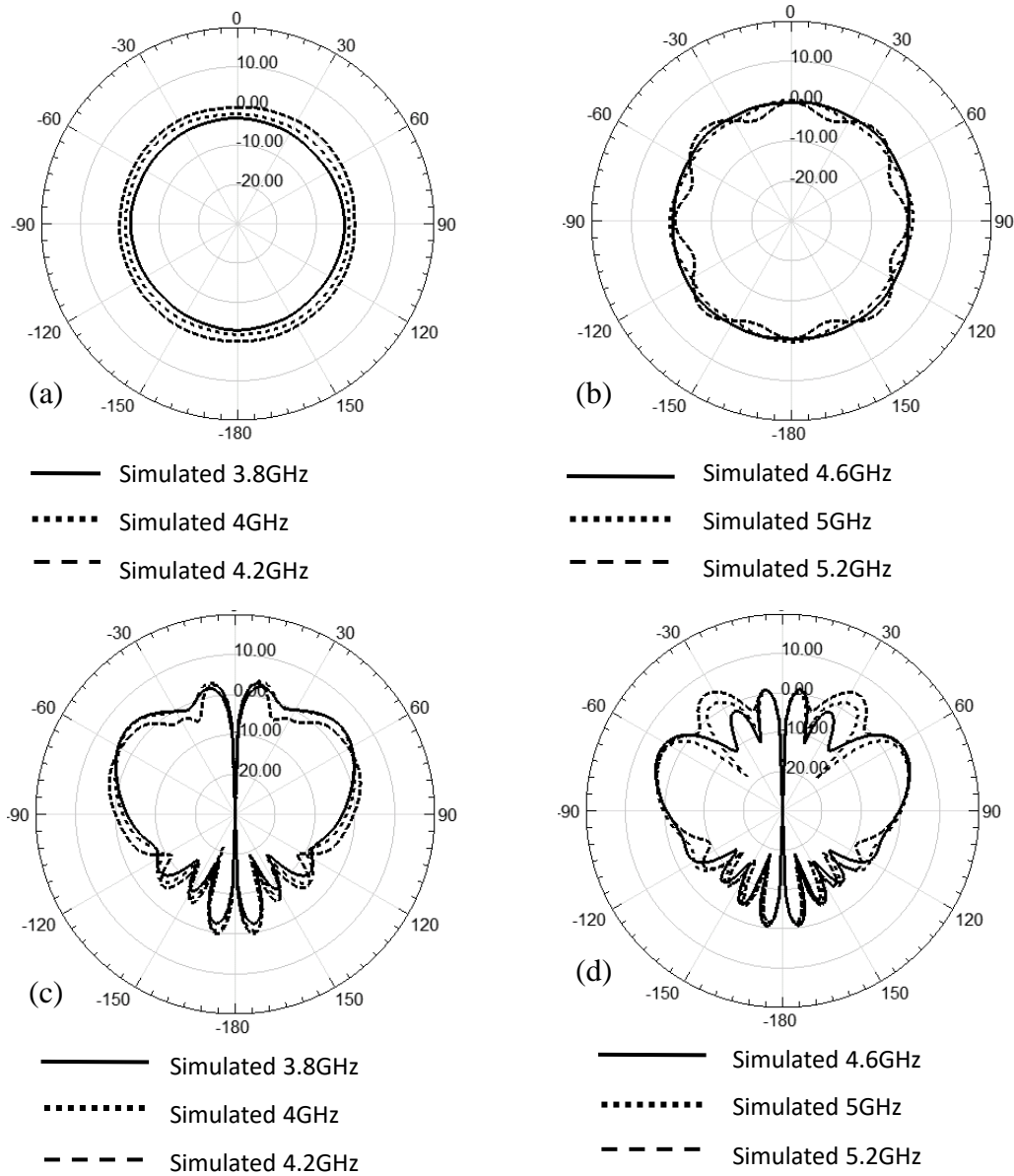
Figure 4-29: Simulated realized gain (a) & (b) Azimuthal pattern of SWA, (c) & (d) Elevation pattern of SWA.

(a)

Measured 3.8GHz

.... Measured 4GHz

– – – Measured 4.2GHz

(b)

Measured 4.6 GHz

.... Measured 5GHz

– – – Measured 5.2GHz

(c)

Measured 3.8GHz

.... Measured 4GHz

– – – Measured 4.2GHz

(d)

Measured 4.6 GHz

.... Measured 5GHz

– – – Measured 5.2GHz
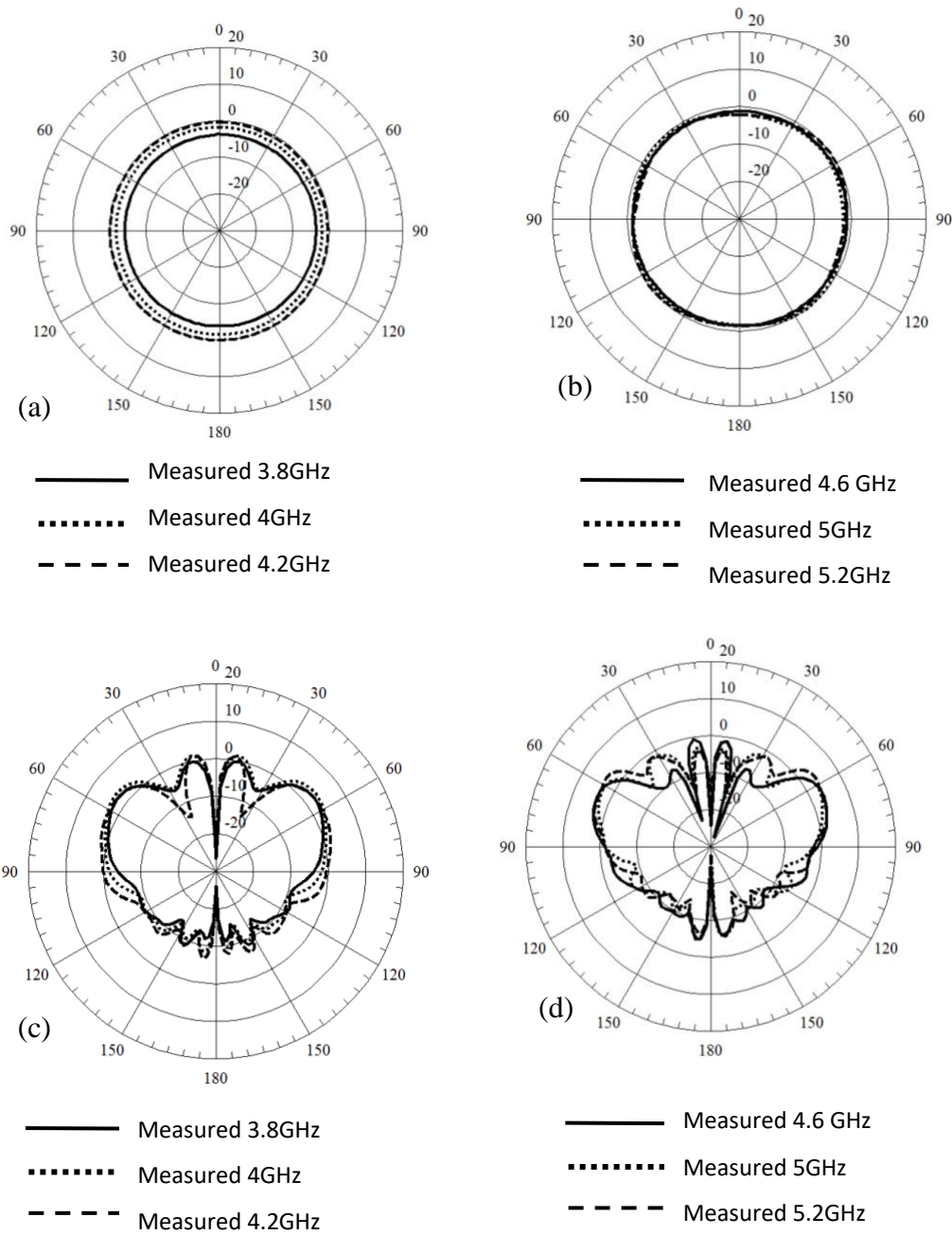
Figure 4-30: Measured realized gain (a) & (b) Azimuthal pattern of SWA, (c) & (d) Elevation pattern of SWA.

The DO standard states that the azimuthal radiation pattern should not have variations greater than 6 dB for each frequency in the DME operating band and should have similar gain as compared to the standard monopole antenna gain. For this purpose, comparison of a quarter-wavelength monopole antenna of height 19 mm, at resonant frequency of 4.2 GHz is simulated and fabricated on the same diameter of ground plane (272 mm). Figure 4-31 shows the simulated and measured S11 of monopole. The simulated and measured realized gain of the proposed SWA and standard monopole antenna is compared at 4.2 GHz is shown in Figure 4-32 (a &b) and Figure 4-33 (a &b). In both cases the gain is almost same as that of monopole antenna with ripples in azimuth plane less than 1 dB. The simulated level of the cross-polarization of SWA in both azimuth and elevation planes is 25 dB less than that of maximum co-polarization as shown in Figure 4-32.
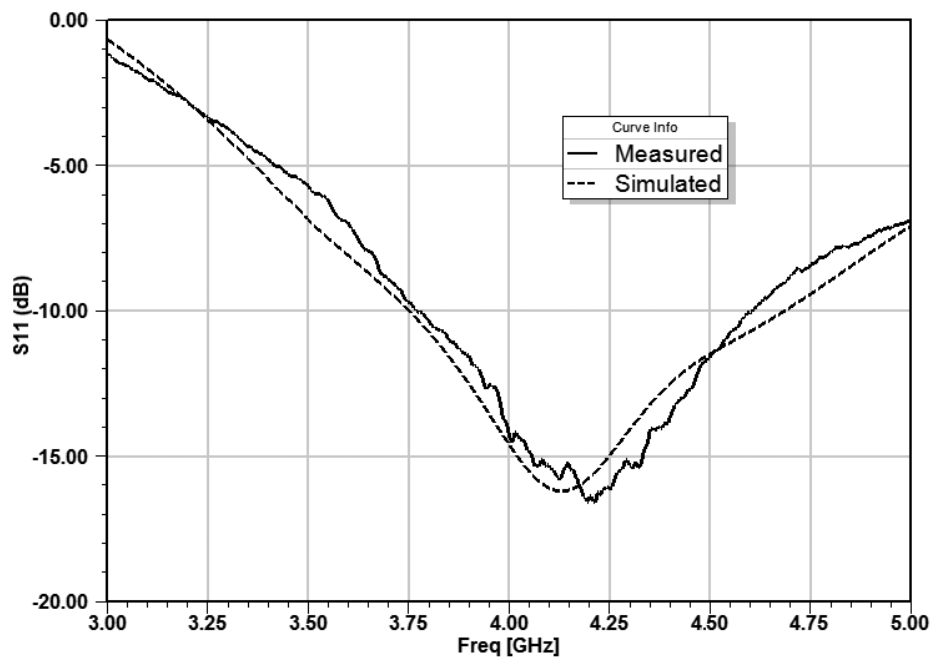
Figure 4-31: Simulated and measured S11 of quarter-wavelength monopole.
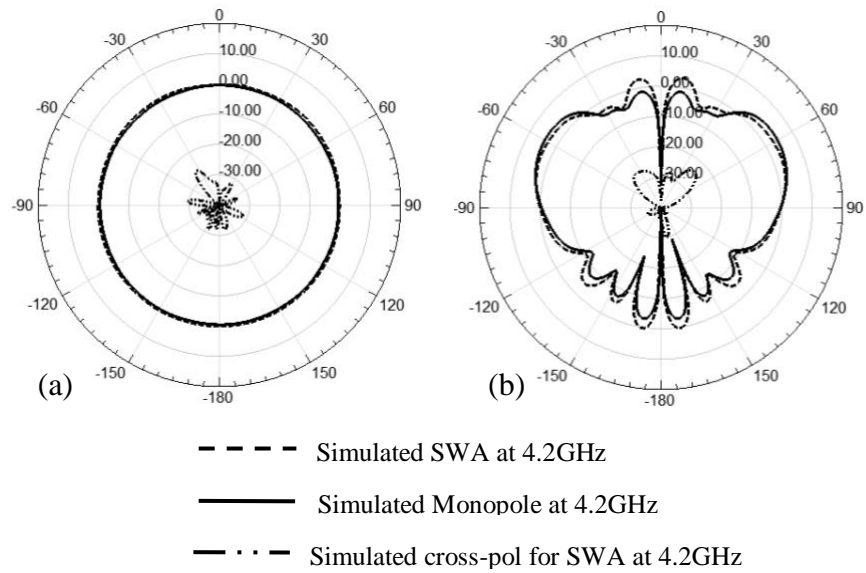
Figure 4-32: Comparison of simulated realized gain of SWA and monopole at 4.2 GHz (a) Azimuthal plane, (b) Elevation plane.
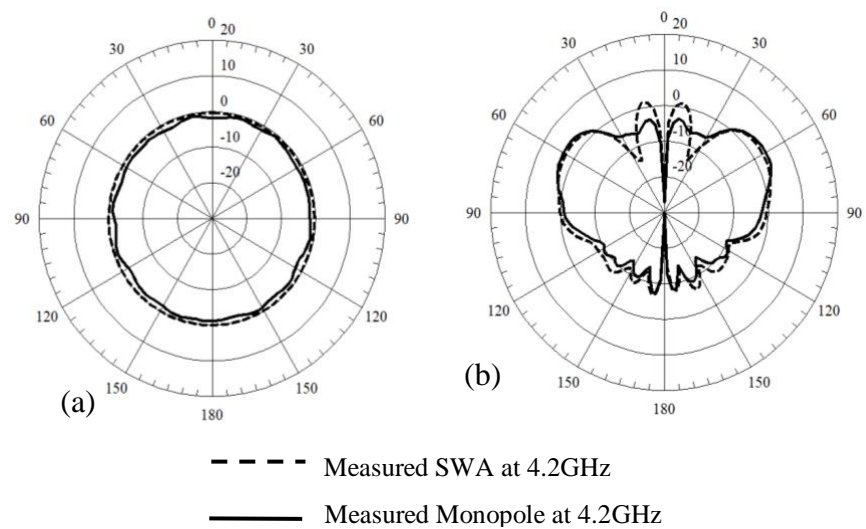
Figure 4-33: Comparison of measured realized gain of SWA and monopole at 4.2 GHz (a) Azimuthal plane, (b) Elevation plane.

4.5   Conclusion

A wideband SWA has been presented in this chapter. The use of circular AMC cells improves the bandwidth of antenna. The fabricated antenna prototype generates vertically polarized omnidirectional radiation pattern similar to that of a monopole. The height of one-fourth scaled antenna is ∼ 7x4=28 mm, considerably reduced as compared to the DME blade antenna (typical height is 55mm to 75 mm). The fabrication of antenna involves multiple dielectric sheets and a ground plane. This has produced airgaps in the structure and has changed the S11 from less than 10 dB to less than 8 dB. This can be improved by placing the first layer with more precaution, using uniform glue and applying uniform pressure to eliminate any airgaps. This low-profile antenna can also be used for other indoor communication applications.

CHAPTER 5   MAGNETO-DIELECTRIC MATERIAL LOADED MONOPOLE ANTENNA

This chapter presents a magneto-dielectric material (MDM) loaded monopole antenna. The presented MDM-based antenna is designed for aircraft DME communication system. At present, blade antennas are used in aircraft for DME operations. These quarter-wavelength blades are located at the upper and lower fuselage of the aircraft. Both the size and location of these antenna makes them prone to physical damages and air drag [24] .Therefore, there is a need to improve these antennas and make them low-profile. The specifications for DME band are listed in

Table 5-1.

Table 5-1: Specifications of DME antenna.

Frequency	DME band
	0.96 – 1.22 GHz
Bandwidth	23%
VSWR / S11	<2 / -10 dB
Radiation Pattern	Omnidirectional with max directivity close to horizon
Polarization	Vertical

5.1   Material loading of antenna

Many techniques have been used in the past to reduce the size of antennas, for example resistive loading [75], reactive loading [76, 77] and material loading [78-81]. The resistive loading of an antenna can help to improve the impedance matching. However, due to resistive losses, efficiency of the antenna is obviously reduced. Reactive loading of antenna includes the use of lumped inductors or capacitors. The impedance of lumped elements is highly frequency dependent which can limit the antenna bandwidth. Material loading with dielectric or magnetic or both can make the antenna size compact. However, one has to find the best match considering the tradeoff of bandwidth or the size of antenna.

5.1.1 Dielectric loading

Dielectric material when used as a substrate for microstrip antenna or as a loading material to any antenna or used in dielectric resonator antenna can shorten the resonant length by factor of up to $\sqrt{\varepsilon_r}$. When the antenna is loaded using a high relative permittivity material, more energy is stored, the quality factor (Q) of antenna is increased and the bandwidth is decreased. Dielectric loaded antennas as presented in the literature [79, 80, 82] offer advantages such as compact size, light weight, low cost and shape versatility (which can also increase the bandwidth when compared to a microstrip antenna).

5.1.2 Magneto-dielectric materials

MDMs are not natural occurring elemental materials, however these materials are synthesized using a mixture of magnetic metal particles and dielectric material. MDM materials are usually powders sintered into a ceramic product. These materials are brittle and can easily break and therefore it is difficult to machine them. Modern material manufacturing industry has shown successful production of materials using magnetic inclusions mixed with dielectric host materials. MDM exhibits both high relative permittivity as well as high relative permeability.

These materials have previously gained significant interest among the antenna designers since they could lead to antenna size reduction without depreciating antenna performance [47, 48, 83]. MDM materials can be isotropic or anisotropic which further broadens the complexity and flexibility of potential antenna designs. The relative permittivity and permeability of MDM are generally frequency dependent.

If an antenna operates in an infinite MDM, i.e. in a media with index of refraction, $n = \sqrt{\varepsilon_r \mu_r}$, the antenna physical dimensions can theoretically be reduced by factor of n. For an antenna operated in air but is partially loaded with MDM, if this material is used in a position where the magnetic field is strong and electric field is weak then the magnetic material properties of this material can be beneficial, without the need for higher permittivity.

5.1.3 Benefits of using magneto dielectric materials

The most common problem seen with the miniaturization of antenna with high-permittivity dielectric material is the impedance mismatch and less bandwidth. The characteristic impedance in

high relative permittivity medium is very low which makes it difficult for impedance matching. The issue of strong field confinement is reduced with the use of MDM of moderate values of permittivity and permeability. The material does not act as a capacitor as in the case of high dielectric material as it has inductance due to the relative permeability. The wave impedance (η) of plane waves propagating in MDM is given by equation (5-1) where η_0 is the free space intrinsic impedance.

$$\eta = \eta_0 \sqrt{\frac{\mu_r}{\varepsilon_r}} \qquad (5\text{-}1)$$

Clearly, for the equal values of ε_r and μ_r, the characteristic impedance is close to the intrinsic impedance of free space and it becomes easy to perform impedance matching. The antenna size reduction factor for dielectric material is $\sqrt{\varepsilon_r}$, whereas in the case of MDM the reduction factor is $\sqrt{\mu_r \varepsilon_r}$. The bandwidth of microstrip patch antenna placed on a MDM with material thickness t is given by equation (5-2) [84].

$$BW = \frac{96 \sqrt{\frac{\mu_r}{\varepsilon_r}}}{\sqrt{2}} \frac{\frac{t}{\lambda_0}}{[4 + 17\sqrt{\mu_r \varepsilon_r}]} \qquad (5\text{-}2)$$

For the case when $\varepsilon_r = \mu_r$, becomes equal

$$BW = \frac{\frac{96t}{\lambda_0}}{\sqrt{2}[4 + 17\varepsilon_r]} \qquad (5\text{-}3)$$

The above two equations can be used to estimate the bandwidth of patch antenna using MDM for different cases of ε_r and μ_r.

- Looking at equation (5-3), if $\mu_r = \varepsilon_r$ and the value of ε_r is small then the patch will have a bandwidth, same as that of patch with air as a substrate.

- If μ_r is very large as compared to ε_r then significant improvement in the bandwidth can be seen.

- Looking at equation (5-3), if $\mu_r = \varepsilon_r$ and if $\varepsilon_r \gg 1$ then the patch bandwidth is almost same as that of patch with ε_r only. The advantage of a material with both μ_r and ε_r is reducing the size of patch by a factor $1/\sqrt{\varepsilon_r \mu_r}$ as compared to only dielectric case where the size is reduced by $1/\sqrt{\varepsilon_r}$ for a same bandwidth.

5.2 Measurement of MDM TTZ500

In the proposed design of loaded monopole antenna, Trans-Tech TTZ500 material is used. It is a Z type hexagonal ferrite (Co_2Z: K) designed for 500 MHz antenna applications. Trans-Tech TTZ500 material is called Z type because of its crystal orientation along Z-axis. This material is available in the form of ceramic slab, thickness from 0.1 inch to 1 inch. Few samples of this material were received as a courtesy from Trans-Tech and were tested for both electric and magnetic properties. X-ray diffraction (XRD) technique was used to study the material properties, details are included as Appendix A.

Dielectric constant and magnetic constant, with respective loss tangents of the MDM were measured. The test fixtures with high stability and repeatable response were used to measure the electric and magnetic characteristic of the material. Dielectric constant was measured using Keysight (formerly Agilent) 85070 dielectric probe kit and Agilent network analyzer N5247A. High temperature probe kit was used to measure the solid sample. A sample of disc with diameter $d > 20\ mm$ and thickness $t > \sqrt{\varepsilon_r}$ is used as shown in Figure 5-1. The measurement setup is shown in Figure 5-2 [85].
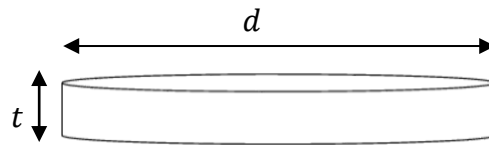
Figure 5-1: Sample for dielectric testing.
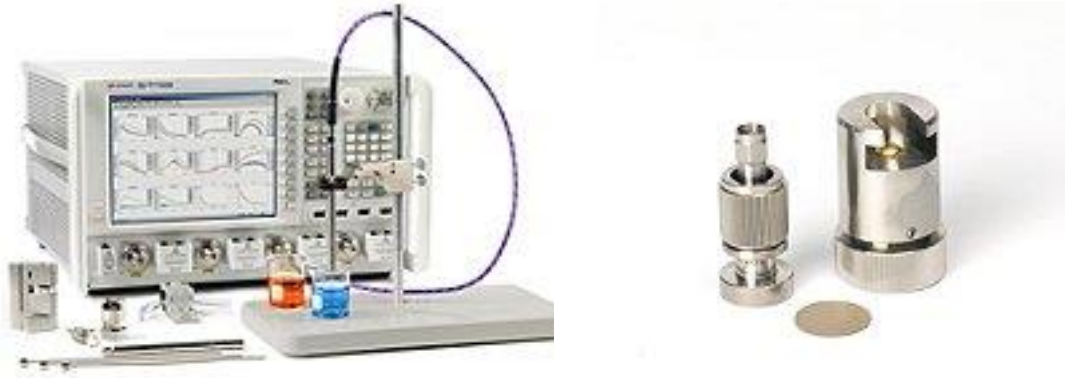
Figure 5-2: Agilent network analyzer N5247A with high temperature test probe to measure complex permittivity.

Measurements were performed for magnetic constant using a Keysight impedance analyzer E4991A (maximum frequency 1 GHz) using 16454A magnetic material test fixture. Inductance method is used to measure the permeability of MDM by placing a torus shaped core wrapped with a wire. Complex permeability is calculated from the inductance values at the end of the core [86]. The sample torus has $c < 22$ mm, $b > 3.1$ mm and $h < 8.5$ mm as given in Figure 5-3 [86].The measurement setup is shown in Figure 5-4 [86]. The samples used for testing were cut through water jet machine and shown in Figure 5-5.
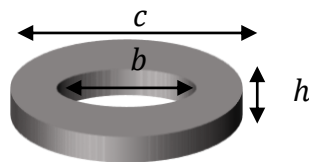
Figure 5-3: Sample for magnetic testing.
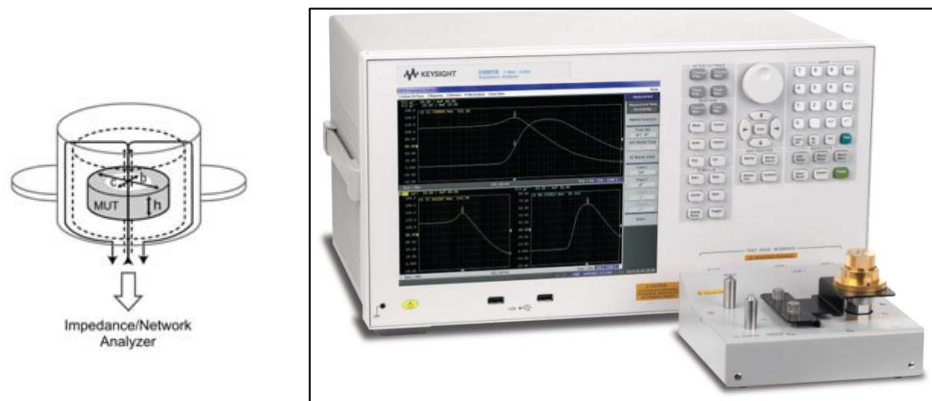
Figure 5-4: Agilent impedance analyzer E4991A with test fixture 16454A to measure complex permeability.

Figure 5-5: Samples for testing the dielectric and magnetic properties of TTZ500.

Table 5-2 shows the comparison of measured and data sheet values for relative permittivity and permeability at different frequencies.

Table 5-2: Measured and data sheet values for relative permittivity and permeability.

Frequency	Permittivity			Permeability			
	Data sheet	Measured		Data Sheet		Measured	
		ε_r	$tan\delta$	μ_r	$tan\delta$	μ_r	$tan\delta$
700 MHz	10.07	10.4	0.02	9.9	0.05	9.3	0.34
900 MHz	-	10.3	0.02	10.1	0.06	9.7	0.65
1000 MHz	-	10.4	0.03	13.8	0.1	11.7	0.9

Measured magnetic loss tangent value was found higher than the values provided in the data sheet. At 700 MHz the measured magnetic loss tangent is 0.34 whereas the data sheet specifies 0.05. At 900 MHz the measured magnetic loss tangent is 0.65 however according to the data sheet it should be 0.06. The difference in these values is almost 10 times. Which could be due to the differences in the samples used for data sheet and sample we tested.

As TTZ500 also has magnetic properties, results of X-ray diffraction (XRD) test can be used to identify the isotropic nature of the material. Isotropic magnet can be magnetized from any direction. On the other hand, crystal direction of an anisotropic magnet is unidirectional so the magnetizing can only be possible from one direction and the magnetic force is strongly oriented toward one direction.

5.3   Design of an MDM loaded monopole antenna

An unloaded monopole antenna is made using a thin wire of diameter 1.3 mm is simulated on a circular ground plane of diameter 300 mm as shown in Figure 5-6. The selected diameter of the ground plane is smaller than DME DO-189 standard ground plane, so that it allows us to place the antenna in a near-field chamber available in our laboratory for antenna testing. The diameter of the wire is kept similar to the inner conductor of SMA connector to be used as a coaxial feed. The antenna consists of a metal wire of height, h, $\frac{\lambda}{4} = 62$ mm, where λ is the wavelength at
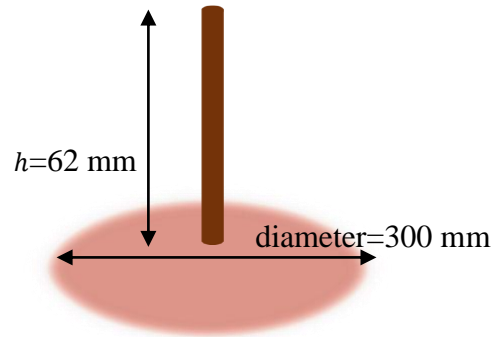
Figure 5-6: Unloaded monopole on a metallic ground.

1.2 GHz, the upper edge frequency of DME band. Optimal placement of material can be determined by analyzing the radiated fields of the monopole antenna using ANSYS HFSS (finite elements method, used in driven mode). Magnetic field of monopole can be affected if loading is done at the base of the monopole and electric field is affected if the loading is done on its tip as shown in Figure 5-7. Figure 5-8, shows a simulation model of loaded monopole, where a disc of MDM has been placed at the tip of the monopole. The ε_r, μ_r and $tan\delta$ used in the simulation are same as measured and given in Table 5-2.
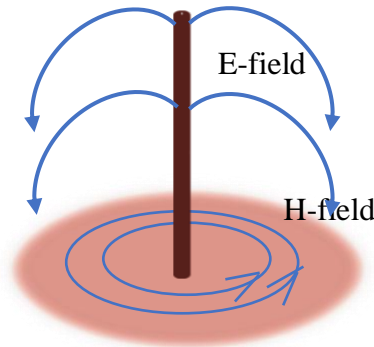
Figure 5-7: Electric and magnetic fields of monopole.

The size of TTZ disc was selected based on two factors. First, a disc with diameter of at least 20 mm was required for the dielectric testing of material. Second, the available TTZ material sample was a slab of 100 mm x 100 mm x 3 mm, which confines the maximum size limit of the disc, as it was used to get few samples out of it.

A parametric study is performed using disc diameter $d1$ in the simulations. With the increase in the $d1$, resonant frequency shifts towards lower frequency. For $d1=28$ mm the resonant frequency is close to 1 GHz as shown in Figure 5-9.
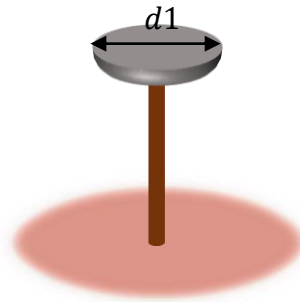
Figure 5-8: MDM disc placed at the top of monopole antenna.
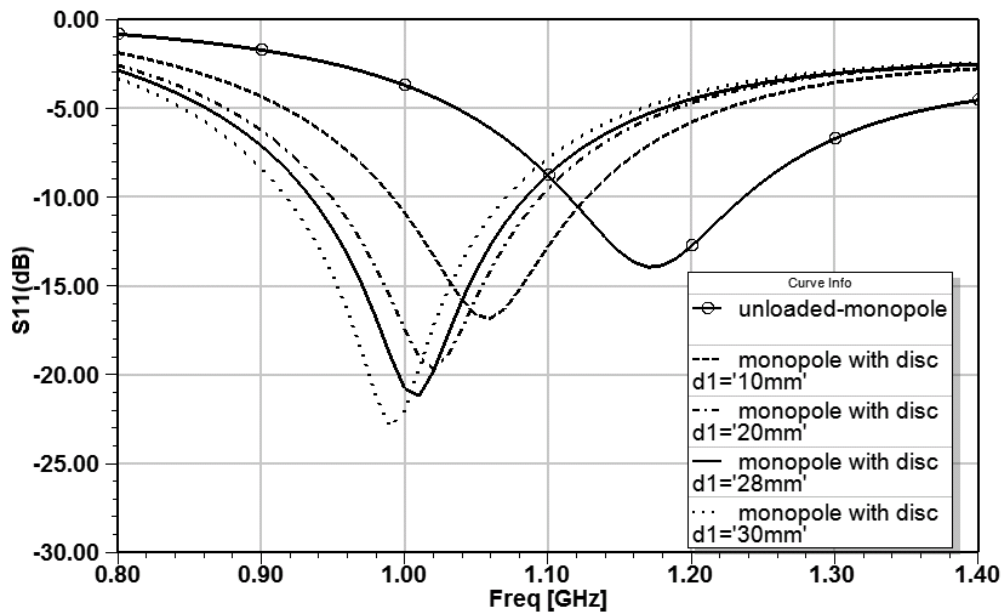
Figure 5-9: Parametric sweep of diameter of disc $d1$.

Figure 5-10, shows a loaded monopole, where a circular ring of MDM having inner diameter, d=15 mm, outer diameter $d2$=22 mm and thickness of 3 mm is placed at the bottom of the monopole. Again, $d2$ has a limitation in terms of required sample size for magnetic testing of material. A parametric study is done on the size of the ring, in simulations as shown in Figure 5-11, where d is the inner diameter of the ring and $d2$ is the outer diameter of the ring. The lower the value of d, the closer the material gets to the wire antenna and the lower is the resonant frequency. Keeping in view the fabrication limitation due to water jet machine, the value of d=15 mm was selected which has moved the frequency close to 1.1 GHz.
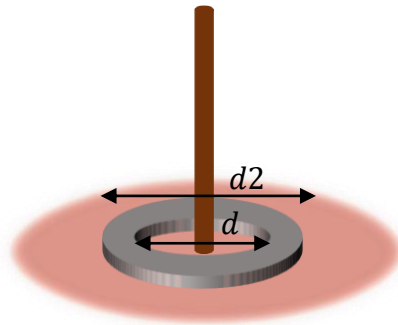
Figure 5-10: MDM ring placed at the bottom of monopole antenna.
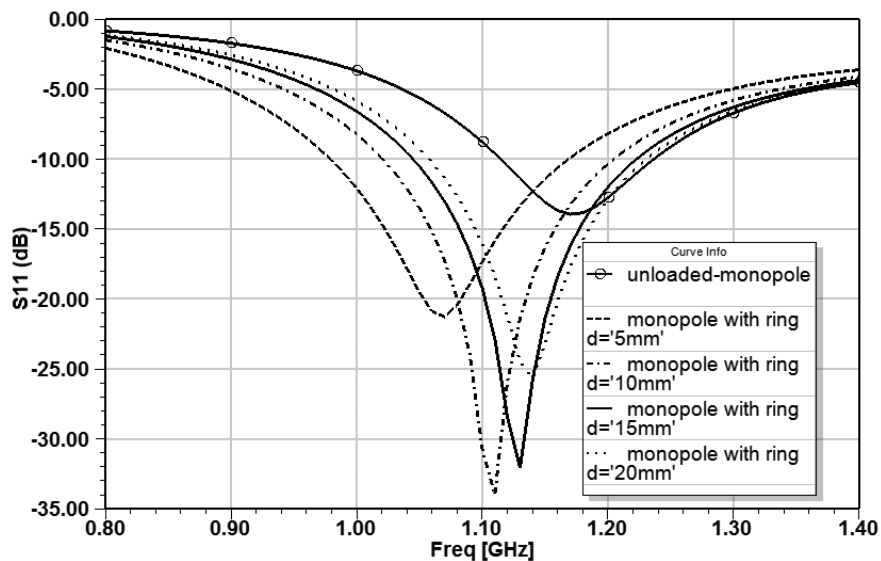
Figure 5-11: Parametric sweep of diameter of ring d.

Figure 5-12 shows a loaded monopole where both a disc and a circular ring of MDM have been placed. The comparison of simulated S11 of unloaded to loaded monopole is shown in Figure 5-13. Loading the monopole with disc and ring has moved the resonant frequency from 1.19 GHz to 0.97 GHz. Meanwhile, the FBW for 10 dB return loss increased from 10% for the unloaded monopole to 18% for the loaded monopole.
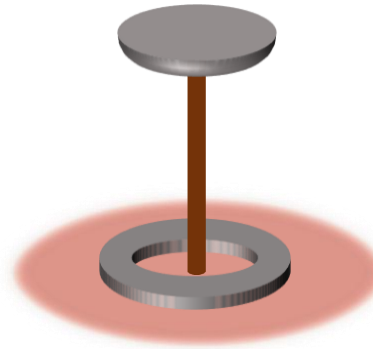
Figure 5-12: MDM disc and ring placed on the monopole antenna.
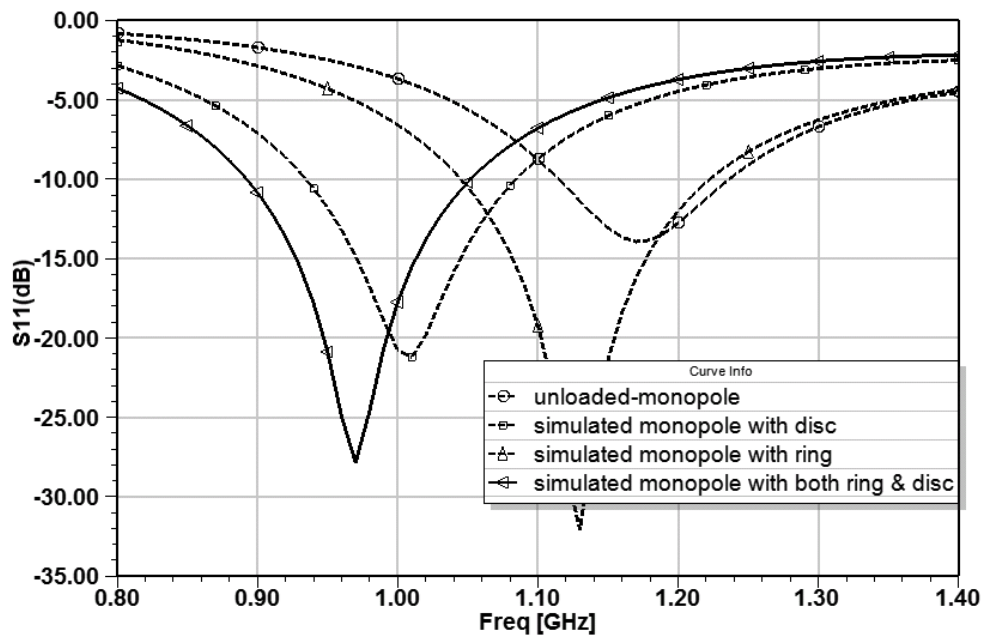
Figure 5-13: Comparison of simulated S11 of monopole with disc, with ring and both ring and disc.

Using the same value of both permittivity and permeability of MDM, the wave impedance in the material is the same as in vacuum as can be seen in equation ((5-1). Therefore, the MDM loading leads to a shrinking of the antenna electrical length (or down-shifting of the operation frequency) without causing reflections at its interface. This is different from the dielectric resonator antennas in which internal reflections are needed to introduce new resonances. Another case is studied in simulations where the disc is only dielectric, and the ring is only magnetic material, using same μ_r and ε_r values as given in Table 5-2. It has been seen in Figure 5-14 the FBW for (a) MDM for both ring and disc is 17.9% and for (b) dielectric material for disc and magnetic material for ring, its 16.8%. Although for (a) the down-shifting of operation frequency is more but for (b) the FBW is more which helps in demonstrating the above statement.

Further simulations were performed to see the impact of only dielectric loading on the monopole. For only top disc loading with ε_r =10, the FBW was 12%, with ε_r = 20, FBW increased to 15% and with both disc and ring and ε_r =10 the FBW was 12%. It shows that the dielectric material can only affect the electric fields at the tip of the monopole and has no influence on the bottom of monopole.
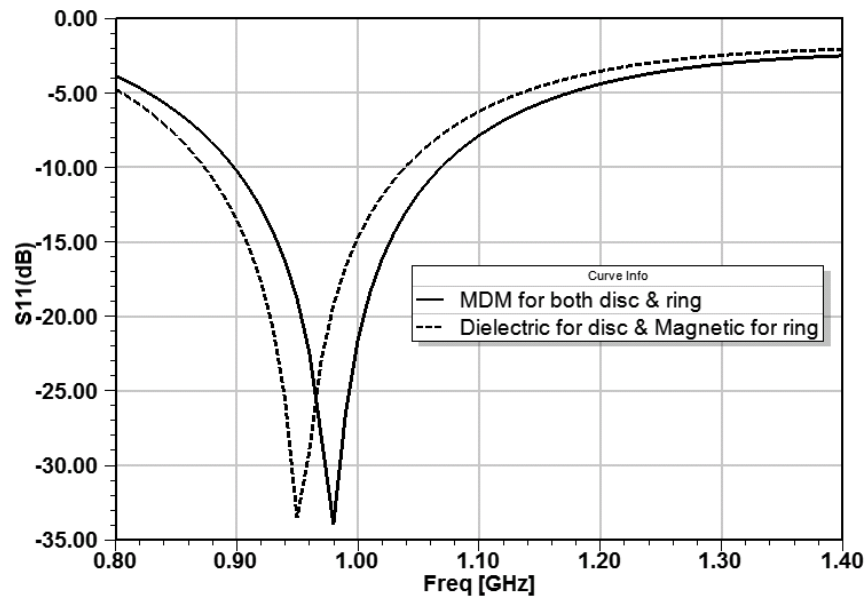
Figure 5-14: Comparison of simulation of MDM for both ring and disc and dielectric material for disc and magnetic material for ring.

To understand the impact of lossy magnetic material on the bandwidth, a less lossy TTZ500 with magnetic $tan\delta = 0.1$ instead of 0.5 was used in the simulation model. Figure 5-15 shows that the bandwidth of the monopole loaded with MDM of magnetic $tan\delta = 0.5$ is 30 MHz greater than the bandwidth of monopole loaded with MDM with a magnetic $tan\delta = 0.1$. However, for the case where the magnetic $tan\delta = 0.1$ the FBW is 14.5% as compared to the FBW of a bare monopole that is 10%. This implies that lossy material with magnetic $tan\delta = 0.5$ and less lossy magnetic $tan\delta = 0.1$, both have effect on the bandwidth of antenna as compared to the bare monopole antenna bandwidth.

The radiation characteristics for the proposed loaded monopole antenna are compared to the unloaded monopole antenna in simulations. Figure 5-16 shows the realized gain at 1.1 GHz for azimuth and elevation planes for unloaded monopole, loaded monopole with ring and loaded monopole with both ring and disc. A decrease of 2 dB gain from unloaded to loaded monopole has been found in the graph, which is due to the lossy nature of MDM. The radiation characteristic that includes the measured gain patterns and efficiency of antenna is discussed in the next section.
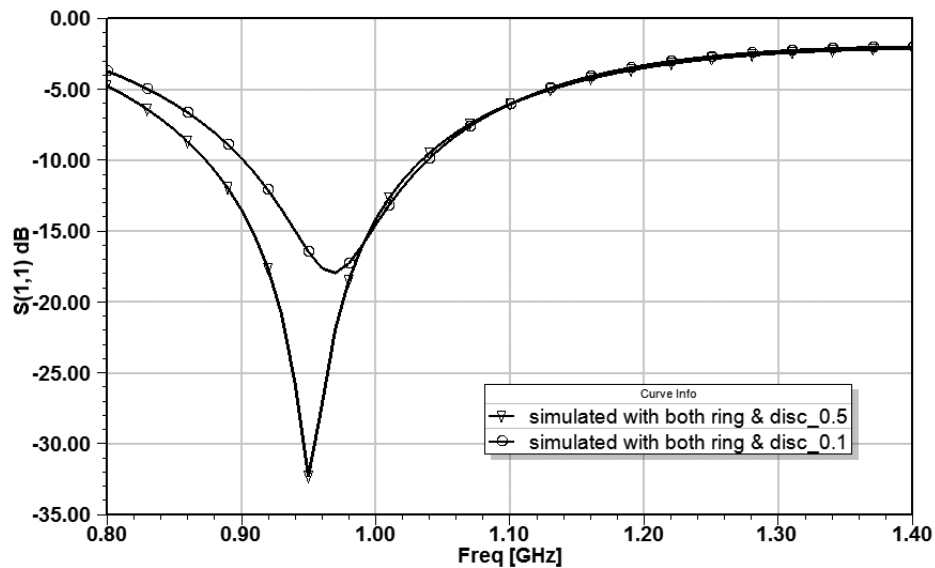
Figure 5-15 Comparison of simulated S11 with magnetic loss tangent 0.1 and 0.5.
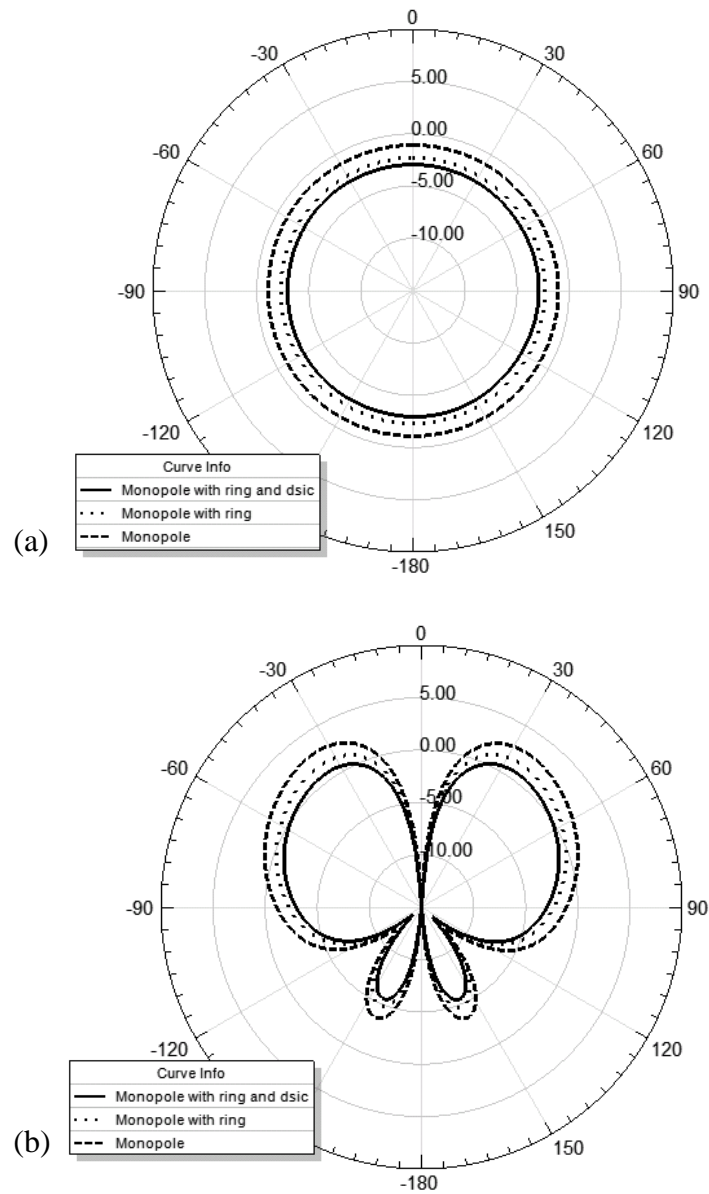
Figure 5-16: Simulated realized gain at 1.1 GHz for monopole, monopole with disc and monopole with both ring and disc (a) Azimuth (H), (b) Elevation (E).

5.4 Fabrication and measurement of a MDM loaded antenna

First, a monopole antenna with height, $h = 62$ mm and plate diameter 300 mm was placed on an aluminum ground plane as presented in Figure 5-6. The return loss and radiation characteristics of unloaded monopole antenna were measured. The MDM disc and ring were made of the chosen simulated dimensions of d, $d1$ and $d2$. The disc and ring diameters were selected using the result of the parametric study, as discussed in the previous section. A ring shaped MDM was placed at the bottom of the antenna and S11 was measured. Next both ring and disc were placed together and S11 and radiation characteristics were measured. Figure 5-17 shows the antenna prototype, where both ring and disc were glued to wire monopole and a styrofoam block was used to give extra stability to the top disc. In Figure 5-17, it is difficult to see the ring as styrofoam is covering it in the photo.
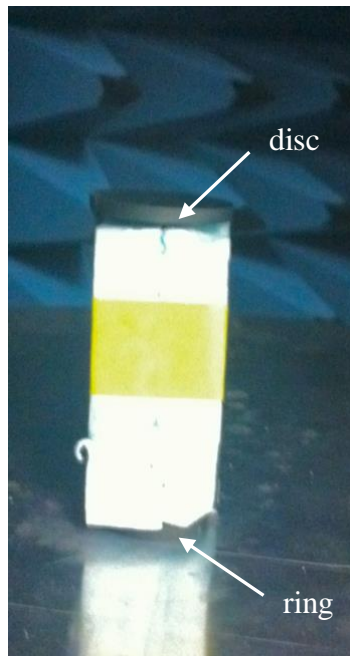
Figure 5-17: Monopole antenna loaded with TTZ material and wrapped by styrofoam.

A comparison of the simulated and measured S11 is shown for unloaded and loaded monopoles in Figure 5-8. The measured results for each case show a good agreement with the simulations by using ε_r, μ_r and $tan\delta$ as given in Table 5-2. In the "ring only" case, the ring is located off centered, which justify the observed change of 50 MHz from the simulated results. The measured resonant frequency of the unloaded monopole is 1.19 GHz, which is shifted to 1.01 GHz by using a disc,

and to 0.98 GHz by using both disc and ring. In terms of physical dimensions, at the lowest frequency 0.89 GHz of band covering measured S11<-10 dB (0.89 to 1.09 GHz), theoretically, a quarter-wavelength in free space is 84.25 mm. The height of loaded monopole in our case is 65 mm, which includes the 3 mm thick disc that make the height approximately one fifth of wavelength. So, the height is reduced by 29.5 % in the case of loaded monopole as compared to unloaded case. The results in Figure 5-18 further shows that the -10 dB FBW of the unloaded monopole is 11.8%, for the monopole with disc it is 15.6%, and for the monopole with both disc and ring it is 20%. Thus, the loaded monopole operation has been shifted to lower operating frequencies while keeping a good bandwidth. Table 5-3 gives the comparison of measured fractional bandwidth for each model. The antenna can be adjusted by shifting the response by 70 MHz to cover the DME band (0.96-1.22 GHz) by tuning the disc and ring dimensions or by optimizing the shape of loading elements as in this case simple ring and disc have been considered. That will bring it to DME band 0.96 GHz to 1.2 GHz instead of 0.89 to 1.09 GHz.
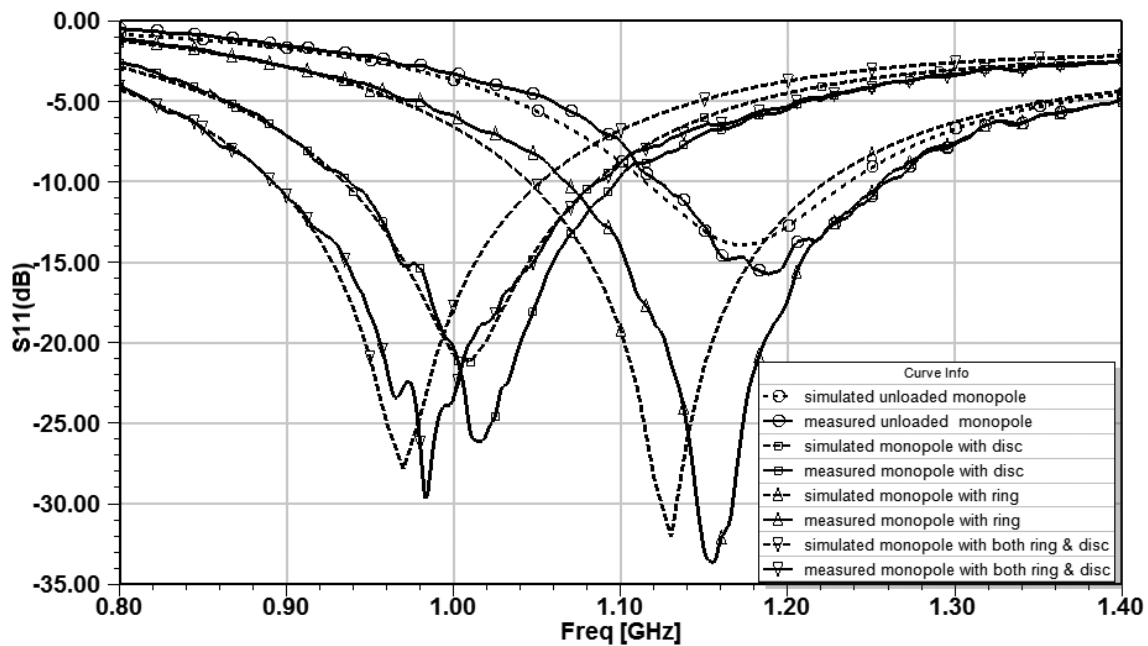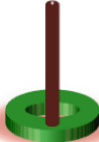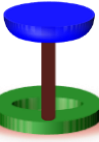
Figure 5-18: Comparison of simulated and measured S11.

Table 5-3: Measured fractional bandwidth.

	Different antenna models	Frequency GHz	-10 dB Fractional Bandwidth
1.		1.12 to 1.26	11.76 %
2.		0.94 to 1.10	15.6 %
3.		1.06 to 1.26	17.2 %
4.		0.89 to 1.09	20.2 %

The radiation pattern of loaded monopole with both disc and ring is similar to that of monopole for all the frequencies in the range 0.89 GHz to 1.09 GHz. The loaded antenna was tested for radiation pattern in a Satimo Starlab test setup. Figure 5-19 shows the antenna in the chamber that can test antennas from 800 MHz to 6 GHz. In this test, the size of the ground plane is not compliant with the requirements of DO-189 due to volume limitations of the test setup. However, the test is still useful to make relative comparisons between loaded and unloaded monopoles.
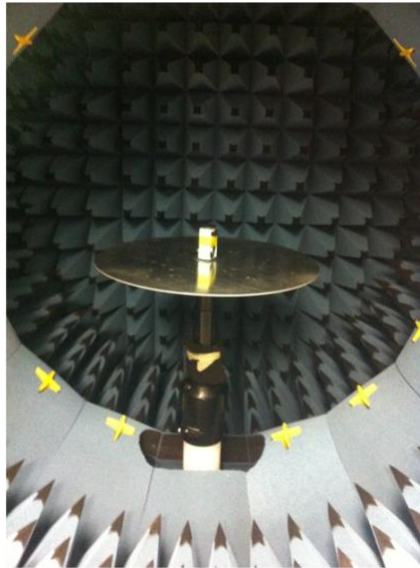
Figure 5-19: Radiation pattern measurement in Satimo Starlab test setup.

The measured realized gain of the antenna is shown in Figure 5-20, at 1.1 GHz, which is the center frequency of DME band, and where S11 measured is -9 dB for both loaded and unloaded monopole antenna.
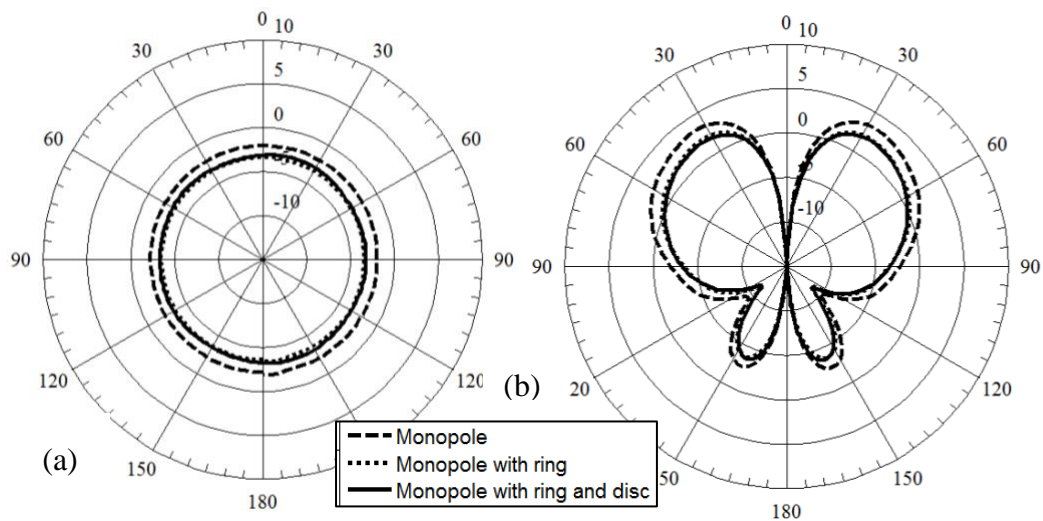
Figure 5-20: Measured realized gain of loaded and unloaded monopole antenna. (a) azimuth plane, (b) vertical plane.

The pattern is identical to monopole antenna, with maximum of 2 dB difference of the loaded monopole because of the magnetic and dielectric losses of the TTZ500 material. It is however not acceptable based on the DO-189 standard, because the gain has to be comparable to that of a bare quarter-wave monopole. The radiation efficiency (η_{rad}) of the antenna is calculated from the total power radiated by the antenna to the total power accepted by an antenna. The total efficiency (η_{total}) also considers the antenna mismatch, conductor and dielectric losses. The measured η_{total} of antenna is computed by the Satimo software. Figure 5-21, compares the η_{total} of unloaded monopole, loaded with ring and loaded with both disc and ring.

The η_{total} of unloaded monopole is maximum at 1.15 GHz due to resonance. It has less value below 1.15 GHz due to mismatch loss. However, the loaded monopole with both disc and ring has an average η_{total} of 55% over the DME band mainly due to magnetic losses. It is one of the disadvantages of this antenna but in small antenna applications of wireless communication system efficiency better than 50% is usually acceptable.
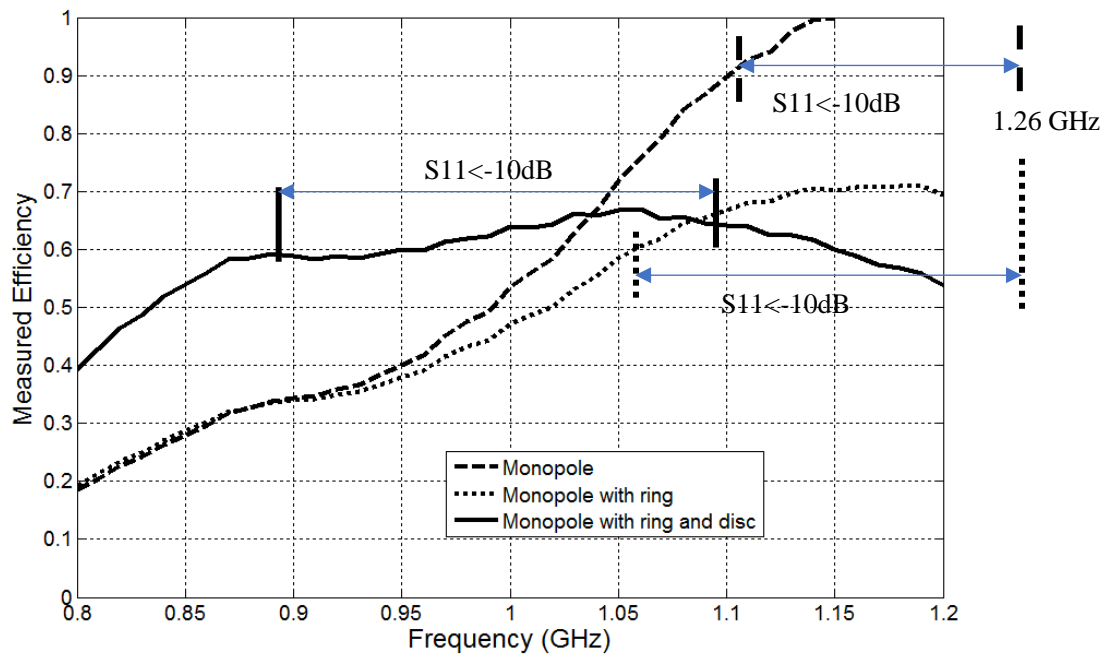
Figure 5-21: Comparison of measured efficiency of loaded and unloaded monopole antenna.

5.5   Conclusion

Design of a monopole antenna with MDM has been presented. In the proposed design the TTZ material is lossy which reduces the efficiency of antenna. The DME band antenna efficiency for the proposed design is better than 55%. The machining of this brittle material was challenging. Other shapes of loaded material can be investigated to see the impact on the electric and magnetic fields. However, the use of a simple disc and ring with approximately same value of ε_r and μ_r reduces the height of a monopole antenna by 29% and almost doubles the fractional bandwidth i.e. from 11.76% to 20.2%. The antenna design has a radiation pattern similar to that of monopole for all the frequencies in between 0.89 GHz to 1.12 GHz. The required frequency of DME band can be achieved by scaling/tuning the shape of disc and ring, to comply with the design requirements.

CHAPTER 6   COUPLED SECTORAL LOOP ANTENNA FOR DME APPLICATIONS

In this chapter we present a novel design technique to enhance the directivity of a low-profile antenna for the use of distance measuring equipment (DME) avionic system. The antenna directivity is improved by using a horizontal grooved ground plane. This solution is attained by solving the beam elevation problem with a circular slot antenna, while achieving an acceptable bandwidth with the use of a matching circuit. The proposed design has a height equal 0.1λ at the lowest operating frequency and the radiation pattern is comparable with that of a quarter-wavelength monopole on the same ground plane dimensions. This proposed antenna can be a good candidate to replace the well-known DME blade antennas.

6.1 Distance measuring equipment system (DME)

In section 2.3 the function of DME system is discussed. The aircraft uses the DME system to continuously display the distance of the aircraft from ground station. It is required to have maximum directivity of the DME antenna at horizon i.e., for θ between 60° to 90° depending upon the height of the aircraft as presented in Figure 6-1. The gain and radiation pattern requirements for DME antenna should be compliant with DO 189 which is previously explained in section 1.2. The specifications of DME antenna is listed in Table 6-1.
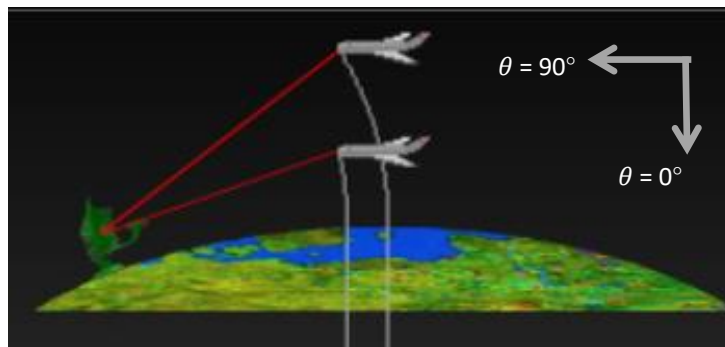
Figure 6-1 : Aircraft using DME communication system at different heights from the control station.

Table 6-1:Specifications of DME system.

Frequency	0.96 – 1.22 GHz
Bandwidth	23%
VSWR / S11	<2 / -10 dB
Radiation Pattern	Omnidirectional with max close to horizon

6.2 Why not blades?

Blade antenna are a popular choice for DME system. These antennas are installed at the lower forward portion of fuselage of aircraft. Blades used for DME are in general monopoles encapsulated in a covering to provide better aerodynamic properties. For the aircraft aerodynamics and mechanical stability external antennas are sensitive factors. During a flight, airstream flows around an antenna and generates drag. Therefore, it is highly required to have an alternate antenna, which is low-profile with height less than that of a blade antenna and with similar radiation pattern as that of a monopole. Having an antenna low-profile, recessed or conformal helps reduce collision with ground equipment during aircraft maintenance and service and reduce in flight aerodynamic drag.

6.3 Monopole antenna and its dependence on the ground plane

A monopole antenna utilizes ground plane as a part of its radiator, therefore its radiation pattern depends on the size of the ground plane. For an infinite ground plane, the peak directivity of a short monopole is at the horizon but for finite size ground plane the main beam will tilt upwards from the ground plane due to edge diffraction. Generally, for a given frequency, the size of the ground plane is increased in order to minimize the upward tilt. Another method (discussed next) is to redesign the monopole to make it to radiate at lower elevation angles. The fuselage of an aircraft is the place where most of the antennas are installed. The fuselage acts as a ground plane and depending upon the frequency and wavelength of antenna, the size of fuselage impacts the radiation pattern.

6.4 Concept of dual magnetic current loop antenna

To replace the quarter-wave monopole with a low-profile antenna, with same polarization and with similar pattern, a circular slot antenna in a ground plane can be a choice. The far-field of a slot is the same as that of a magnetic loop due to the equivalence theorem [87] as shown in Figure 6-2. The fields of a narrow slot can be found from an equivalent magnetic current along the axis of slot. If antennas are dual it is possible to write the field expression of one antenna from the field of other the antenna by using principle of duality. Following this, an infinitesimal electric dipole is equivalent to an infinitesimal magnetic current loop, but when the two have finite length (or finite radius for the loop) they are no longer equivalent. However, we can say that they have similar (not equivalent) radiation patterns and polarization. shown in Figure 6-2.
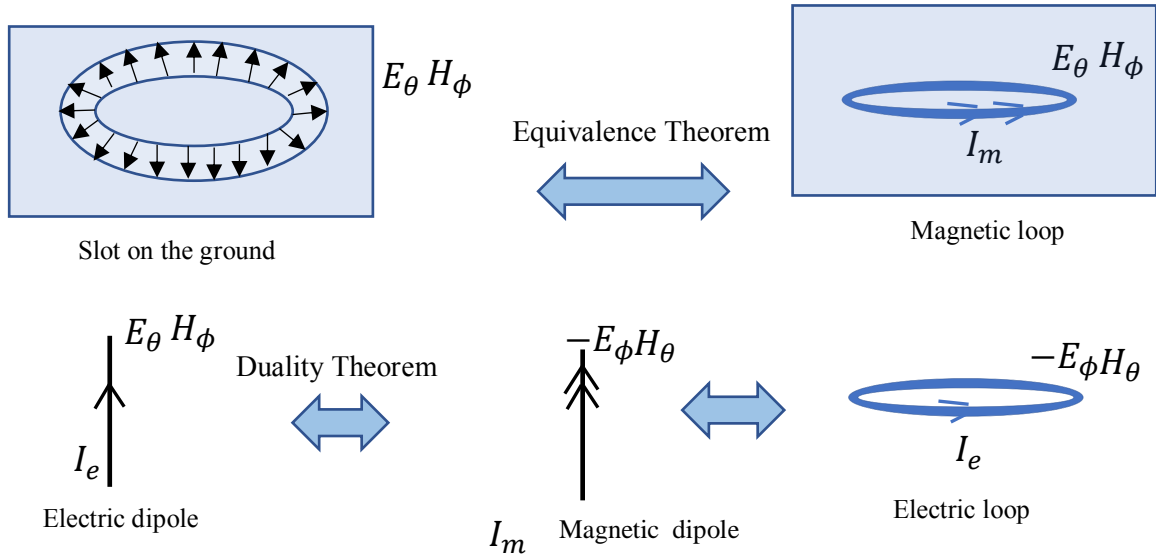
Figure 6-2: (a) Slot in a ground plane equivalent to magnetic loop, (b) Electric dipole is dual of an electric loop.

The far-field electric and magnetic fields of ideal dipole is given in equation (6-1) and (6-2) The far-field electric and magnetic fields of a small loop of electric current is given in equation (6-3) and (6-4). Where η_o is the intrinsic impedance, k is the propagation constant in free space, I_d is the constant current for dipole, l is the length of dipole, a is the radius of loop, I_m is the magnetic current for magnetic dipole, and θ is the angle with the monopole vertical axis in the elevation plane.

$$E_\theta = j\eta_o k I_d l sin\theta \frac{e^{-jkr}}{4\pi r} \hat{\theta} \qquad (6\text{-}1)$$

$$H_\phi = jk I_d l sin\theta \frac{e^{-jkr}}{4\pi r} \hat{\Phi} \qquad (6\text{-}2)$$

$$E_\phi = -jk I_m l sin\theta \frac{e^{-jkr}}{4\pi r} \hat{\Phi} \qquad (6\text{-}3)$$

$$H_\theta = j I_m l w\varepsilon sin\theta \frac{e^{-jkr}}{4\pi r} \hat{\theta} \qquad (6\text{-}4)$$

In the proposed design the loops are not infinitesimal and the radiated field (E and H) of loop is given by equation (6-5) and (6-6) , where J_1 is the first order Bessel's function and θ is the angle with the monopole vertical axis in the elevation plane.

$$E_\phi(\theta) = k\eta_o I_m a J_1(kasin\theta) \frac{e^{-jkr}}{2r} \qquad (6\text{-}5)$$

$$H_\theta(\theta) = -\frac{E_\phi}{\eta_o} = -k I_m a J_1(kasin\theta) \frac{e^{-jkr}}{2\eta_o r} \qquad (6\text{-}6)$$

Figure 6-3 shows two concentric loops, with radii a and b and azimuthal magnetic source currents I_{ma} and I_{mb} respectively.
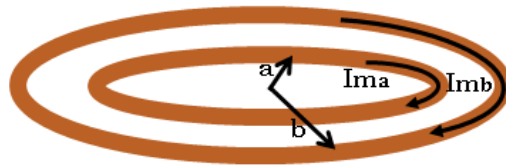
Figure 6-3: Two concentric loops of radius a & b with magnetic currents I_{ma} and I_{mb}.

The total E-field due to two loops is given by equation (6-7). Where in equation (6-8) is approximate E-field of two loops. Where R, is the relative magnitude and phase difference of the magnetic currents and can control the directivity of the radiating source.

$$E = \left(I_{ma}kaJ_1(kasin\theta) + I_{mb}kbJ_1(kbsin\theta)\right)\frac{e^{-jkr}}{2r} \tag{6-7}$$

$$E \propto \left(kaJ_1(kasin\theta) + RkbJ_1(kbsin\theta)\right); \quad where \; R = \frac{I_{mb}}{I_{ma}} \tag{6-8}$$

The directivity is defined by equation (6-9). The average electric field (ave ($|E\theta|$)) is calculated over the theta $0 \leq \theta \leq 90°$. This is assuming no radiation in the range $90° \leq \theta \leq 180°$ due to the presence of an infinite metallic ground plane at $z = 0$.

$$D = 10log_{10}\left[\frac{|E_\theta|^2}{ave(|E_\theta|^2)}\right] \tag{6-9}$$

Figure 6-4 shows the directivity plot for a dipole, one loop (R=0) and after trying multiple cases for R we have found R= - 0.35 as a ratio of two loop currents where the directivity of two loop at
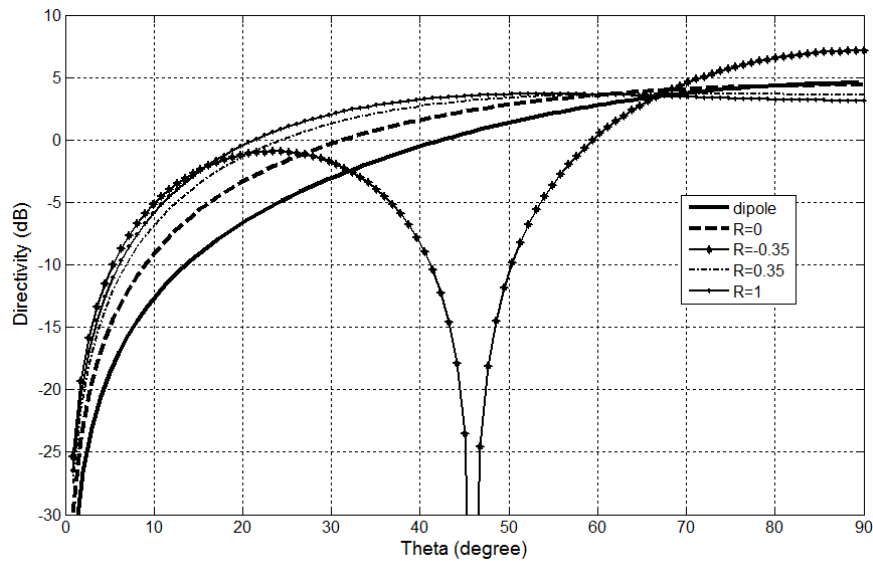
Figure 6-4: Plot of directivity of two magnetic current loops with inner loop radius $a = 0.2\,\lambda$ and outer loop radius is $b = 0.4\,\lambda$.

the horizon $\theta=90°$ is better than a dipole for $a = 0.2\,\lambda$, and $b = 0.4\,\lambda$ (the choice of a and b is made by the physical size of antenna model shortly presented). We cannot control the theoretical value of R numerically (the current ratio of two loops) in the simulation model (physical realization of two loops), because one loop excites the second loop by coupling. Therefore, in the simulation model the size of both loops will be optimized to get the maximum coupling.

6.5 Physical implementation of dual-loop concept

To simplify the feeding mechanism for two slots/ two loops in a practical antenna, Figure 6-5 shows possible physical implementation. The loop of radius a is resulting from the radial E-field at the edge of the upper metal disc, whereas the loop of radius b results from the radial E-field at the edge of the lower metal disc. In practice, only the upper disc is directly excited (e.g. with a coaxial feed line) and electromagnetic coupling of the first loop excites the other. This concept will be applied to the coupled sectorial loop antenna proposed in [88], to which we will introduce a horizontal groove acting as second loop underneath the upper plate.
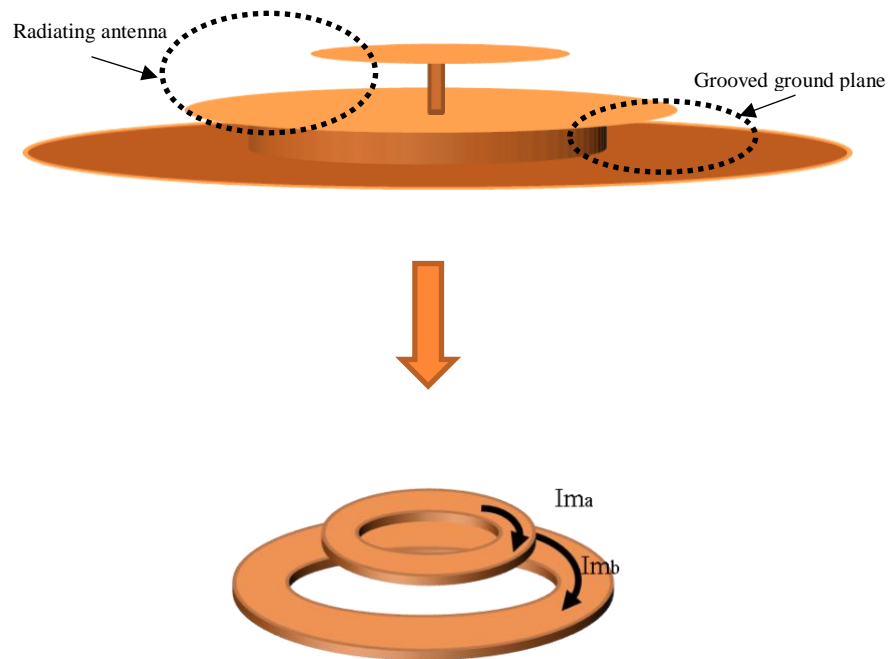
Figure 6-5 : Realization of dual magnetic loop concept, CSLA acting as inner loop and placed on grooved ground plane which is acting as outer loop, and two concentric magnetic loop currents.

6.6 Design of horizontal grooved antenna

The design starts by first simulating the top disc. For that, the coupled sectorial loop antenna (CSLA) [88] was selected over a ground plane as illustrated in Figure 6-6. The antenna consists of four fins top-loaded with a top disc with an annular slot. Top disc and each fin are made of dielectric Rogers RO4003 $\varepsilon_r = 3.55$ and $tan\delta = 0.0027$. One side of each fin has metal and only the lower side of the top-disc has metal. Each fin is shorted to the ground plane and has a slot on one side. A SMA connector is used to feed the antenna right in the middle where four fins meet and connects. Next, the principle of operation is discussed. The antenna fins work in similar manner as that of shorted pins as discussed earlier in the design of TCAS antenna in Chapter.3. An annular slot in the top plate and slots in the fins of the antenna are optimized for broadband impedance matching. Isometric view of the simulation model of the antenna is shown in Figure 6-6, where the diameter of the top plate is 120 mm and height of the antenna from the ground plane is 17.5 mm.
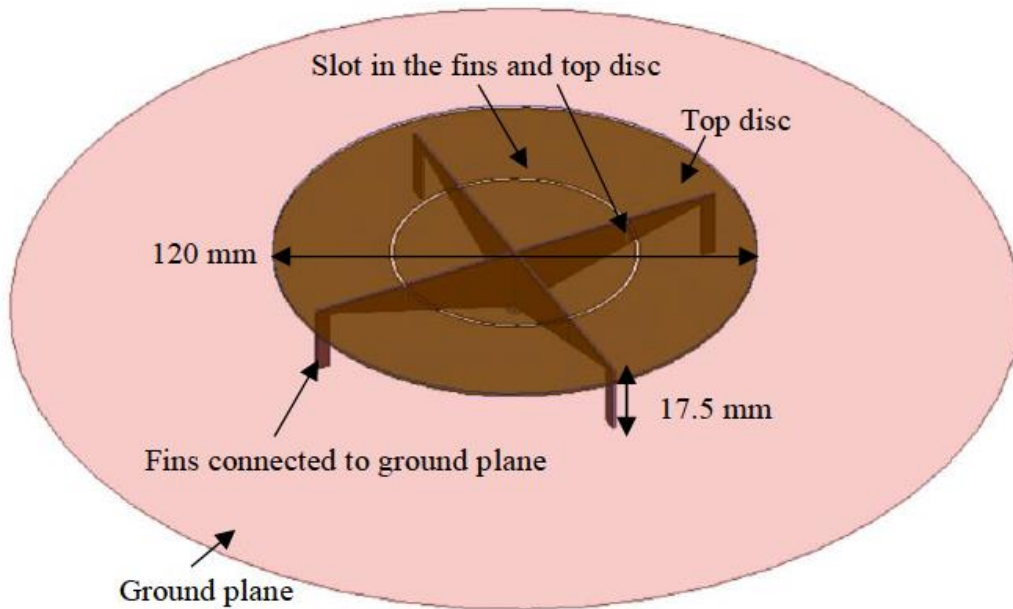
Figure 6-6: Simulation model of CSLA antenna on a finite ground plane.

Figure 6-7 shows the CSLA with a finite ground plane (diameter of 250 mm) placed on a cylindrical ring which is placed on a finite horizontal ground plane of diameter 420 mm. This cylindrical ring has a diameter (210 mm) and forms a horizontal annular groove. As explained earlier, placement of groove beneath the CSLA acts as a second loop. This groove is excited using the top antenna. The goal is to optimize the length and height of the groove such that it receives maximum coupling from the top antenna and generates a relative excitation between the two equivalent magnetic current loops and enhance radiation at horizon.

The proposed dimensions of $d1$, $d2$ and height of groove h in Figure 6-7 selected from the parametric study in HFSS. Figure 6-8 and Figure 6-9 shows the realized gain and S11 for these parameters. By finding a good compromise between the realized gain (max values) at $\theta=90°$, $\phi = 0°$ and S11 values (over the DME band), $d1=250$ mm, $d2=210$ mm and $h= 14$ mm are chosen. For DME band there is a requirement of S11<-10 dB see Table 6-1. However, in Figure 6-9 for the case selected, the S11 is less than -6 dB, therefore, external impedance matching circuit is required, which is discussed later in this chapter.
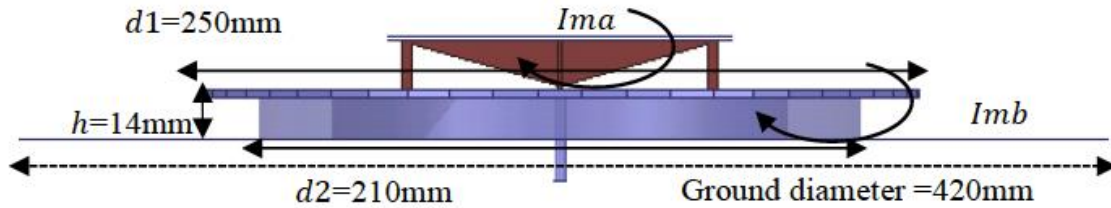
Figure 6-7: Simulation model of proposed design CSLA over grooved ground plane.
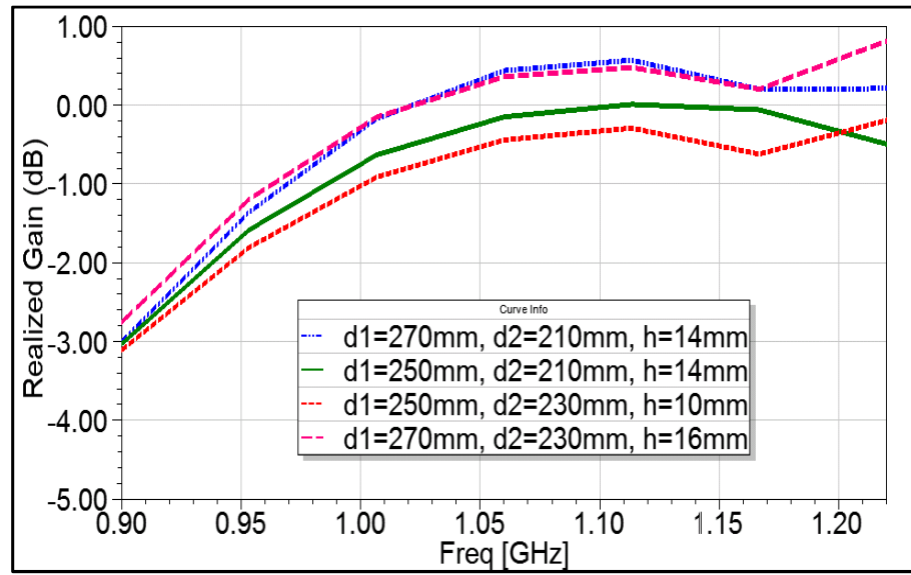
Figure 6-8:Simulated realized gain at horizon (θ=90°) for different values of h, $d1$ and $d2$.
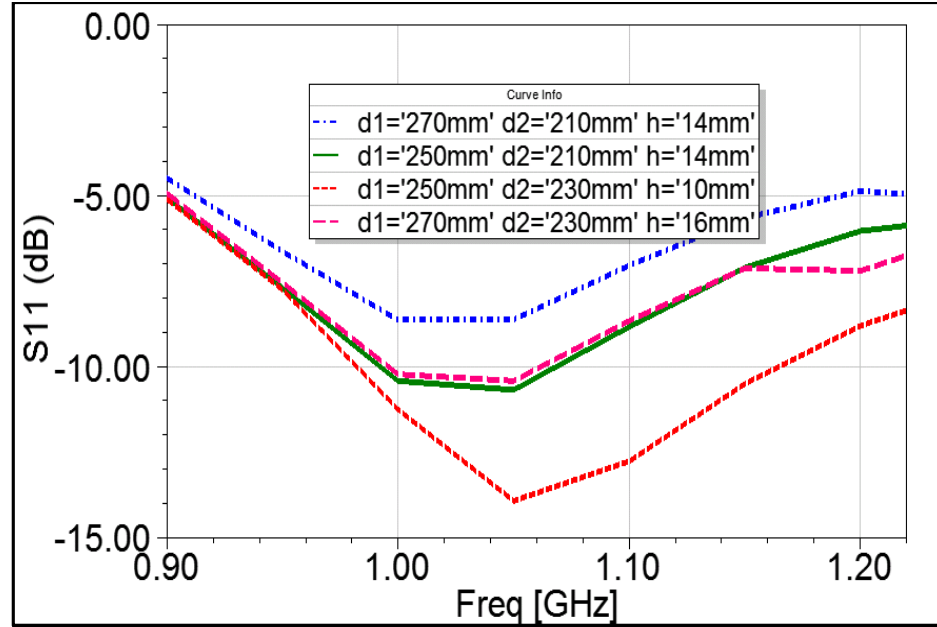
Figure 6-9: Simulated S11 for different h, $d1$ and $d2$.

Figure 6-10(a) and Figure 6-10(b) compares the near-field plane cuts of the antenna with and without the horizontal grooved finite ground plane. It can be seen here that the second loop which is the groove is effectively excited.

(a)

(b)
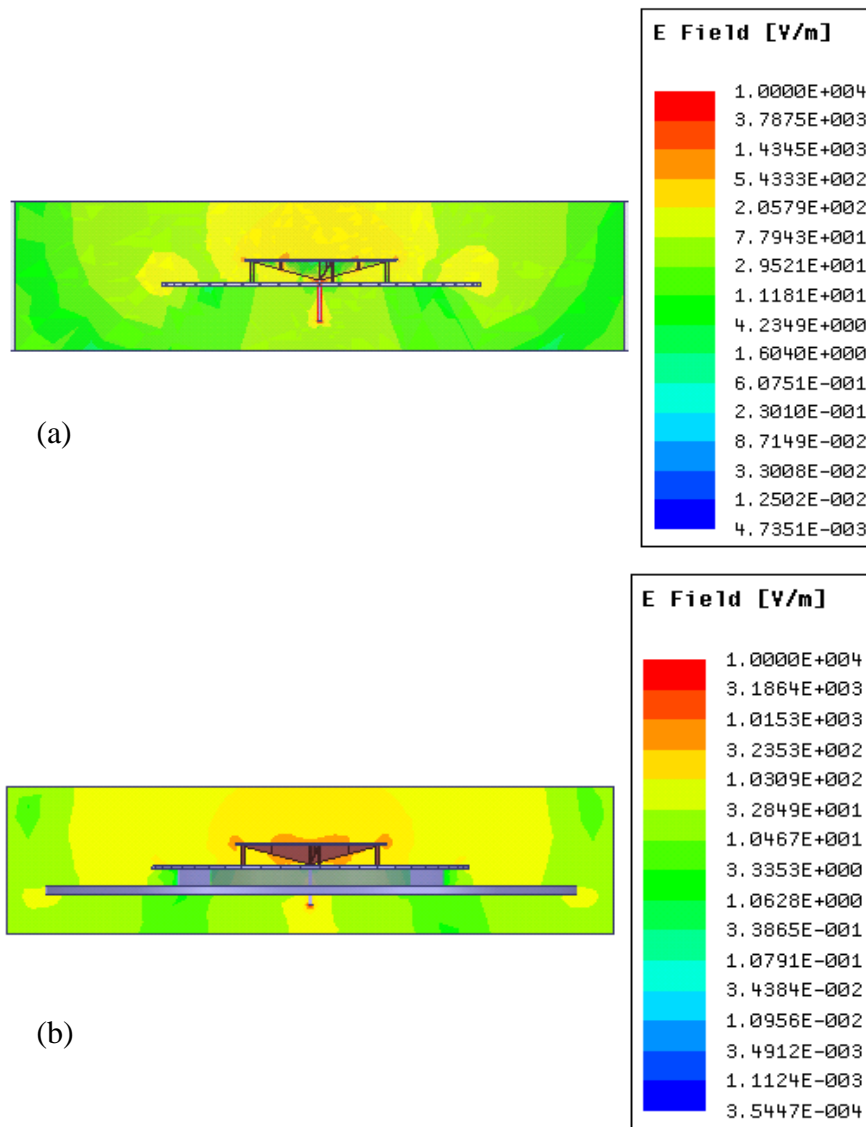
Figure 6-10: Electric field magnitude in the vicinity of (a) CSLA only, (b) CSLA with grooved ground plane.

The simulated realized gain of the quarter-wave monopole ($f_r = 1.13$ GHz), CSLA alone and CSLA on a grooved ground plane (without matching circuit) is compared in Figure 6-11. It can be seen that the presence of grooved ground plane has increased the gain at horizon ($\theta=90°$) for the full band as compared to the standard quarter-wavelength monopole and CSLA.
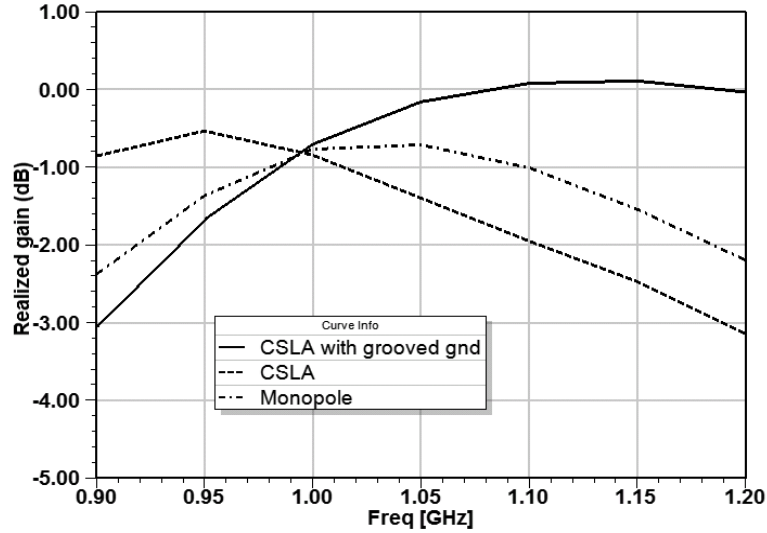
Figure 6-11: Comparison of simulated realized gain for CSLA, CSLA with grooved ground and quarter-wave monopole.

A comparison of simulated realized gain for monopole, CSLA and CSLA with grooved ground plane for both azimuth and elevation planes for 1 GHz, 1.1 GHz and 1.2 GHz is given in Figure 6-12. For ($\theta=90°$) for three different cases for each frequency shown in (a), (b) and (c) the CSLA with grooved ground has better gain. At the same time, it is worth to see that the first null in the elevation pattern for CSLA is at $\theta=100°$ and for monopole and CSLA with grooved ground plane it is at $\theta=125°$. This is due to the different ground size of CSLA (when measured alone) as compared to the grooved CSLA and monopole. The pattern in both azimuthal and elevation is similar to monopole. The height of monopole is 67 mm and for our proposed design it is 34 mm.
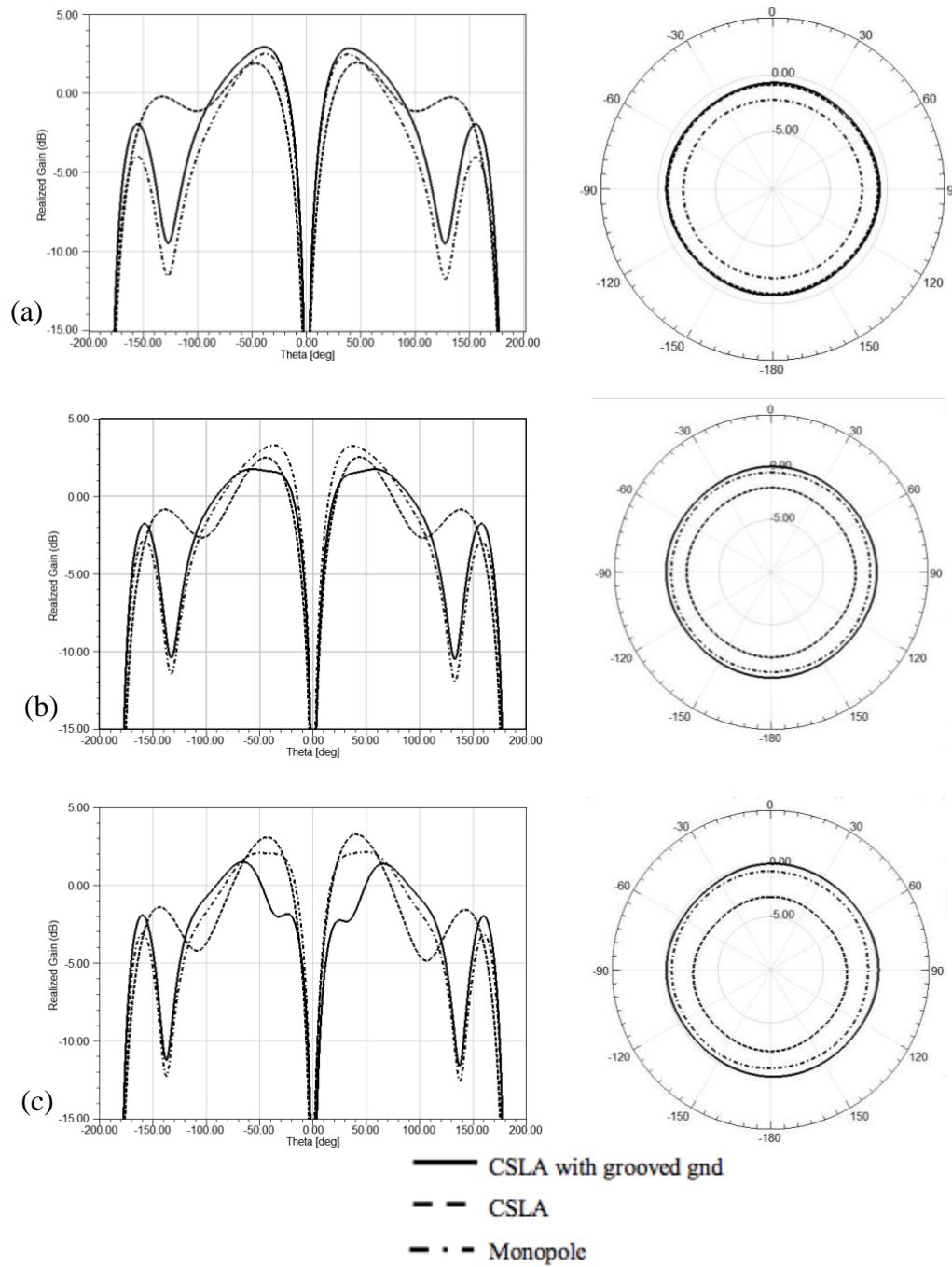
Figure 6-12 : Comparison of simulated realized gain both elevation and azimuth for (a) 1GHz, (b) 1.1 GHz, (c) 1.2 GHz.

6.7 Fabrication of prototype and testing

The CSLA antenna placed on a ground plane was fabricated and is shown in Figure 6-13(a) and placed on a grooved ground plane is shown in Figure 6-13(b) and tested for the return loss and radiation characteristics. Due to the physical limitations and considering the space available for the testing inside SATIMO Starlab system the infinite size of grooved ground plane was truncated to 420 mm.
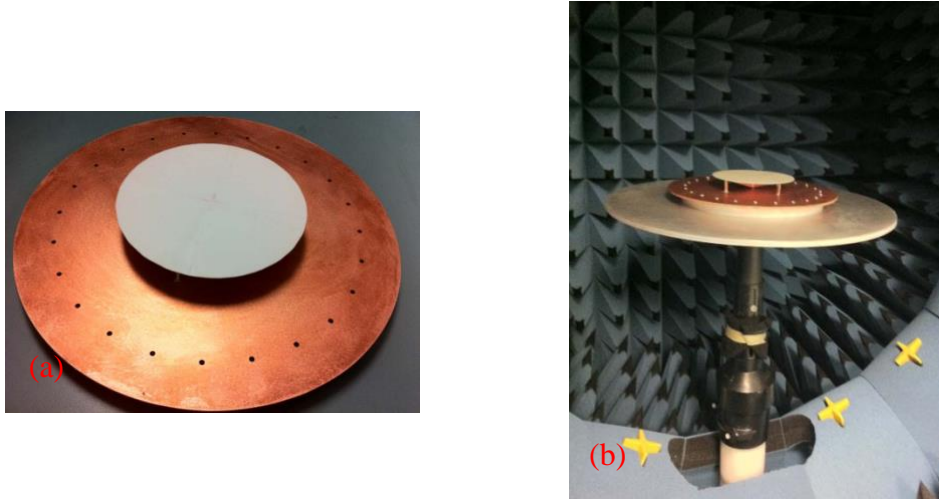
Figure 6-13:Fabricated prototype (a) CSLA (b) CSLA with grooved ground plane.

For the return loss, both antennas alone (without the grooved ground plane) and antenna place on the grooved ground plane show good agreement with the simulation results as seen in Figure 6-14. The measured realized gain of the quarter-wave monopole, CSLA alone and CSLA on a grooved ground plane are compared in Figure 6-15. As shown for the simulated results, the presence of grooved ground plane has increased the gain at horizon for measured results as well. Figure 6-16(a) and (b) shows the elevation and azimuthal plane of realized gain at 1.1 GHz respectively. As can be seen, the use of the grooved ground plane has changed the vertical radiation pattern of the antenna by reducing the gain below $\theta=60°$ and increasing it above $\theta=60°$, as required.
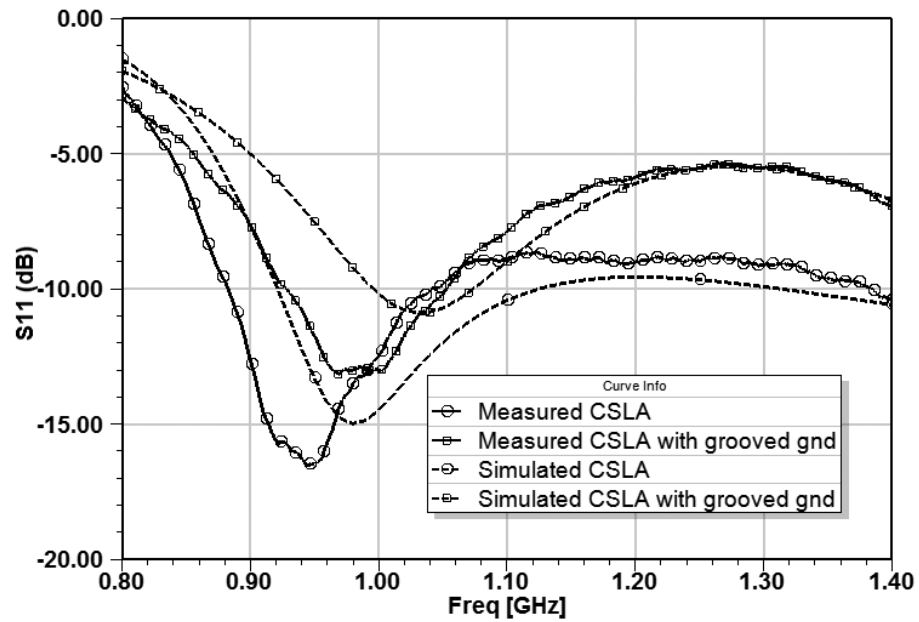
Figure 6-14: Comparison of S11 simulated and measured antenna.
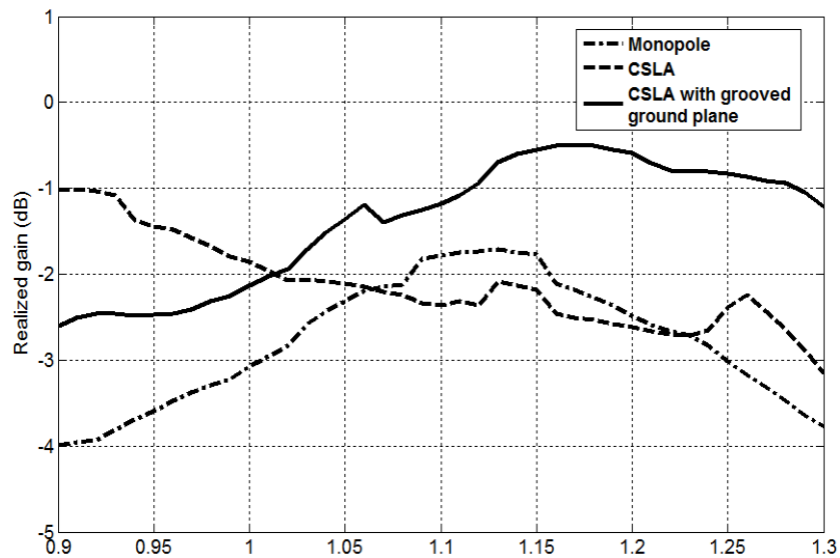
Figure 6-15: Comparison of measured realized gain for CSLA, CSLA with grooved ground (without matching) and monopole.
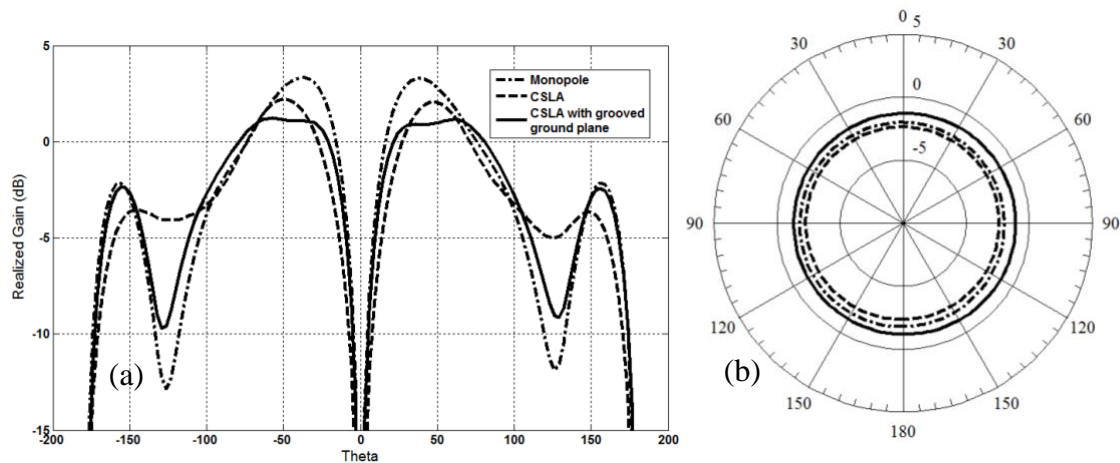
Figure 6-16: Comparison of measured realized gain for CSLA, CSLA with grooved ground and monopole.

6.8 Matching of fabricated CSLA with grooved ground plane

For DME band it is required to have S11< -10 dB. As it can be seen from Figure 6-14, measured S11 for CSLA is less than -8 dB and for CSLA with grooved ground plane it is less than -6 dB for 0.96 -1.22 GHz. It is clear that this antenna is not meeting the -10 dB requirement for S11 and consequently a matching network is used. Figure 6-17 shows a lumped LC matching network using double tuned impedance matching [89] that can be used to improve the antenna with grooved ground plane return loss (measured) better than -10 dB.
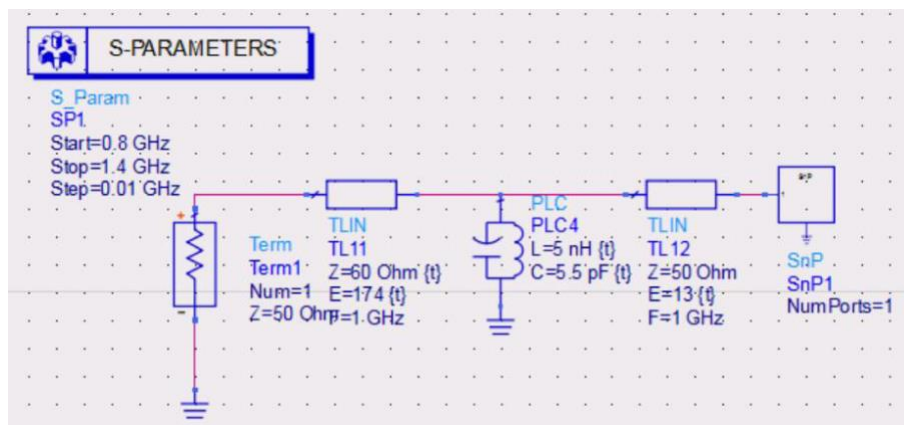
Figure 6-17: Passive circuit matching in ADS.

The circuit is designed in ADS and schematic shows the tuning of different parameters like E (electrical length of transmission line or impedance transformer), Z (impedance), L (inductance) and C (capacitance) for DME frequency band. This circuit is called double tuned matching network because matching is done in two steps. An LC circuit (PLC4) produces another resonance at 1.17 GHz and then an impedance transformer (electrical length 174° and impedance 60Ω) is used to match it to the 50Ω impedance using impedance transformer (TL11). The matched and unmatched return loss responses of measured full antenna are given in Figure 6-18. This circuit has not been fabricated. The purpose of this proposed circuit here is to demonstrate a method to improve S11. After using the matching network, the S11 <-10 dB for DME band (red curve). Assuming the matched S11 shown in Figure 6-18 the realized gain for antenna with grooved ground is further improved especially for frequencies above 1.05 GHz. This improvement factor can be determined by using following relation (6-10) versus frequency. The realized gain after the matching network is given in Figure 6-19, where it can be seen that gain is improved by 0.5 to 1 dB after using matched S11 for frequencies above 1.05 GHz.
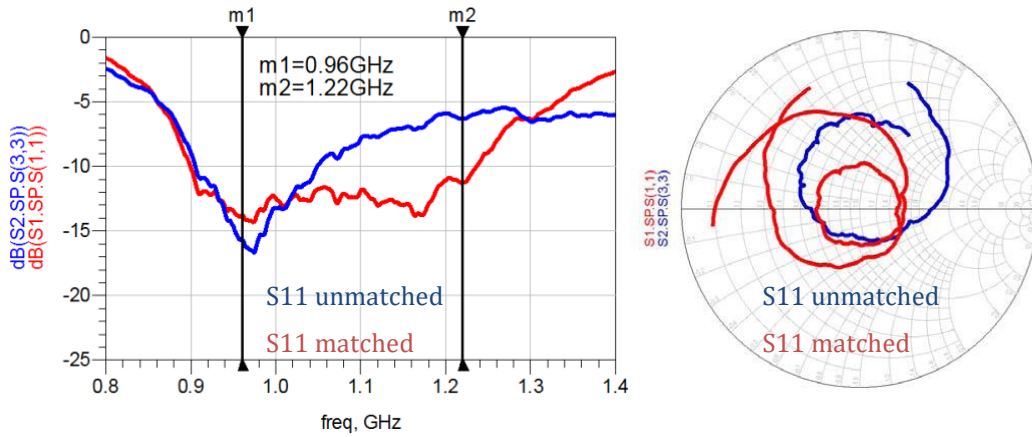
Figure 6-18: Matching of measured S11 of CSLA with grooved ground plane.

$$gain_{imp} = 10\, log10\left(\frac{1 - |S11_{matched}|^2}{1 - |S11_{unmatched}|^2}\right) \qquad (6\text{-}10)$$

124
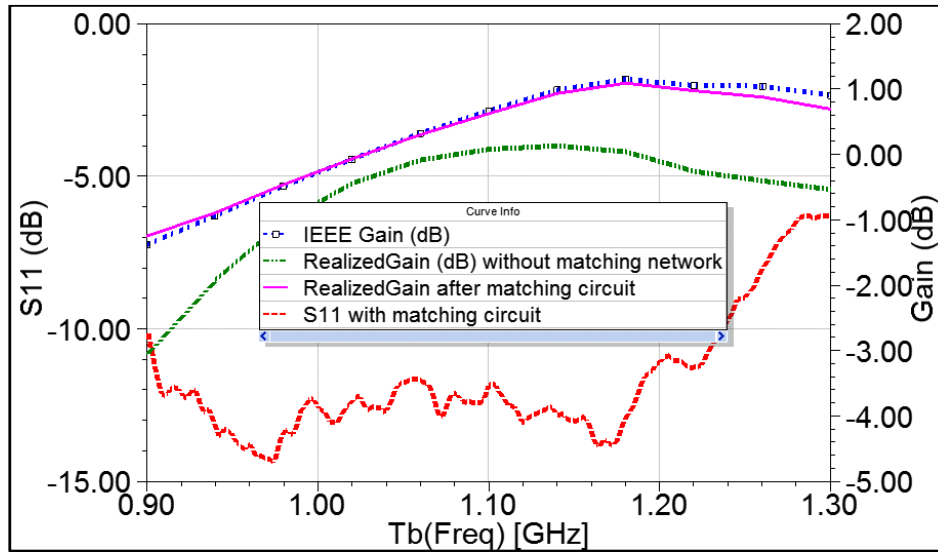
Figure 6-19:Improvement of realized gain with matching circuit.

6.9 Drag calculations for blade antenna and proposed antenna

In an aircraft there are two types of aerodynamics drag. First, induced drag which is mainly because of the wings, and second parasitic drag is due to anything protruding from the surface of the fuselage. The parasitic drag could be because of landing gears, external antennas, externally mounted navigation/strobe lights, fuel caps, temperature probe, external handles and fuel vents. Drag estimation is a well-established part of any aircraft design process. The following factors take a major influence on the drag: size of the obstacle (effective surface), form and orientation relative to the surface of aircraft, speed of aircraft and location of installation. In 1960's a lot of empirical data was measured in wind tunnels for all kind of objects and surfaces was collected [90],[91]. This systematically collected data which is the basis for engineering handbooks, is still in use today. Using this data, experts in the field can predict drag effects within a few percent precisions quite quickly which would normally take many days of time to find a good numerical model and run all the aerodynamic analyses. If a blade is installed horizontally, it will generate drag as a kind of lift, which it would not generate when installed vertically. So, the calculation of drag considers all effects that are caused by the boundary layer of the airflow. For instance, if the proposed antenna is installed within the boundary layer there would hardly be any difference in drag regardless of form and size. This boundary layer is the region where the viscous forces are significant [92]. In

case of aircraft it is the region close to the aircraft body where the fluid dynamics forces are strong. But things can change significantly if the antenna reaches outside the boundary layer even if only partially. The boundary layer is in itself a complicated multi-variable function including the shape of the aircraft and speed. To address the problem of how to assess two antenna candidates with respect to aerodynamic drag following points need to be considered.

a) There is no simple formula in drag estimation. If there is one, then we should fully understand the constraints under which it is valid. The handbook method is the most efficient way to analyse a specific configuration within a few percentage uncertainties.

b) The contribution of smaller antennas to overall drag is usually quite small [91]. Therefore, searching for the difference between two small contributions in presence of a dominant contribution is not easy.

c) Full numerical aerodynamic analysis may or may not give better insight for this purpose, but for sure it will involve significant efforts. It is better to apply this method after finding the approximate handbook method [93].

d) A lower antenna profile doesn't guarantee lower drag as it depends on the shape of the outer boundary of antenna [94]. But it definitely raises the chances to find an installation spot within the boundary layer. This can be an important factor in particular if the antenna is added after the aircraft shape was frozen, because all the nice locations are usually occupied during the design process.

e) There are cases where blade antennas improved drag. However, they were not installed on the aircraft body or fuselage instead they are hiding in winglets [25].

As we are not the expert of this field, based on all the points mentioned above from the literature and industry expert discussions, the drag calculation is done by using handbook empirical formulae. Using approximate empirical formulas as given in equation (6-11), (6-12) and (6-13) , [95] drag coefficient is calculated for the off-the-shelf DME blade antenna [96] in Figure 6-20 (a) and the proposed antenna model in Figure 6-20 (b), while considering the same size of the footprint c of the antennas on the aircraft. It is worth to mention here that the proposed antenna is covered by a cylindrical radome.

In these equations, C_d is the drag coefficient, h is the height of the antenna, c is the chord length or footprint, area of antenna wetted is defined as the surface area of antenna in contact with air (in this case it is the area of cylindrical radome), area of aircraft is the surface area of the wings, C_f is

the skin friction coefficient, R_e is the Reynolds number, p is the air density, v is the speed of aircraft, μ is the viscosity of air.

(a)

(b)
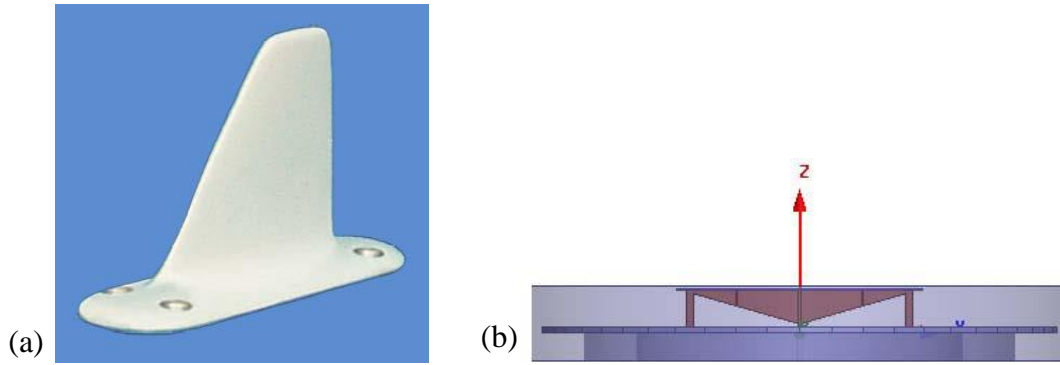
Figure 6-20:Drag models for (a) Blade antenna (b) Proposed antenna.

$$C_d = C_f \left[1 + \frac{h}{c}\right] \frac{area\ of\ antenna\ wetted}{area\ of\ aircarft} \tag{6-11}$$

$$C_f = \frac{0.455}{log10(R_e)^{2.58}} \tag{6-12}$$

$$R_e = \frac{pvc}{\mu} \tag{6-13}$$

By using the appropriate values of each variable [95] & [97]

p =1kgm^{-3}

v =590mph=260msec^{-2}

μ =1.45x10^{-5}kgmsec^{-3}

c =0.250m

area of aircraft=surface area of wings=85m^2

wetted area of blade antenna=0.0059m^2

wetted area of proposed antenna=0.076m^2

The drag coefficient C_d for the blade is approximately 2.94x10^{-6}=0.0249 counts and for proposed antenna it is 3.49x10^{-6}= 0.0349 counts. Where 0.0001=1 count. The above-calculated values are quite close and are calculated from approximate formulas, which do not include all the physical/environmental effects. As the height of proposed antenna is less and shape is dome as compared to blade antenna, it is more attractive candidate for less aerodynamic drag. The proposed design beats the blade in terms of directivity at horizon. Experimental testing, e.g. in a wind tunnel, is however required to have more accurate assessment of the drag.

In Figure 6-21 comparison of drag coefficient of different shapes are given. As can be seen any shape with sharp edges or corners have large drag, while streamlined bodies have the least drag. If the low-profile antennas are covered by radome of such shapes the drag can significantly be reduced. The commercial blade antenna is also covered by radome which has smooth corners but still the height is comparatively large as compared to the low-profile antenna, which plays an important role in increasing the drag.
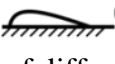
Figure 6-21:Measured Drag coefficient of different shapes of objects [7].

6.10 CONCLUSIONS

A new technique to increase the directivity of low-profile antennas at the horizon has been studied and verified with both simulation and prototype. The realization of two loop concept into grooved ground plane antenna shows advantageous results over monopole antenna. The antenna was fabricated with high precision from machining of individual parts to the assembly. The fabricated antenna is tested for S11 and radiation characteristics. The height of the proposed fabricated antenna from the top of the ground plane to the top plate of the antenna is 34.5 mm, including the thickness of middle plate. At the lowest frequency of DME band the electrical height of the antenna is 0.11 λ. The radiation pattern is similar to that of a monopole however there is an advantage of height reduction from 0.25 λ to 0.11 λ. Even with its reduced height, this antenna has more gain or directivity than the quarter-wave monopole (or blade antenna) at horizon. Based on simple calculations, its drag coefficient remains small and comparable to that of blade used for DME.

CHAPTER 7   CONCLUSIONS AND FUTURE WORK

This chapter summarizes the work presented in this dissertation, its scope and future improvements. This research work is a part of two academia-industry projects. The first project is to research and develop low-profile antennas for aircrafts. The main collaborators in this project are École Polytechnique de Montreal (POLY), École de Technologie Supérieure (ETS), Concordia University, Bombardier Aerospace (BA) and MacDonald Dettwiler and Associates (MDA Corporation).

The second project is Electromagnetic Platform for lightweight Integration/Installation of electrical systems in Composite Electrical Aircraft (EPICEA) and the collaborators are Axessim (France), Bombardier aerospace, École Polytechnique de Montreal, Ingegnerai dei sistemi (Italy) and Onera (France). The work presented here, i.e. the design of a multiband antenna for aircraft communication system is a part of this project.

7.1   Summary of the Contributions

In this dissertation we have presented four novel antenna designs for three different communication systems VHF, TCAS and DME of an aircraft. These antenna designs can be low-profile alternatives to the existing state-of-the-art and can further be adapted to be used by industry. The state-of-the-art blades or whip antennas are presently used in both commercial and military aircrafts. These antennas are near to quarter-wavelength in height, which causes the aerodynamic challenges such as high drag and aeroacoustics noise. Both high drag and aeroacoustics noise impacts aircraft's overall performance and are directly related to aircraft fuel consumption, speed and range. The proposed designs in this dissertation are reduced height antennas, meeting all the requirements of the specific aircraft communication system with a radiation pattern similar to those of existing blades.

These antenna designs can also be utilized for indoor communication system and for other platforms that require low-profile, conformal and omnidirectional antennas such as ships, trains and automobiles.

1. A dual-band antenna is presented in Chapter 3. It complies with all the requirements of VHF and TCAS (omni) antenna in terms of S11 and radiation characteristics. The use of top-loaded monopole with shorting pins and shorted stub help to reduce the antenna height.

Near E-field for VHF has been tested in an EMC chamber. This test method is helpful in validating the radiation performance of antenna especially for the case when compact antenna ranges are not available for such a low frequency. This antenna is also tested for return loss for both aluminum and composite ground planes at both VHF and TCAS frequency.

2. In Chapter 4, a surface wave antenna is presented where surface waves are generated by loading the patch antenna with circular AMC cells. The effect of this is to broaden the antenna matched impedance bandwidth to 30% (in simulations). The working prototype showed 24% fractional bandwidth for S11<-8 dB due to air gaps found in the fabrication. The required S11 <-10 dB for DME can be fixed by tuning the AMC cells. This antenna can be scaled down for DME band communication system.

3. A monopole loaded with magneto-dielectric material is discussed in Chapter 5. It shows that the resonant frequency is lowered for a given length of monopole without sacrificing the matched impedance bandwidth. Due to the lossy nature of MDM the radiation efficiency achieved is ~ 60% which is acceptable for many antenna applications. The FBW is 21% that makes our designed antenna useable for DME communication system.

4. In Chapter 6 a new technique to increase the directivity of a low-profile antenna at the horizon has been presented. A grooved ground plane is used to implement the dual-loop antenna concept. Around horizon ($\theta = 60°$ to $90°$), the radiation of candidate antenna is same as that of standard monopole for DO-189 (minimum operational performance standards for airborne DME system) standard compliance. A well-known CSLA [11] antenna is used as primary radiator and grooved ground plane is placed underneath the antenna. The antenna is matched by using double tuned matching network to compliance with the DME bandwidth. Based on simple empirical calculations, its drag coefficient remains small and comparable to that of blade used for DME.

All the above antennas are fabricated and measured for return loss and radiation characteristics. The measured results are found in good agreement with the simulation results of HFSS. Table 7-1 summarizes the simulated and measured performance of our proposed designs.

Table 7-1: Comparison of simulated and measured results of proposed designs.

Proposed design	Height	Width	System Requirement	Simulated	Measured
Chapter 3 VHF and TCAS Dual-band antenna	0.03λ where λ is at 118MHz	0.23λ where λ is at 118MHz	118-137 MHz S11<-6 dB FBW 14.9%	117 to 137 MHz	117 to 137 MHz
	0.04λ where λ is at 1.03GHz	0.28λ where λ is at 1.03GHz	1.03 to 1.09 GHz S11<-10 dB FBW 5.6%	1.02 to 1.10 GHz	0.99 to 1.08 GHz
			Dual-band configuration	120 to 137 MHz 1.02 to 1.05 GHz	120 to 137 MHz 1.0 to 1.08 GHz
Chapter 4 DME SWA	0.07λ where λ is at 3.84 GHz	2.3λ where λ is at 3.84 GHz	0.96 to 1.2 Scaled DME 3.84 to 4.88 GHz S11<-10 dB FBW 23%	3.8 to 5.2 GHz where S11 < -10 dB	4.1 to 5.25 GHz where S11 < -8 dB
Chapter 5 DME Magneto-dielectric loaded monopole	0.20λ where λ is at 0.96 GHz	0.09λ where λ is at 0.96 GHz	0.96 to 1.2 GHz S11<-10 dB FBW 23%	0.86 to 1.05 GHz	0.89 to 1.09 GHz
Chapter6 DME CSLA grooved ground plane	0.1λ where λ is at 0.96 GHz	0.8λ where λ is at 0.96 GHz	0.96 to 1.2 GHz S11<-10 dB FBW 23 %	0.99 to 1.2 GHz where S11<-6 dB	0.9 to 1.22 GHz where S11 <-10 dB (With matching in ADS)

The upper bound for fractional bandwidth of small antenna, ($ka \leq 0.5$) for VSWR s, can be calculated from equation ((7-1) [27], where a is the radius of spherical volume circumscribing the maximum antenna dimension and η is the radiation efficiency of antenna.

$$FBW_{ub} = \frac{1}{\eta}\left[\frac{1}{ka} + \frac{1}{(ka)^3}\right]^{-1}\frac{s-1}{\sqrt{s}} \tag{7-1}$$

Table 7-2: Comparison of theoretical upper bound of FBW and simulated FBW for proposed designs.

Proposed design	Height (h)	Width (w)	FBW (Sim)	FBW (M)	a	ka	η (M)	s (M)	Q_{lb}	Theoretical FBW_{ub}
VHF	0.03 λ	0.23 λ	21.2%	21.2%	0.12 λ	0.75	0.9	3	3.33	34%
TCAS	0.04 λ	0.28 λ	3.8%	4.3%	0.14 λ	0.88	0.9	2	2.3	30%
DME-SWA	0.07 λ	2.3 λ	31%	23.5%	1.2 λ	7.54	0.9	2.3	0.12	705%
DME-MDM	0.20 λ	0.09 λ	19.8%	20.2%	0.20 λ	1.26	0.6	2	3.35	90%
DME-CSLA	0.1 λ	0.8 λ	20.1%	30.2%	0.4 λ	2.51	0.9	2	0.41	170%

According to Wheeler the antenna is considered as small antenna when $ka \leq 0.5$. In the above Table 7-2 it can be seen that none of the design is exactly small antenna rather they are low-profile antennas. The height of proposed antennas is quite low as compared to the diameter or width of the structure. Using equation (7-1), gives a theoretical estimate of upper bound FBW that can be determined for a given volume /size of an antenna. However, in the Chu-limit, it is assumed that

the antenna occupies the volume of a sphere of radius a. Here the antenna is far from being spherical, so the formula may not apply.

7.2 Future Work

Some of the suggested future work and improvements are as follows.

1. In Chapter 3, the dual-band antenna has a both VHF and TCAS band. The TCAS antenna has two modes, omnidirectional and directional. In the proposed dual-band antenna, the omnidirectional mode of TCAS is only considered. This can be made directional by adding a feeding network, which includes switches and beam forming parasitic elements. The VHF Comms antenna can also be extended to VHF band 108 MHz to 156 MHz by optimizing the antenna-radiating model.

2. In Chapter 4, a patch antenna excites AMC cells. The bandwidth of this proposed design can further be enhanced by using a broadband antenna instead of patch antenna. Such that the full-scaled antenna can cover DME band (0.96-1.22 GHz) as well as inflight telephony system (824 MHz to 895 MHz) simultaneously. The one-fourth scaled antenna can be used for telemetry police (4.9 GHz to 6.4 GHz) and Telemetry Advanced Range Instrumentation Aircraft (ARIA) (4.16 GHz to 4.25 GHz).

3. The use of magneto-dielectric material in Chapter 5 can be explored for other material loading /coating having less magnetic loss. There is need for more work to be done on magnetic materials properties to make them less lossy. The shape of loading elements can also be looked into, to make the antenna broadband.

4. The grooved ground plane used with CSLA in Chapter 6 can also be applied to other proposed antennas to get more radiation towards the horizon for DME band applications.

The general improvements required in all the prototypes are as follows:

1. The radome of the antennas needs to be designed and tested for any changes in the characteristics of antenna. The radome helps to protect antenna from weather condition and provide mechanical stability to the antenna. The shape of the radome can play important role in finding the drag or noise produce by these designs.

2. As the proposed designs are low-profile, more than one antenna (dual-band antenna and DME antenna) can be placed together and a radome covering both antennas simultaneously can effectively reduce the drag caused by two antennas placed individually.

3. The tuning parameters of the all the antenna designs need to be defined. As in the environment where multiple antennas are placed, they can influence each other and change the antenna characteristic. By knowing the tuning parameters, the antennas performance can be optimized accordingly.

4. All the antennas should be tested for both aluminum and composite ground planes. As, an increasing number of the aircrafts nowadays are composite electric aircraft (CEA).

5. To understand aerodynamics improvements with proposed designs, antenna drag should be studied for all the proposed antenna models.

6. The wind tunnel testing of antenna will give better experimental values of parasitic drag caused by their shapes and can be compared with the state-of-the-art blades.

7.3 Publications of research papers

7.3.1 Conference proceedings

1. Ikram, A. & Laurin, J.J. (2016). "Reducing the height of a monopole antenna by using magneto dielectric material." 17th International Symposium on Antenna Technology and Applied Electromagnetics (ANTEM 2016), Montreal, QC.

2. Ikram, A. & Laurin, J.-J. (2014). "On the increase of the directivity of a low-profile aircraft antenna". 8th European Conference on Antennas and Propagation (EuCAP 2014), The Hague, Netherlands (p. 338-342).

7.3.2 Articles

Two articles are under preparation of submission.

1. Design and fabrication of low-profile dual-band antenna for aircraft TCAS and VHF communication system.

2. Low-profile surface wave antenna for aircraft DME communication system.

BIBLIOGRAPHY

[1]   T. M. Macnamara, "The Antenna Sitting Process," Chichester, UK: John Wiley & Sons, Ltd, 2010, ch.3, pp. 99.

[2]   Minimum Operational Performance Standards for Airborne Distance Measuring Equipment (DME) Operation Within the Radio Frequency Range of 960-1215 MHz, Document No. RTCA/DO-189, 1985.

[3]   Minimum Operational Performance Standards for Airborne Radio Communication Equipment Operating Within The Radio Frequency Range (VHF), 117.975-137 MHz, Document No. RTCA/DO-186A, 2005.

[4]   Minimum Operational Performance Standards for Traffic Alert and Collision Avoidance System II Airborne Distance Measuring Equipment (TCAS) Operation Within the Radio Frequency Range of 1030-1090 MHz, Document No. RTCA/DO-185B, 2008.

[5]   D. Kotz, "ADS-B In An Older Plane? - Plane & Pilot Magazine," Aug-2017, [Online].Available: https://www.planeandpilotmag.com/article/ads-b-older-plane/

[6]   M. del Carmen Redondo Gonzalez, "Analysis of Conformal Antennas for Avionics Applications," M.S. thesis, Dept. Elect. Eng., Univ. of Gothenburg, Sweden, 2007.

[7]   F. J. Hale, "Aircraft Forces and Subsystems," in Introduction to aircraft performance, selection, and design, 1st ed. Canada: John Wiley & Sons Inc, 1984, ch.2, pp. 16-18.

[8]   [Online]. Available: https://gardn.org/.

[9]   L. J. Chu, "Physical Limitations of Omni-Directional Antennas," (in English), Journal of Applied Physics .1948, vol. 19, no. 12, pp. 1163-1175, 1948.

[10]   J. E. Cermak. et al, "Drag Force on Microwave Antenna ," Gabrial Electronics, Inc Maine, U.S.,   1983.   [Online],   Available: https://mountainscholar.org/bitstream/handle/10217/173137/CERF_Cermak_Peterka_B enkiewicz_2.pdf?sequence=1.

[11]   A. Elsherbini and K. Sarabandi, "Very Low-Profile Top-Loaded UWB Coupled Sectorial Loops Antenna," IEEE Antennas and Wireless Propagation Letters, vol. 10, pp. 800-803.

[12]   S. Henely, "TCAS II," in The Avionics Handbook, CRC Press LLC, 2001, ch.18.

[13]   T. M. Macnamara, "Aircraft Systems Using Antennas," in Introduction to AntennaPlacement and Installation, UK: John Wiley & Sons, Ltd, 2010, ch.2, pp. 76

[14]   U.S. Department Fedral Aviation Authority,"Introduction to TCAS II V7.1," [Online].Available:httpswww.faa.govdocumentLibrarymediaAdvisoryCircularTCASIIV.I ntrobooklet.pdf. [Accessed: 26-Apr-2018].

[15]   T. M. Macnamara, "Aircraft Systems Using Antennas," in Introduction to Antenna Placement and Installation, Chichester, UK: John Wiley & Sons, Ltd, 2010, pp. 78.

[16]   C. Balanis and D. DeCarlo, "Monopole antenna patterns on finite size composite ground planes," IEEE Transactions on Antennas and Propagation, vol. 30, no. 4, pp. 764-768, 1982.

[17]   J. A. Birken, R. F. Wallenberg and O. Milton, "Advanced Composite Aircraft Electromagnetic Design and Synthesis," 1981 IEEE International Symposium on Electromagnetic Compatibility, Boulder, Colorado, USA, 1981, pp. 1-8.

[18]   C. L. Blake, "Composites - Their Electrical and Electromagnetic Impact," presented at the IEEE 1976 International Symposium on Electromagnetic Compatibility, Washington, DC, USA, 2016, pp. 1–4."

[19]   F. A. A. U S Department of Transportation, "Acceptable Methods, Techniques, and Practices Aircraft Inspection and Repair," 1998, pp.191, [Online]. Available: https://www.faa.gov/documentLibrary/media/Advisory_Circular/AC_43.13-1B_wchg1.pdf.

[20]   Online], Available: http://www.appropedia.org/Composites_in_the_Aircraft_Industry

[21]   [Online]. Available: http://www.sensorantennas.com/product/tcas-ii-antenna/

[22]   [Online]. Available: http://www.aeroexpo.online/prod/sensor-systems/product-184807-40558.html

[23]   [Online]. Available: http://www.sensorantennas.com/wp- content/uploads/2015/01/S65 8280-10.pdf

[24]   T. M. Macnamara, "Antenna Used on Aircraft," in Introduction to Antenna Placement and Installation, UK: John Wiley & Sons, Ltd, 2010, ch.5, pp.149.

[25]   John H. Hanusa et al., "Very high frequency line of sight winglet antenna," US Patent 7737898 B2, Jun.15, 2010.

[26]   J. Volakis,"Small Antenna" in Antenna Engineering Handbook, 4th Edition. New York, NY:McGraw-Hill Education, 2007, ch.6.

[27]   D. F. Sievenpiper et al., "Experimental Validation of Performance Limits and Design Guidelines for Small Antennas," IEEE Transactions on Antennas and Propagation, vol. 60, no. 1, pp. 8-19.

[28]   S. Palud, F. Colombel, M. Himdi, and C. Le Meins, "Wideband Omnidirectional and Compact Antenna for VHF/UHF Band," IEEE Antennas and Wireless Propagation Letters, vol. 10, pp. 3-6.

[29]   S. Palud, F. Colombel, M. Himdi, and C. Le Meins, "Reduced-height wideband conical antennas in the VHF/UHF bands," pp. 3761-3765, Feb 07 2009.

[30]   M.-S. Kim, C.-Y. Park, C.-M. Cho, and S.-M. Jun, "A multi-band smart skin antenna design for flight demonstration," presented at the The 8th European Conference on Antennas and Propagation (EuCAP 2014), 2014.

[31]   W.-C. Liu and C.-S. Chen, " Design Of Missile-Mounted SIW Antenna With High Directivity For Data Transmission," Progress In Electromagnetics Research C, vol. 38, pp. 79-88, 2013.

[32]   P. Wongsakulphasatch, C. Phongcharoenpanich, and S. Kawdungta, "Compact flat monopole antenna for small aircraft of VHF communication system," in 2012 IEEE Asia-Pacific Conference on Antennas and Propagation (APCAP), pp. 27-28.

[33] C.-F. Wang, L. B. Kong, F.-G. Hu, Z. Yang, and Z.-W. Li, "Electrically small magnetodielectric coated monopole antenna at HF band," pp. 78-79.

[34] G. Goubau, N. N. Puri, and F. K. Schwering, "Diakoptic theory for multielement antennas," IEEE Transactions on Antennas and Propagation, vol. 30, no. 1, pp. 15-26, 1982.

[35] S.-H. Yeh and K.-L. WONG, "A broadband low-profile cylindrical monopole antenna top loaded with a shorted cross patch," Microwave and Optical Technology Letters, vol. 32, no. 3, pp. 186-188, 2001.

[36] Z. Shen and J. Wang, "Top-Hat Monopole Antenna for Conical-Beam Radiation," IEEE Antennas and Wireless Propagation Letters, vol. 10, pp. 396-398.

[37] N. Takanori and K. Yasuhiro, "A Low Profile and Wideband Top-Loaded Monopole Antenna with Shorting Posts," pp. 1-4, 2000.

[38] Y. L. Dazhi Yang and Z. Shen, "A broadband top cap monopole antenna," presented at the IEEE Antennas and Propagation Society Symposium, 2003., pp. 24-27.

[39] N. M. Y. Y. Woo-Jin Kim, "Low-Profile Top-Loaded Monopole Antenna with Oblique Shorting Pins," in Proceedings of the 40th European Microwave Conference, pp. 1476-1479.

[40] L. Cobos, H. D. Foltz, and J. S. McLean, "A modified Goubau-type antenna with two octaves of impedance bandwidth," in IEEE Antennas and Propagation Society Symposium, 2003., pp. 3051-3054 Vol.3.

[41] F. Y. Rahmat-Samii and A. Kishk, "A Novel Surface Wave Antenna with a Monopole Type Pattern: A Thin Periodically Loaded Slab Excited by a Circular Disk," in IEEE Antennas and Propagation Society International Symposium, 2005, pp. 742-745.

[42] A. Sutinjo, M. Okoniewski, and R. H. Johnston, "Investigation Into the Vertical Monopole-Like Radiation Mechanism of a Horizontal Dipole on a Periodic Patch-Loaded Grounded Slab," IEEE Antennas and Wireless Propagation Letters, vol. 6, pp. 344-348.

[43] F. Yang and Y. Rahmat-Samii, Electromagnetic Band Gap Structures in Antenna Engineering. Cambridge University Press, 2009, pp. 266.

[44] Z. Chen and Z. Shen, "Wideband Flush-Mounted Surface Wave Antenna of Very Low Profile," IEEE Transactions on Antennas and Propagation, vol. 63, no. 6, pp. 2430-2438.

[45] F. Erkmen, C.-C. Chen, and J. Volakis, "UWB magneto-dielectric ground plane for low-profile antenna applications," IEEE Antennas and Propagation Magazine, vol. 50, no. 4, pp. 211-216, Oct 15 2008.

[46] F. Namin, T. G. Spence, D. H. Werner, and E. Semouchkina, "Broadband, Miniaturized Stacked-Patch Antennas for L-Band Operation Based on Magneto-Dielectric Substrates," vol. 58, no. 9, pp. 2817-2822.

[47] B.-Y. Park, M.-H. Jeong, and S.-O. Park, "A Magneto-Dielectric Handset Antenna for LTE/WWAN/GPS Applications," IEEE Antennas and Wireless Propagation Letters, vol. 13, pp. 1482-1485.

[48]   Y. Cheon, J. Lee, and J. Lee, "Quad-Band Monopole Antenna Including LTE 700 MHz With Magneto-Dielectric Material," IEEE Antennas and Wireless Propagation Letters, vol. 11, pp. 137-140.

[49]   J. Lee, J. Heo, J. Lee, and Y. Han, "Design of Small Antennas for Mobile Handsets Using Magneto-Dielectric Material," IEEE Transactions on Antennas and Propagation, vol. 60, no. 4, pp. 2080-2084.

[50]   B. Seok and Y. Mano, "A Small Meander VHF & UHF Antenna by Magneto-dielectric Materials," in 2005 A*sia-Pacific Microwave*, vol. 4, pp. 1-3.

[51]   A. Henderson, "Electrically short monopole antennas with dielectric or ferrite coatings," Proceedings of the Institution of Electrical Engineers, vol. 125, no. 9, pp. 793-803(10), Sep 1978.

[52]   L. Huitema, T. Reveyrand, J.-L. Mattei, E. Arnaud, C. Decroze, and T. Monediere, "Frequency Tunable Antenna Using a Magneto-Dielectric Material for DVB-H Application," IEEE Transactions on Antennas and Propagation, vol. 61, no. 9, pp. 4456-4466.

[53]   A. Ikram and J.-J. Laurin, "On the increase of the directivity of a low profile aircraft antenna," in *European Conference on Antennas and Propagation 2014*, pp. 338-342.

[54]   L. Huang, "Low-profile patch antennas with enhanced horizontal omnidirectional gain for DSRC applications," IET Microwaves, Antennas &amp; Propagation, vol. 12, no. 2, pp. 246-253(7), Mar 2018.

[55]   B. Lv, X. Wang, C. Zheng, J. Huangfu, C. Li, and L. Ran, "Radiation Enhancement for Standard Patch Antennas Using a Loosely Grooved Ground Plane," IEEE Antennas and Wireless Propagation Letters, vol. 11, pp. 604-607.

[56]   Z. Guangping, "Shorting-pin loaded annular ring microstrip antenna," in IEEE Antennas and Propagation Society International Symposium. 1998 Digest. Antennas: Gateways tothe Global Network. Held in conjunction with: USNC/URSI National Radio Science Meeting, vol. 2, pp. 900-903.

[57]   H.-F. Chen, M.-Y. Lin, and K.-H. Lin, "A V-shape Edge-Groove Design for a Finite Ground Plane to Reduce Pattern Ripples of a Monopole," IEEE Antennas and Wireless Propagation Letters, vol. 7, pp. 561-564.

[58]   D.-H. Kwon, "Transformation Electromagnetic Design of an Embedded Monopole in a Ground Recess for Conformal Applications," IEEE Antennas and Wireless Propagation Letters, vol. 9, pp. 432-435.

[59]   L. Rufail and J.-J. Laurin, "Aircraft Cavity-Backed Nonprotruding Wideband Antenna," IEEE Antennas and Wireless Propagation Letters, vol. 11, pp. 1108-1111.

[60]   [Online]. Available: http://www.b737.org.uk/communications.htm#Antennae

[61]   U.S. Department Federal Aviation Authority, "Introduction to TCAS II V7.1," [Online].Available: httpswww.faa.govdocumentLibrarymediaAdvisoryCircularTCASIIV.Introbooklet.pdf.[Accessed: 26-Apr-2018]

[62]   [Online].   Available: https://www.cobham.com/communications-and
         connectivity/aerospace-communications/antennas/aircraft-
         communicationantennas/business-and-regional-jets-antennas/atc-dmedatasheet/docview/.

[63]   [Online]. Available: http://www.sensorantennas.com/product/vhfuhf-antenna/.

[64]   L. Akhoondzadeh-Asl, J. Hill, J.-J. Laurin, and M. Riel, "Novel Low Profile Wideband
         Monopole Antenna for Avionics Applications," IEEE Transactions on Antennas and
         Propagation, vol. 61, no. 11, pp. 5766-5770.

[65]   F. Yang, Y. Rahmat-Samii, and A. Kishk, "Low-profile patch-fed surface wave antenna
         with a monopole-like radiation pattern,"IET Microwaves, Antennas &amp;
         Propagation, vol. 1, no. 1, pp. 261-266, 2007.

[66]   C. A. Balanis, Advanced Engineering Electromagnetics, 2nd Edition. Wiley Global
         Education, 2012, p. 1040.

[67]   A. Al-Zoubi, F. Yang, and A. Kishk, "A Low-Profile Dual-Band Surface Wave Antenna
         With a Monopole-Like Pattern," IEEE Transactions on Antennas and Propagation, vol. 55,
         no. 12, pp. 3404-3412.

[68]   A. Bhattacharyya, "Effects of ground plane and dielectric truncations on the efficiency of a
         printed structure," IEEE Transactions on Antennas and Propagation, vol. 52, no. 1, pp. 303-
         308, Feb 2004.

[69]   J. R. James, P. S. Hall, and C. Wood, Microstrip Antenna. IET, 1981, pp. 304.

[70]   D. Sievenpiper, R. Broas, and E. Yablonovitch, "Antennas on high-impedance ground
         planes," vol. 3, pp. 1245-1248.

[71]   D. Sievenpiper, R. Broas and E. Yablonovitch, "Antennas on high-impedance ground
         planes," 1999 IEEE MTT-S International Microwave Symposium Digest
         (Cat.No.99CH36282), Anaheim, CA, USA, 1999, pp. 1245-1248 vol.3.

[72]   Daniel Frederic Sievenpiper, "High-Impedance Electromagnetic Surfaces," PhD
         dissertation, Dept. Elect. Eng Univ of California, Los Angeles, 1999.

[73]   Yongxi Qian, D. Sievenpiper, V. Radisic, E. Yablonovitch and T. Itoh, "A novel approach
         for gain and bandwidth enhancement of patch antennas," Proceedings RAWCON 98. 1998
         IEEE Radio and Wireless Conference (Cat. No.98EX194), Colorado Springs, CO,
         USA,1998, pp. 221-224.

[74]   A. Foroozesh and L. Shafai, "Application of combined electric- and magnetic-conductor
         ground planes for antenna performance enhancement," Canadian Journal of Electrical and
         Computer Engineering, vol. 33, no. 2, pp. 87-98, 2008.

[75]   C. Deng and Y.-j. Xie, "Design of Resistive Loading Vivaldi Antenna," IEEE Antennas
         and Wireless Propagation Letters, vol. 8, pp. 240-243.

[76]   W. Richards and S. Long, "Matching microstrip antennas using reactive loads," in 1986
         Antennas and Propagation Society, vol. 24, pp. 431-434.

[77]   J. Oh and K. Sarabandi, "Ultra-wideband, miniaturized, low profile, omnidirectional
         antenna using a novel reactive loading approach," in 2012 IEEE Antennas and Propagation

Society International Symposium and USNC/URSI National Radio Science Meeting, pp. 1-2.

[78]   D. Guha and Y. M. M. Antar, "Four-Element Cylindrical Dielectric Resonator Antenna for Wideband Monopole-Like Radiation,", IEEE Transactions on Antennas and Propagation, vol. 54, no. 9, pp. 2657-2662, Sep 2006.

[79]   D. Guha, D. Ganguly, S. George, and Y. M. M. Antar, "Monopole-type dielectric resonator antenna with improved bandwidth characteristics," in 2014 IEEE International Symposium on Antennas and Propagation & USNC/URSI National Radio Science Meeting, pp. 1988-1989.

[80]   D. Guha, B. Gupta, and Y. M. M. Antar, "Hybrid monopole-DRA: New geometries for improved ultra-wideband operation," in *2010 IEEE International Symposium Antennas and Propagation and CNC-USNC/URSI Radio Science Meeting*, pp. 1-4.

[81]   L. Huitema, M. Koubeissi, C. Decroze, and T. Monediere, "Handheld dielectric resonator antenna for ultra-wideband applications," in 2010 International Workshop on Antenna Technology: "Small Antennas, Innovative Structures and Materials" (iWAT), pp. 1-4.

[82]   D. Guha, Y. M. M Antar, A. Ittipiboon, A. Petosa, and D. Lee, "Improved Design Guidelines for the Ultra Wideband Monopole-Dielectric Resonator Antenna," IEEE Antennas and Wireless Propagation Letters, vol. 5, pp. 373-376.

[83]   C. Niamien, S. Collardey, A. Sharaiha, and K. Mahdjoubi, "Compact Expressions for Efficiency and Bandwidth of Patch Antennas Over Lossy Magneto-Dielectric Materials," IEEE Antennas and Wireless Propagation Letters, vol. 10, pp. 63-66.

[84]   R. C. Hansen and M. Burke, "Antennas with magneto-dielectrics," (in English), Microwave and Optical Technology Letters, vol. 26, no. 2, pp. 75-78, 2000.

[85]   "Keysight 85070E Dielectric Probe Kit 200 MHz to 50 GHz," (2017), [Online]. Available: https://literature.cdn.keysight.com/litweb/pdf/5989-0222EN.pdf?id=364444.

[86]   "Keysight 16454A Magnetic Material Test Fixture," (2017), [Online]. Available: http://literature.cdn.keysight.com/litweb/pdf/16454-90020.pdf

[87]   W. L. Stutzman and G. A. Thiele, "Some simple radiating system and antenna practice,"in Antenna Theory and Design, New York, NY, US: John Wiley & Sons, 1997, pp. 68-76.

[88]   A. Elsherbini and K. Sarabandi, "Very Low-Profile Top-Loaded UWB Coupled Sectorial Loops Antenna," IEEE Antennas and Wireless Propagation Letters, vol. 10, pp. 800-803, 2011.

[89]   A. R. Lopez, "Double-Tuned Impedance Matching," IEEE Antennas and Propagation Magazine, vol. 54, no. 2, pp. 109-116, 2012.

[90]   A. Cimarelli, M. Madonia, D. Angeli, and A. Dumas, "Aerodynamic Study of Advanced Airship Shapes," Journal of Aerospace Engineering, vol. 30, no. 3, 2017.

[91]   F. J. Hale, "Aircraft Forces and Subsystems," in Introduction to aircraft performance, selection, and design, 1st ed. Canada: John Wiley & Sons Inc, 1984, ch.2, pp. 16-18.

[92]   D. F. o. M. A. J. E. Cermak. et al, " Gabrial Electronics, Inc, U. S. Maine, 1983. [Online], Available:,

https://mountainscholar.org/bitstream/handle/10217/173137/CERF_Cermak_Peterka_Bi, and enkiewicz_2.pdf?sequence=1.

[93] [Online], Available: https://gardn.org/.

[94] L. J. Chu, "Physical Limitations of Omni-Directional Antennas," Journal of Applied Physics, vol. 19, no. 12, pp. 1163-1175, 1948.

[95] E. Torenbeek, Advanced Aircraft Design (Conceptual Design, Technology and Optimization of Subsonic Civil Airplanes). John Wiley & Sons, 2013, pp. 440.

[96] [Online], Available : http://www.sensorantennas.com/products/s65-5366-7l/

[97] M. Sadraey, Aircraft Performance. VDM Publishing, 2009.

[98] R. Furushima, S. Tanaka, Z. Kato, and K. Uematsu, "Orientation distribution–Lotgering factor relationship in a polycrystalline material—as an example of bismuth titanate prepared by a magnetic field," Journal of the Ceramic Society of Japan, vol. 118, no. 1382, pp. 921-926, 2010.

APPENDIX

As the sample is a sintered ceramic product, which means it is prepared by powdered material under high temperature and pressure without melting them. Since the lattice are hexagonal and slightly magnetic, some peaks are seen in the XRD plot. These peaks correspond to the expected peaks related to the hexagonal phases that are usually found for this kind of ferrite. Due to sintering of the powder, the crystalline domains are randomly oriented in the sample. If the intensity is normalized by the peak intensity of 11,000 the normalized intensity is close to 0 instead of 1 for all the theta. Looking at the pattern in Figure A-1, it does appear that it is close to an isotropic XRD pattern, As the lotgering number closer to 0 than 1 [98], which means that particles are randomly orientated.
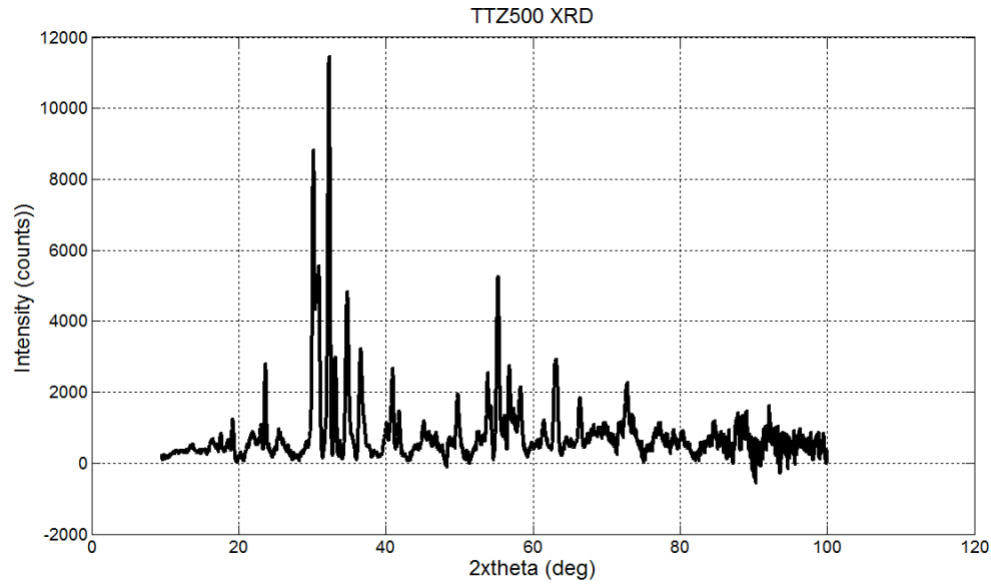

Figure A-1 : XRD of TTZ500 sample.